Continuous Flow Microwave Sterilisation Focussing on Aqueous Media

By

Jordan David Burcher-Jones

Thesis presented in partial fulfilment of the requirements for the degree of Master of Engineering (Electrical and Electronic) in the Faculty of Engineering at Stellenbosch University

The financial assistance of the National Research Foundation (NRF) towards this research is hereby acknowledged. Opinions expressed and conclusions arrived at are those of the author and are not necessarily to be attributed to the NRF.

Supervisor: Professor JB De Swardt

March 2020

Declaration

By submitting this thesis electronically, I declare that the entirety of the work contained therein is my own, original work, that I am the sole author thereof (save to the extent explicitly otherwise stated), that reproduction and publication thereof by Stellenbosch University will not infringe any third party rights and that I have not previously in its entirety or in part submitted it for obtaining any qualification.

Date: March 2020

Abstract

This thesis contains details regarding the research and development of a continuous flow, temperature controlled, microwave heating sterilisation unit. The microwave hardware design promotes the propagation of the fundamental TE_{10} mode for rectangular waveguide structures at $2.45\ \mathrm{GHz}$. The system design incorporates a single mode applicator chamber which considers the microwave heating patterns within the system. The heating patterns were predicted through rigorous electromagnetic thermal coupled simulations.

The temperature control system operates by maintaining output magnetron power whilst varying the media flow rate. The system has a controllable temperature range between $60\ ^{\circ}\mathrm{C}$ and $95\ ^{\circ}\mathrm{C}$ resulting in a variable system output flow rate between $3.3\ \mathrm{l/h}$ and $6\ \mathrm{l/h}$. The constant output power produced by the magnetron can be set to either $700\ \mathrm{W}$, $350\ \mathrm{W}$ or $210\ \mathrm{W}$, using a technique called saturable reactor control and this is demonstrated and explained in the project. The magnetron and high voltage supply were obtained from a conventional microwave oven.

Calibration techniques for various stages in the system are discussed and implemented to ensure measured data obtained is accurate and repeatable.

The materials used to transport the targeted media inside the treatment chamber were selected based on a low dissipation factor ($tan\delta$), effectively making the materials “invisible” to microwave radiation. This allows for selective heating of the media to be treated inside the system.

The microwave sterilisation treatments were conducted with a strain of *Lactococcus lactis* (NZ9000) with an antibiotic marker (chloramphenicol at $10\ \mu\mathrm{g/ml}$) suspended in sterile saline. The experiments conducted and observations made during development suggest that the designed system is a successful, effective, sterilisation solution.

Opsomming

Hierdie tesis bevat besonderhede rakende die navorsing en ontwikkeling van 'n deurlopende vloei, temperatuurbeheerde, mikrogolfverwarmingsterilisasie-eenheid. Die ontwerp van die mikrogolf-hardeware bevorder die voortplanting van die fundamentele TE_{10} modus vir reghoekige golfleier strukture by 2,45 GHz. Die stelselontwerp bevat 'n enkel-modus toediener wat die mikrogolfpatroon in die stelsel in ag neem. Die verwarmingspatrone is voorspel deur streng elektromagnetiese termiese gekoppelde simulasies.

Die temperatuur beheerstelsel werk deur die magnetron uittree drywing te handhaaf terwyl die media se vloeitempo verander word. Die stelsel het 'n beheerbare temperatuurbereik tussen 60 °C en 95 °C, wat lei tot 'n veranderlike uittree tussen 3,3 l / h en 6 l / h. Die konstante uittree drywing wat deur die magnetron gelewer word, kan op 700 W, 350 W of 210 W ingestel word met behulp van 'n tegniek genaamd versadigde reactor beheer, en dit word in die projek gedemonstreer en verduidelik. Die magnetron en hoogspanning krag toevoer is verkry uit 'n konvensionele mikrogolfoond.

Kalibreringstegnieke vir verskillende fases in die stelsel word bespreek en geïmplementeer om te verseker dat die gemete data akkuraat en herhaalbaar is.

Die materiaal wat gebruik word om die geteikende media binne die toediener te vervoer, is gekies op grond van 'n lae verlies faktor ($tan\delta$), wat die materiaal effektief 'onsigbaar' maak vir mikrogolf straling. Hierdeur kan selektiewe verhitting van die media binne die stelsel behandel word.

Acknowledgements

I, Jordan Burcher-Jones, would like to thank:

- Professor JB De Swardt for his continuous guidance and keen interest throughout the duration of this project.
- Doctor Anton Du Preez van Staden for his insight and help regarding the microbiology section and all live bacterial tests.
- Fiona Burcher-Jones for language editing and proof reading of this document.
- Terence Jones for assisting in Afrikaans translation for the abstract.
- Bernard van der Merwe for always making time to chat about design issues we faced in the EHG.
- Michelle de Castro for doing everything in her abilities to reduce the stress incurred during this thesis by giving me her time, love and support.
- Wessel Croukamp who always greeted me with a smile before discussing the fabrication of waveguide related hardware in this project and always being available to give me guidance in the workshop.
- Wynand van Eeden for his assistance while manufacturing the PCB in this project.
- Jenny Martin who ordered all the components I required for this project.
- To all my peers and friends who helped me stay motivated.

Dedication

This thesis is dedicated to my mother and father who made it their mission to provide me with the best tools in the toolbox of life.

Table of Contents

Chapter 3 - Initial Investigation

Chapter 4 - Simulations and Applicator Design

Chapter 5 - Experimental System Overview

Chapter 6 - Hardware

Chapter 7 - Software

Chapter 8 - Control System Design

Chapter 9 - Microbial Experiments

Chapter 10 - Recommendations and Conclusions

List of Figures

List of Tables

List of Abbreviations

AC	Alternating Current
ADC	Analogue to Digital Converter
bps	Bits Per Second
CST	Computer Simulation Technology
dB	decibels
dBm	decibels relative to one milliwatt
DC	Direct Current
E. coli	Escherichia coli
E-field	Electromagnetic field
EHG	Electro Heating Group
EM	Electromagnetic
EMC	Electromagnetic Compatibility
EMI	Electromagnetic Interference
FAO	Food and Agriculture Organisation
GHz	Gigahertz
H-field	Magnetic field
IDE	Integrated Development Environment
IR	Infrared
ISM	Industrial, Scientific and Medical
ITU	International Telecommunication Union
kW	Kilowatt
MHz	Megahertz
ml	millilitre
mm	millimetre
ms	millisecond
NTC	Negative Temperature Coefficient
PC	Personal Computer
PCB	Printed Circuit Board
PEC	Perfect Electrical Conductor
PTFE	Polytetrafluoroethylene (or Teflon)
PWM	Pulse Width Modulation
RLC	Resistor, Inductor, Capacitor
s	seconds
SUWI	Stellenbosch University Water Institute
TE	Transverse Electric
TEM	Transverse Electromagnetic
TM	Transverse Magnetic
TM	Temperature Magnetron
TRIAC	Triode for Alternating Current
TT	Temperature Transformer
USB	Universal Serial Bus
V	Volts
VNA	Vector Network Analyser
W	Watts
WHO	World Health Organisation
WISA	Water Institute of Southern Africa

Chapter 1
Introduction

This document represents a study in support of previous projects which have been undertaken within the Electrical & Electronic Department of Stellenbosch University's Engineering Faculty's Electro Heating Group (EHG). It contains details of a project designed to sterilise liquid media using microwave energy.

1.1 Chapter Summary

This chapter looks at the previous works completed by the EHG under the supervision of Professor JB de Swardt. The objectives for this project are defined and an outline of the project development process is seen. A summary of each chapter in this document is also presented.

1.2 Background

The first published work of the EHG of interest is AE Oberholzer's "Development of a Continuous Flow Sterilisation System Using Microwaves" in 2016. This work showed the effective use of conventional microwave components and parts as far as possible. The system was tested in a laboratory environment which yielded successful results. The experimental system can be seen in Figure 1 below.

Figure 1 - AE Oberholzer's Final System [1]

The system focussed on liquid media and had a coiled pipe inside the multimode microwave cavity. This can be seen in Figure 2 a) below.

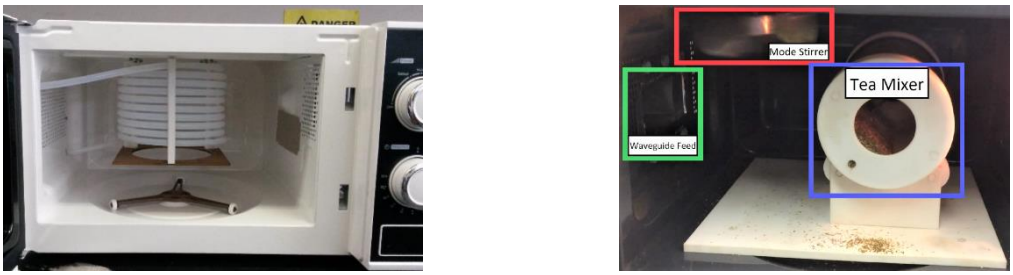

a) b)

Figure 2 - a) AE Oberholzer's Treatment Cavity [1] *b) JP van der Merwe's Treatment Cavity* [2]

The second pertinent published work of the EHG is JP van der Merwe's "Magnetron Output Power Controller Used in the Application of Rooibos Tea Sterilisation" in 2018. This work also shows the effective use of conventional microwave components as far as possible. Due to the nature of the

application, the inside of the microwave cavity was altered to hold and mix a dry media. This can be seen in Figure 2 b) above.

JP van der Merwe's system was tested with application specific criteria. It was found that although there was a reduction in microbial growth compared to the control, the system did not reduce the *E. coli* growth below the South African Rooibos standard [2]. This suggests that the system should be refined and re-tested with the aim of meeting the South African Rooibos standard. This goal provides a basis into the study of microwave sterilisation for dry media.

The published works both used the same Triode for Alternating Current (TRIAC) power control techniques to control the output power of the microwave magnetron. The nature of this technique leads to the use of two high voltage transformers which adds to the cost of the system when compared to the use of a single high voltage transformer seen in conventional microwave ovens. Both systems also use expensive circulators which are in place to protect the magnetron from reflected power. Both systems also made use of a generic microwave multimode cavity (conventional microwave oven) seen in Figure 1.

The published works of the EHG have future recommendations which highlight the downfalls of each system and served as a starting point for the design of the system presented in this document.

1.3 Objectives

The objectives of this project are therefore to:

- To develop a system capable of sterilising liquid to an industry standard.
- To develop a predictable system where insight can be gained through simulation.
- To have a continuous flow system as opposed to a batch system.
- To have a cost-effective design.
- To have a system of comparable/better efficiency seen from other conventional sterilisation techniques.
- To detect when a treatment sample is no longer present in the treatment chamber.
- To ensure the temperature is controlled.

1.4 Project Development

The work on this project was addressed in the following order:

- Short courses provided by Stellenbosch Electrical & Electronic Engineering department were attended. These included courses in Electromagnetics, EMC, Microwave Electronics and Methods of Moments. The courses were intended to give broader detail in the field of high frequency design. A course in Food Science was also taken to gain better understanding of industrial sterilisation techniques currently used in the food industry.

- A fully comprehensive safety analysis for the laboratory environment was conducted to ensure lab practices are carried out in a way which puts no individuals at risk. The lab is amply fitted with safety signage throughout. These notices clearly inform people of the dangers present. A risk assessment can be seen in Appendix B.

- The conventional microwave oven as well as the circuit diagram was studied to gain a good working understanding of how microwave ovens work.

- A simple proportional control system was created to control the heat of a lightbulb. This was done to get familiar with practical control systems as well as to understand the TRIAC switching capabilities used in previous projects.

- Experiments were conducted on conventional microwave ovens to further understand the problem of hot spots generated by standing waves inside a multimode cavity. Mode stirrers and turntables were also investigated.

- Initial microwave sterilisation tests were conducted with the Microbiology Department of Stellenbosch University. These experiments were carried out very early on in the project development cycle. This was done to get an understanding of microbiology practices and testing procedures which could influence the development of the system.

- Simulations investigating single mode structures were conducted. The simulations aimed to predict microwave interactions so that the design could be “tweaked” and made the best it could be. This led to quicker project development as no time was wasted fabricating and testing faulty structures.

- The chosen simulated structure was fabricated.

- Investigation into temperature sensors, liquid pumps and motor drivers was conducted and a printed circuit board (PCB) was designed and built for this hardware.

- Investigations into waveguide power sensing was conducted. This was necessary as the reflected power in the system could be harmful to the magnetron.

- Investigation into the processing and sending of data was done so that a microcontroller could be selected.

- A calibration procedure was designed for the system and implemented.

- A control strategy was chosen and designed and implemented in software.

- Final experimental system sterilisation tests were designed and conducted to determine if the experimental design would be successful.

- The experimental system was further refined to remove non-essential hardware to create a minimum viable product.

- Temperature sensors were attached to the magnetron as well as the high voltage transformer to determine the duration the system could operate for without over-heating or needing to be turned off.

- A presentation of this project was planned and conducted at the Stellenbosch University Water Institute/Water Institute of Southern Africa (SUWI/WISA) mini-symposium on the 17th of October 2019. This was done to gain industry specific exposure and criticism.

1.5 Thesis Format

1.5.1 Chapter 2 – Literature Study

The literature studies presented in this section define and give an understanding into the background of radiation and positions microwave radiation in the electromagnetic (EM) spectrum. The literature also explores and introduces microorganisms and how they react to sterilisation methods. Finally, the literature highlights the phenomenon of the non-thermal microwave specific effect.

1.5.2 Chapter 3 – Initial Experiments

The content in this chapter gives specific insight into some of the practical problems surrounding this project. Magnetron power control experiments were conducted and sterilisation in a multimode cavity performed. Furthermore, sterilisation in a single mode cavity was attempted, yielding valuable lessons.

1.5.3 Chapter 4 – Simulations and Applicator Design

This chapter aims to show the evidence available when making design decisions with regards to the applicator. Modal patterns are understood mathematically and confirmed with electromagnetic simulations. Thermal coupled electromagnetic simulations are then presented to show the different heating patterns created. Moving media simulations are mentioned and a rigorous applicator design is presented.

1.5.4 Chapter 5 – Experimental System Overview

This chapter aims to illustrate all the different aspects of the project and how they relate to each other. The block diagram images specifically show the experimental system designed for this project relating to hardware, software and their interactions.

1.5.5 Chapter 6 – Hardware

This chapter shows the design decisions undertaken in this project with regards to: Microwave waveguide structures, media transport, power supplies and electronic hardware. The hardware in this section was designed in a modular fashion. This meant that further revision and optimisation of a specific area would be possible without disrupting the entire hardware system.

1.5.6 Chapter 7 – Software

This chapter shows the calibration steps taken to ensure accurate results were obtained from the system. The calibration includes the microprocessor's analogue to digital converter (ADC), temperature sensors and software timing information. The chapter further discusses how data is packaged, sent and received and shows software flow diagrams. The chapter ends by highlighting various software packages used during the duration of this project.

1.5.7 Chapter 8 – Control System Design

This chapter starts off with a short literature study regarding control theory. The control system for this project was then designed and begins by identifying and deriving a mathematical model for the system. The control system specifications are stated. The designed control system was simulated and altered to meet the system requirements. Finally, the control system was implemented in a live test.

1.5.8 Chapter 9 – Microbial Experiments

This chapter gives details of the methods used to prepare the media which was tested in the continuous flow system designed for this project. A step by step experimental checklist is presented

which shows the apparatus used. The temperature responses for the treated media analysed and comments are made with regards to the control system designed.

1.5.9 Chapter 10 – Recommendations & Conclusions

This chapter discusses and highlights potential recommendations for further improvements to the system designed in this project. The chapter then draws conclusions relating to the overall system objectives outlined in chapter 1.

Chapter 2
Literature Study

2.1 Chapter Summary

The literature studies presented in this section define and give insight into the different types of radiation and positions microwave radiation in the electromagnetic (EM) spectrum. Microwave radiation is discussed in further detail because of its useful properties when interacting with certain substances. The study further explains how to generate microwave radiation with the use of a magnetron and discusses various techniques used to control the output power of the magnetron.

The chapter also explores the different types of microorganisms and shows typical growth characteristics as well as discusses how to kill microorganisms. Sterilisation methods are discussed, and sterilisation standards are outlined.

Finally, the literature ends by highlighting the phenomenon of the non-thermal microwave specific effect and evidence for this is presented.

2.2 Background to Radiation

Radiation is the broad term given to energy which travels as a particle or as a wave [3][4].

2.2.1 Types of Radiation

Particle radiation consists of atomic matter which has both energy and mass [5]. Atoms are made up of protons, neutrons and electrons. Protons and neutrons make up the atom's nucleus and are positively charged. Orbiting the nucleus are negatively charged electrons [6]. These are illustrated in Figure 3.

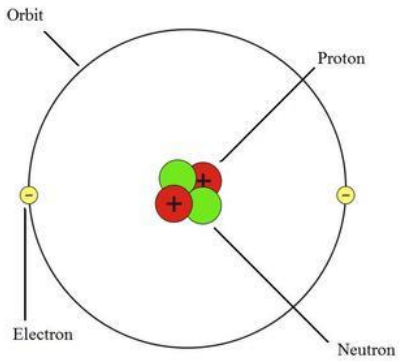

Figure 3 - Atom Diagram [7]

2.2.1.1 Particle Radiation

Particle radiation can interact with other atoms with enough energy to remove electrons from another atoms' orbit. This violent chemical change can damage living tissue. Radiation of this nature is referred to as ionising radiation [8].

2.2.1.2 Wave Radiation

Wave radiation consists only of energy and has no weight [5]. These waves are characterised by frequency. The energy associated with the radiation is directly proportional to the frequency of the wave, this can be seen in the equation below:

$$\mathrm{E} = hf\ , \tag{1}$$

where E is energy, h is Planck's constant and f is frequency [9]. Wave radiation is created when an atomic particle is forced to accelerate by an induced electric field. The nature of this movement creates an oscillating electric and magnetic field which travels at right angles to one another [10]. This is illustrated in Figure 4.

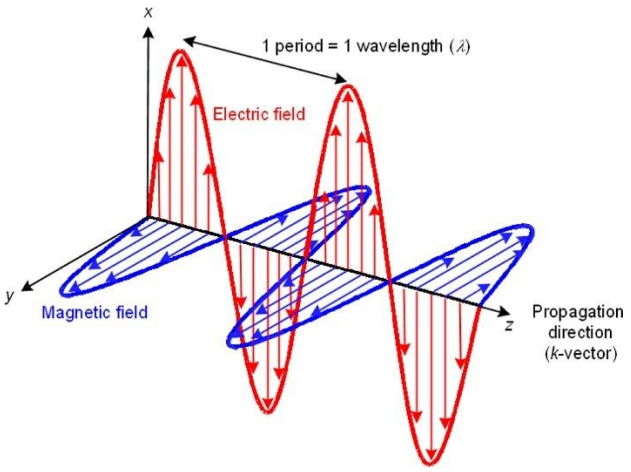

Figure 4 – Graphical Representation of Oscillating Electric and Magnetic Waves [11, p. 2]

2.2.2 The EM Spectrum

The EM spectrum refers to categorising electromagnetic energy in relation to two extreme points. These points are characterised by wavelength and frequency. Figure 5 shows that the spectrum extends from very low frequency waves ($< 50\mathrm{Hz}$) through to high frequency Gamma Rays ($> 10^{19}\mathrm{Hz}$).

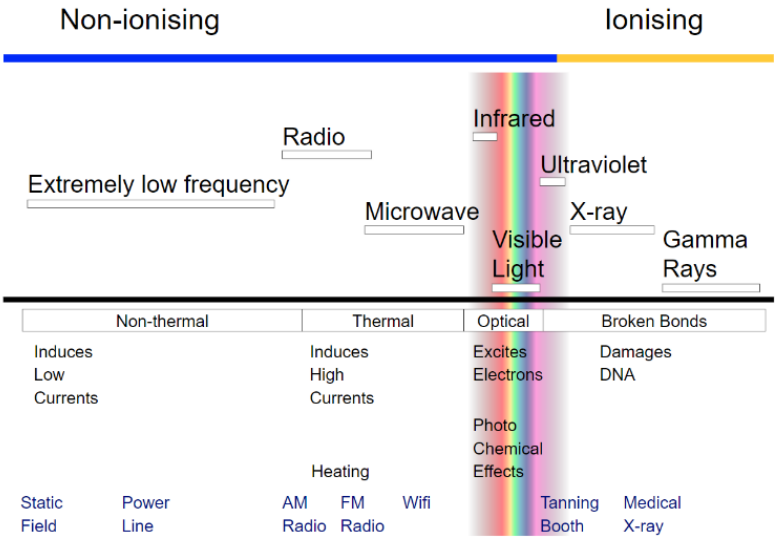

Figure 5 – The Electromagnetic Spectrum [12]

2.3 Microwave Radiation

The microwave region exists in between the infrared and radio wave regions of the EM spectrum. This region is roughly defined between $1\ \mathrm{GHz}$ and $300\ \mathrm{GHz}$ [13]. Magnetron tubes are commonly used in the generation of EM radiation. These tubes were initially used by the military for close-range radar applications. After the Second World War, magnetron manufacturers desperately looked for alternative peacetime applications for microwave energy. By this stage it was common knowledge that radio waves could heat certain materials and this potential had been demonstrated before the war at the Chicago World's Fair in 1933 [14]. Ultimately, attempts to find a new market for magnetron tubes led to a patent being filed in 1946 by Percy Spencer who described the ability to heat food with microwave radiation [14][15].

2.3.1 Microwave Generation

The magnetron is comprised of several key components placed together in specific orientations to generate oscillating EM fields. Figure 6 shows a labelled diagram of a common magnetron typically found today in commercial microwave ovens.

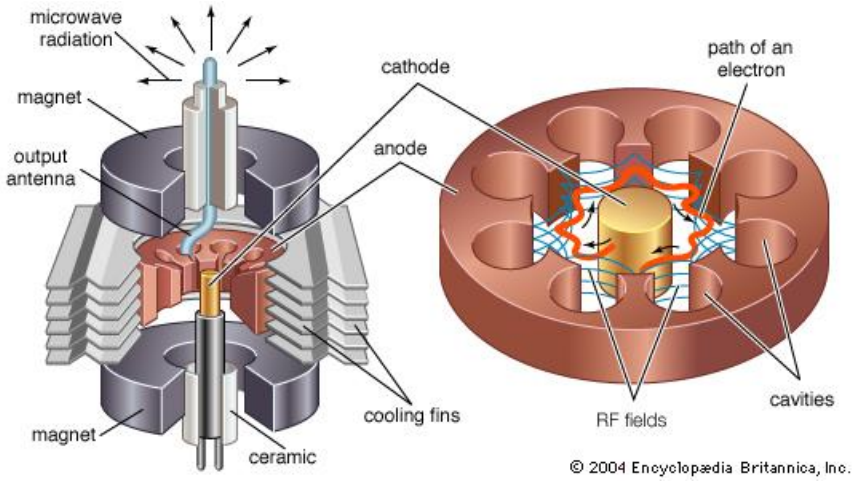

Figure 6 – Magnetron Diagram [16]

At the heart of the magnetron exists a copper rod known as the cathode (negative charge). This copper rod is suspended in a vacuum enclosed by a copper ring known as the anode (positive charge). Together, the cathode and the anode create an electric ($\mathbf{E}$)-field. The cathode has a filament made from a material which has a high electron emission when heated. An example of a material with this characteristic is thoriated tungsten which begins releasing free electrons when heated to $2400\ ^{\circ}\mathrm{C}$ [17]. The filament is heated when the magnetron turns on by applying a potential difference across the filament [18].

The free electrons have enough energy to move easily within the $\mathbf{E}$-field as they are attracted to the anode. At this stage the free electrons can be visualised as a cloud of electrons which are randomly placed within the vacuum tube. This can be seen in the first image depicted in Figure 7.

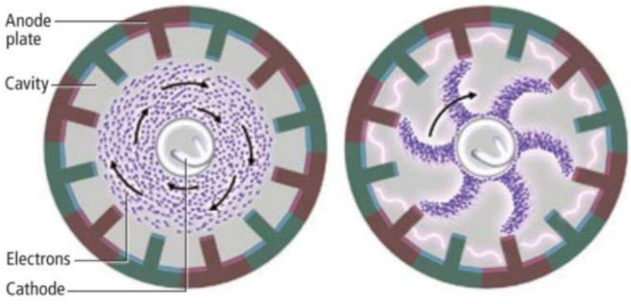

Figure 7 – Electron Interactions Inside Magnetron Tube [19]

The vacuum tube is then suspended between two strong permanent magnets. This subsequently means that the cloud of free electrons is now inside a magnetic ($\mathbf{H}$)-field. The $\mathbf{H}$-field interacts with the accelerating electrons and causes them to spiral as they leave and return to the filament. The force experienced by the electrons is called Lorentz force [20]. This spiral creates a space-charge pinwheel which rotates around the cathode. This can be seen in the second image depicted in Figure 7.

The tips of the pinwheel interact precisely with the walls of the cut grooves on the inside of the anode's copper ring. This can be seen in Figure 8 as each wall of a single groove will be made slightly more negative than the consecutive wall which is furthest away from the tip of the pinwheel. This effect creates an oscillating EM wave [17][18][21] and is known as the π-mode of operation [2].

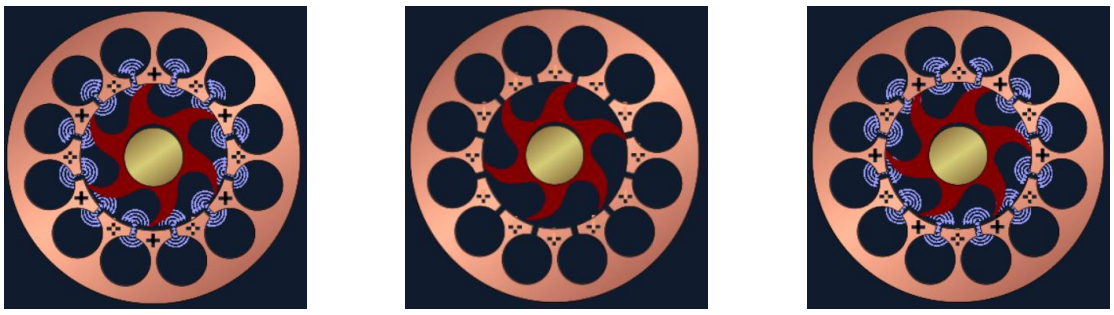

a) b) c)

Figure 8 – a) Positive Cycle b) Neutral Cycle c) Negative Cycle [18]

Lastly, an antenna is placed within the cavities created by the shape of the anode. This allows the oscillating EM wave to get coupled out of the magnetron vacuum tube [21]. The microwave energy is now in a useable form.

2.3.2 Microwave Power Control

Commercial microwave oven magnetrons reach their π-mode of operation when there is a potential difference between the anode and cathode which exceeds $3500\ \mathrm{V}$ [2].

With the fundamental understanding of the inner workings of the magnetron obtained by section 2.3.1, if the $\mathbf{E}$ or $\mathbf{H}$-field can be controlled then the π-mode of operation of the magnetron can be controlled. Alternatively, if the temperature of the filament is controlled, then the density of the electron cloud circulating the cathode can be controlled. Figure 9 shows the circuitry for a conventional microwave oven magnetron.

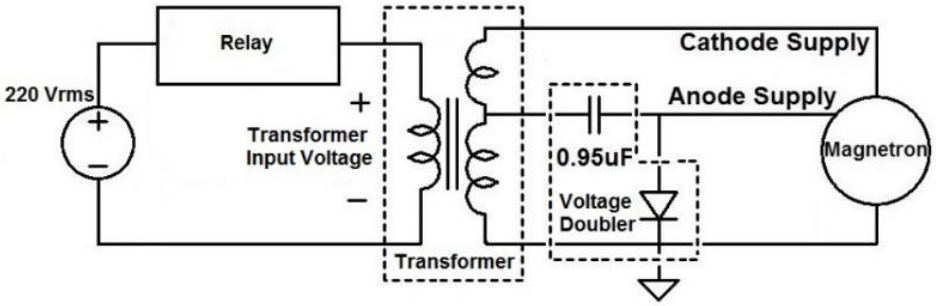

Figure 9 – Conventional Magnetron Power Supply [2]

Methods used to control the **E**-field involve controlling the main supply voltage. This can be done in several ways:

2.3.2.1 Duty Cycle Control

This method aims to control the average anode current within the magnetron. This type of control is achieved by turning the magnetron "on" (at full power) for a period of time followed by a period of time where the magnetron is completely "off" (zero power). Although this type of control is very simple and effective, it may not be applicable for sterilisation purposes as the media can rapidly cool in the "off" cycles and thus not fully sterilise the media [2][22]. This means that particular care must be taken to ensure that the media is kept at the target temperature to ensure sterilisation.

2.3.2.2 Variable Transformer Control

This method physically lowers and increases the peak voltage at the output of the high voltage transformer. This type of control method is linear and may be adjusted accurately. The problem with this method is that a mechanical system is required to change the winding ratio of the transformer. This introduces mechanical wear and tear on the system and may also prove too slow for digital control [2][22].

2.3.2.3 TRIAC Control

This method aims to alter the shape of the incoming mains sinusoidal signal. This method has an advantage over the normal duty cycle control method as the "off" periods are spread out through each half cycle of the signal. The disadvantage of this type of control is that it relies heavily on external circuitry such as zero crossing detection circuitry which is used to synchronise the TRIAC switching with that of the supply signal [2].

This method, however, can introduce unwanted higher order harmonics into the system which could cause inefficiency as well as lower component life spans [2].

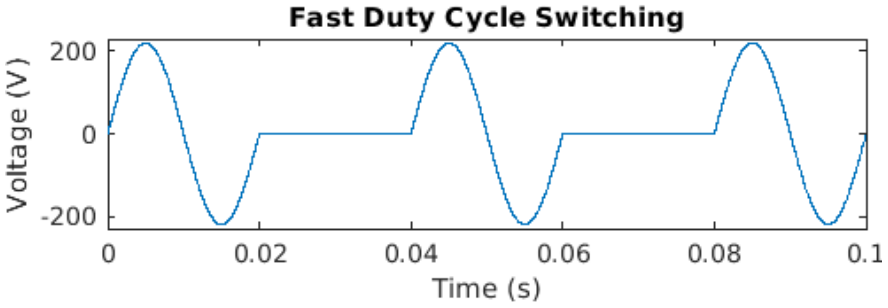

a)

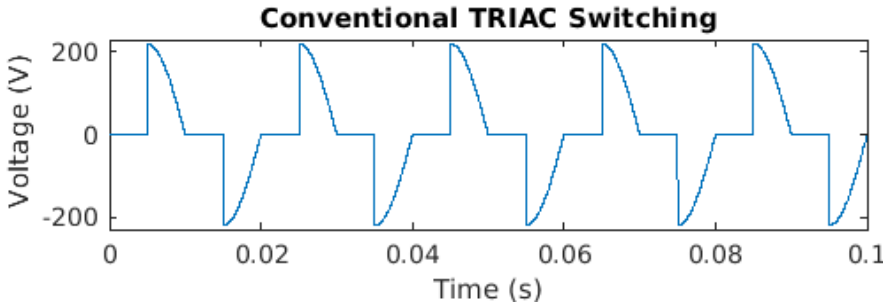

b)

Figure 10 - a) Duty Cycle Control Waveform b) TRIAC Control Waveform

Figure 10 graphically illustrates the difference in wave shape between the duty cycle control wave form and the TRIAC control waveform.

2.3.2.4 Inverter Power Supply Control

This type of power supply thrives by being able to switch at higher frequencies. These power supplies are much smaller than conventional microwave power supplies and can be accurately controlled. The control technique implemented with these power supplies is similar to that of the duty cycle control method, with the added benefit that the "on" and "off" cycles can be a lot closer together. This method, however, does not make use of conventional microwave oven parts [2][23]. This type of power supply is currently being introduced to commercial microwave ovens and works by taking the main alternating current (AC) supply and converting it to a direct current (DC) signal for the magnetron tube [24].

2.3.2.5 Variable Electromagnet Control

This technique aims to alter the $\mathbf{H}$-field created by the strong permanent magnets within the magnetron. This method of control is very expensive because strong electromagnets are required and must be installed in an orientation which opposes the permanent magnets. These electromagnets also need to be powered by an external power supply [2][22].

2.3.2.6 Saturable Reactor Control

This method aims to control the output power by controlling the anode current of the magnetron. This method is commonly used in lower power magnetron applications [22].

The premise that this control uses is based on the fact that voltage-current relationships are non-linear when transformer core saturation is achieved [25]. A series resonant circuit can be derived from Figure 9. The transformer can be modelled as an ideal transformer with a series inductor (L). Similarly, there exists some form of series resistance (R) and the circuit is completed with the high voltage capacitor (C). The equivalent resistor, inductor, capacitor (RLC) circuit is shown in Figure 11 below.

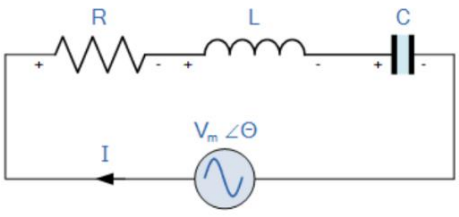

Figure 11 - RLC Equivalent Circuit [26]

To understand how this circuit can be characterised in order to control output power, the total impedance (Z_{TOT}) needs to be considered [26]:

$$Z_{TOT} = \sqrt{R^2 + X_{TOT}^2}\,, \tag{2}$$

where

$$X_{TOT} = |X_L - X_C|\,, \tag{3}$$

and

$$X_L = \omega L\,, \tag{4}$$

$$X_C = -\frac{1}{\omega C}, \tag{5}$$

where:

$$\omega = 2\pi f. \tag{6}$$

Figure 12 below shows how the capacitive and inductive elements change their impedance with respect to frequency. Figure 13 to the right of Figure 12 shows how the value $|Z_{TOT}|$ changes with respect to frequency.

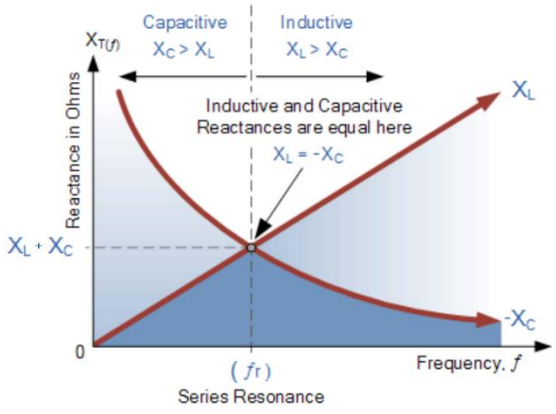

Figure 12 - Capacitive and Inductive Impedance Versus Frequency [26]

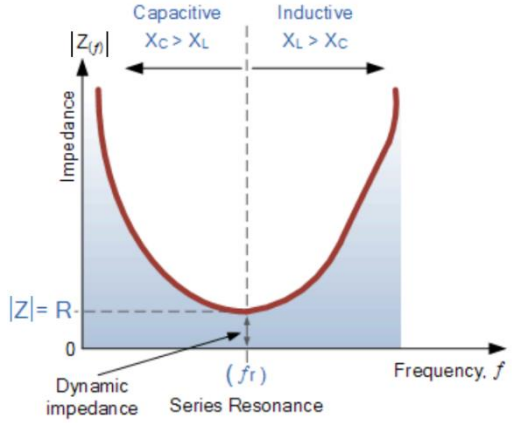

Figure 13 - Capacitive and Inductive Impedance Combined Versus Frequency [26]

Figure 13 shows that $|Z_{TOT}|$ is at a minimum value when $X_L = X_C$. The frequency at this point is known as the resonant frequency (f_r) and can be derived to have the following relationship within the resonant circuit as:

$$f_r = \frac{1}{2\pi\sqrt{LC}} \tag{7}$$

It can be seen from Figure 14 that at the resonant frequency, the circuit current is at a maximum. This subsequently also means that the circuit can operate at maximum power.

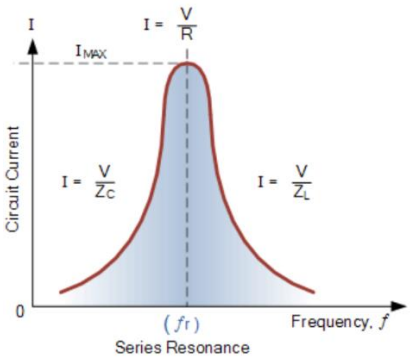

Figure 14 - Current vs Resonant Frequency [26]

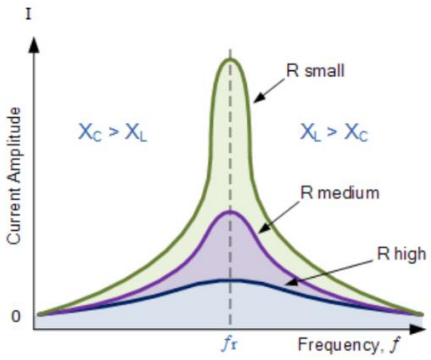

Figure 15 - Current vs Resonant Frequency (The effect of R) [26]

Figure 15 shows the effect of the series resistance and that it is desirable to keep the value of R as small as possible to yield the greatest output current and power.

The resonant frequency in commercial domestic microwave ovens is usually designed to be 15% higher than that of the incoming supply frequency [22]. This means that the circuit is operating slightly below full power and the resonant circuit is more capacitive.

To use this theory in a live control system would require the ability to control the saturation of the reactor core. This can be done by a means of DC winding around the reactor core which is orthogonal to the AC winding. The effect of this configuration means that if a variable current flows through the DC winding it will send the reactor core into different stages of saturation thus allowing the power to be controlled variably [25]. This theory can also be used as a fixed power limitation if particular care is taken when choosing the values in the RLC circuit.

To create a fixed power limiter, Equation 7 on the previous page, illustrates that if the capacitance value is made smaller, the resonant frequency will rise and subsequently results in a decrease in the circuit current and overall circuit power. Evidence of this can be seen in Figure 16 a) and b).

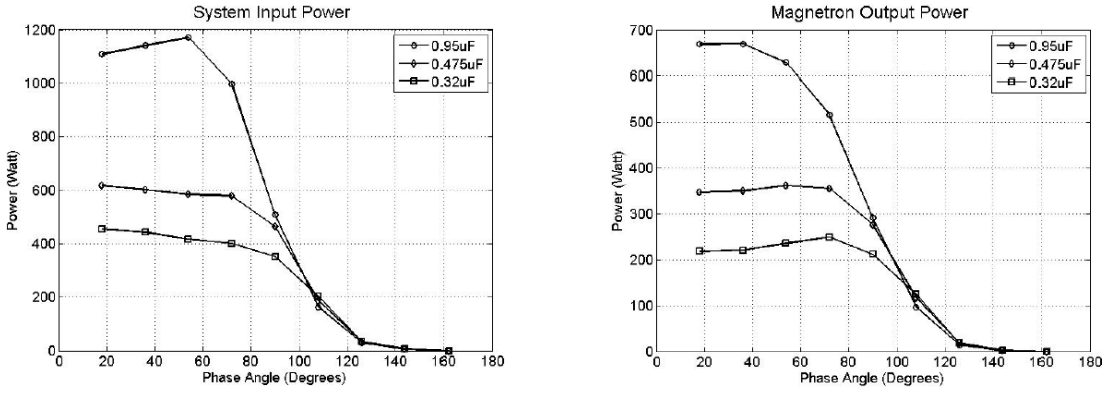

a) b)

Figure 16 - a) System Input Power, b) Magnetron Output Power [20][22]

Note that the "Phase Angle (Degrees)", seen on the x-axis of Figure 16, relates to the firing angle of a TRIAC as the magnetron used in [2][23] was further controlled in this manner.

2.3.3 Microwave Heating

The Industrial, Scientific and Medical (ISM) frequency bands are pre-determined frequency ranges defined by the International Telecommunications Union (ITU). These frequency bands are set aside for radio frequency uses other than telecommunications [27].

Microwave heating is commonly around the $2.45\,GHz$ ISM band. This band, however, also accommodates induction heating and various other communications methods such as WiFi and Bluetooth [27].

2.3.3.1 Polarisation Theory

Microwave heating is a by-product of how microwaves interact with a dielectric medium. The applied electric field across this dielectric medium causes the electrons surrounding the nucleus of an atom to disperse within the atom in such a way as to give the atom positive and negative edges opposite each other. This effect is called polarisation and the displacement is called the "dipole moment" of the atom [2]. This can be seen in Figure 17 below.

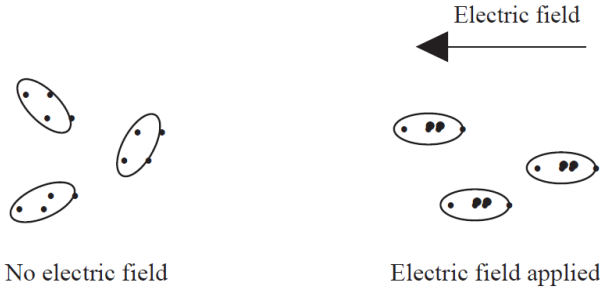

Figure 17 – Orientation of Polarised Molecules in an Electric Field [28]

Since the magnetron is producing an oscillating EM wave, the atomic particles are subsequently always trying to align themselves with the changing electric field [29]. This means that the atoms are physically rotating back and forth in the presence of the electric field. The act of the motion described overcomes frictional forces on an atomic level, which has the by-product of heat [28].

2.3.3.2 Advantages and Disadvantages of Microwave Heating

Microwave heating has multiple proven benefits over other conventional heating systems [2]. These benefits include steep temperature gradients which result in rapid heating [2]. Rapid heating often means that treatment times are shortened [2][28]. The shorter treatment times of microwave heating have several advantages for the food processing industry. These benefits include better product taste, texture and leaves the product with more nutrients when compared to other conventional heating types [2].

Microwave heating has the benefit of selectively heating what is inside the treatment chamber. This is because the microwave radiation specifically polarises the water molecules present. This means that the actual media rises in temperature whilst the container itself is not directly heated by the microwave treatment [2][28]. Microwave heating can also evenly heat any shape of medium provided that the depth of the medium is smaller than that of the penetration depth of the microwaves [2][28]. These key advantages further result in a higher heating efficiency (80% and higher) and can be precisely controlled [28]. Lastly, microwave heating has the benefit of being silent and does not directly produce a waste product or exhaust gas [28].

Microwave heating has a few undesirable characteristics. These include the fact that un-even heating will be achieved if standing waves are present inside the treatment chamber. Secondly, "edge over-heating" can occur where objects with sharp edges get hotter than the bulk material because superposition of the waves happens at the edges of the material [2]. Thirdly, electrical discharge can easily occur if conductive materials are placed inside the treatment chamber [28]. Lastly, leakage microwave radiation is harmful to living organisms. This means that a faulty system has the potential to put human beings at risk [2].

2.3.3.3 Factors Influencing Microwave Heating

2.3.3.3.1 Dielectric Properties

The ability for a material to absorb microwave energy is directly proportional to the amount of penetration the microwaves can achieve through a material. Some materials are transparent to microwave energy and some materials are reflective to microwave energy. To determine whether a material is transparent to microwaves or not, it is often helpful to look at the dissipation factor which is defined by Equation 8 below [30]:

$$tan\delta = \frac{\varepsilon''}{\varepsilon'}, \tag{8}$$

where ε' is the dielectric constant which is determined by the ability for a material to be polarised by an external **E**-field and subsequently hold energy within the material [30].The variable ε'' is the dielectric loss factor which is determined by the ability for a material to release the absorbed energy as heat [30].

Large values of $tan\delta$ mean that the material is very absorptive to microwave energy, which means materials with this property will heat up [30]. Small values of $tan\delta$ mean that the material is transparent to microwave energy, which means materials with this property do not heat up. Materials with these properties are best suited when used as the containers for the item that is to be treated by microwave energy [30].

2.3.3.3.2 Moisture

Liquid water is strongly polar. This means that it can absorb microwave energy easily. *When liquid water* is mixed with other materials, it is then called *absorbed water*. The dielectric properties of *liquid water* and *absorbed water* are very different. The maximum heating capacity for *liquid water* occurs at $18\ \mathrm{GHz}$ whereas the maximum heating capacity for *absorbed water* can occur well below that [22].

Absorbed water exists in two states. The first state is called *free water,* which is found in capillaries and cavities (free space). *Free water* has a much higher dielectric constant as the water molecules are free to rotate. The second state is called *bound water*, which has a lower dielectric constant as the molecules are less rotationally free [22].

2.3.3.3.3 Volume

The volume or mass of a material is directly proportional to the amount of microwave power which can be absorbed. There also exists a minimum volume which should be present in the treatment chamber. This volume will absorb microwave energy and means less power will be reflected. Reflected power can damage the magnetron. The general rule of thumb for adequate absorption is $250\ \mathrm{ml}$ of water for every $1\ \mathrm{kW}$ of microwave power [31].

2.3.3.3.4 Geometry and Location

The shape of the material can have a significant effect on the effective absorption of microwave power. If the material has non-uniform thickness, then it will lead to non-uniform heating. For the greatest heating profile, the surface area to volume relationship needs to be maximised [31].

2.4 Microorganisms

Microorganisms account for a large majority of the Earth's living matter and play a key role in its ecosystem [32]. There are seven categories into which these microorganisms can be divided. They are: fungi, algae, viruses, protozoa, archaea, multicellular parasites and bacteria. Although most of these organisms live in symbiosis with their environment and respective hosts (e.g. plants and

humans), some of them can be pathogenic. Cell structures of microorganisms can be described as unicellular, multicellular or as cell clusters [32].

2.4.1 Types of Microorganisms

The types of microorganisms which are usually associated with food spoilage are fungi, bacteria, bacteriophage (a type of virus) and protozoa [31]. These microorganisms will be looked at in more detail throughout this section.

2.4.1.1 Protozoa

Protozoa are unicellular microorganisms which account for the majority of microorganisms in the world based on numbers, biomass and diversity [32]. They are categorised into four main subsections and are defined by the way in which they move. The first being *flagellates* which have a whip-like structure. The second being *ciliates,* which have small pulsing hair-like structures. The third is *amoeboid,* which have temporary protrusions from the surface of the structure which they use for movement. The fourth is *sporozoans*, and do not move by their own means. Protozoa cells have a nucleus and their cell wall is made from cellulose [32].

2.4.1.2 Bacteria

Bacteria are unicellular microorganisms described as *prokaryotic* cells which means that they do not have a nucleus surrounded by cell membranes [32]. These cells reproduce by a means of binary fission (microbial count doubles every reproductive cycle) [2]. Most bacteria have a *peptidoglycan* cell wall structures [32] which means that they contains *glycosaminoglycan* chains with short peptides [33].

2.4.1.3 Fungi and Fungal Spores

Fungi are mostly multicellular microorganisms which absorb organic material from their surroundings. They are called *eukaryotic* cells, which means they have a nucleus surrounded by cell membranes [32]. The cell walls are comprised of chitin and they reproduce by a means of unicellular spores [34].

2.4.1.4 Bacteriophage (Virus)

Bacteriophages are a type of virus which infect bacteria [31]. Viruses are non-cellular and simply consist of DNA surrounded by protein. These microorganisms are not technically “living” as they require a host (bacteria in this case) in order to survive [32]. Viruses tend to infect *prokaryotic* and *eukaryotic* cells [32].

2.4.2 Bacterial Growth Characteristics

Binary fission, discussed in section 2.4.1.2, can occur as regularly as every twenty minutes, or as long as eighteen hours. These times depend on what type of bacteria is being considered and the environment in which the bacteria is trying to live [2].

The general growth characteristics for bacteria observed in a closed environment [1] are displayed in Figure 18 below and consist of four main stages.

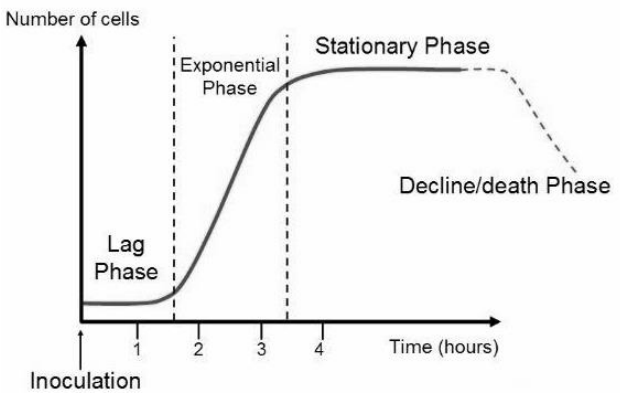

Figure 18 - Bacterial Growth Curve [35]

The Lag Phase occurs because the bacteria needs to adapt to its new environment and to source nutrients [2].

The Exponential Phase occurs once the bacteria have acclimatised to the new environment and have the required nutrients to start metabolic processes for binary fission. The constant logarithmic increase in cells is called the "generation time" [1]. This is the growth phase where most bacterial research is carried out [2].

The Stationary Phase occurs because there is a depletion of nutrients and limited space for further bacterial growth. It cannot be determined whether or not the growth rate at this point is equal to the death rate, or if no new growth occurs at all at this stage [1].

The Death Phase occurs because the nutrients in the environment have been fully depleted and the bacteria are seen to die at the same constant generation time seen in the exponential phase [1][2].

2.4.3 Understanding How to Kill Bacteria

The bacterial cell consists of multiple different parts which all contribute to a healthy life span for each cell. The cell structure of a typical bacterium is shown in Figure 19 below. The cell wall, cytoplasmic membrane, nucleoid and ribosome will be focussed on.

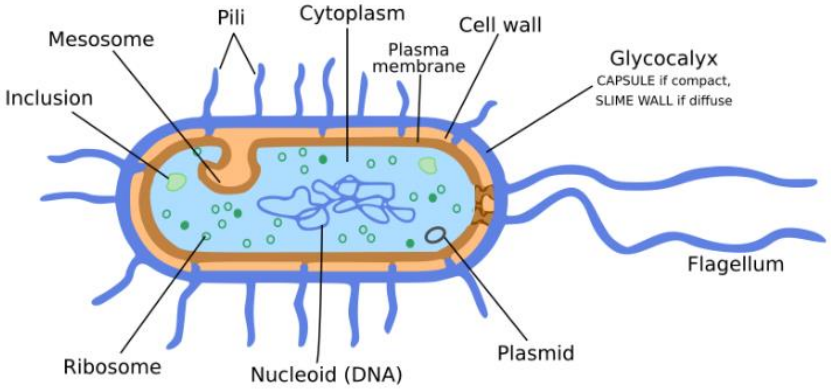

Figure 19 - Bacterial Cell Diagram

2.4.3.1 Cell Wall

The cell wall is responsible for giving the cell and all its contents strength to hold their shape. The material that makes up the cell wall is discussed in the section above and in simple terms, consists of protein-sugar molecules. Without the cell wall, the cell would burst when differences in osmotic pressures occur between the cytoplasm and the environment [36].

There are two basic types of bacterial cell wall structures. These are called Gram-positive and Gram-negative. Gram-negative cell structures have an extra outer membrane. This outer membrane is made from complex lipopolysaccharides that help the bacteria become more resistant to external substances in their environment, such as antibiotics [37]. Figure 20 illustrates the differences between Gram-positive and Gram-negative.

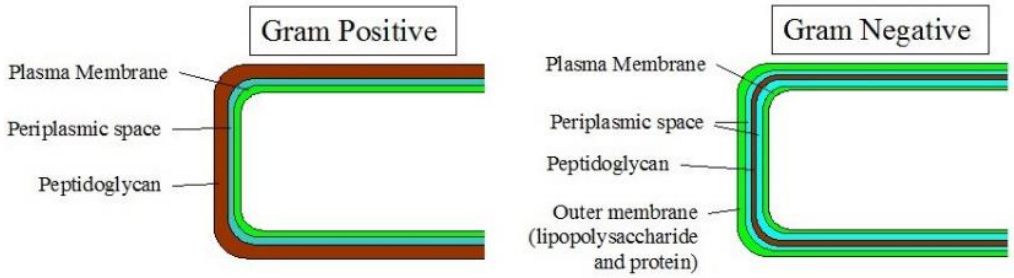

Figure 20 - Gram Positive vs Gram Negative [37]

The difference in cell wall structure means that cells will react differently to changes in the environment [1].

2.4.3.2 Cytoplasmic Membrane

The cytoplasmic membrane occurs in other living cells and is composed of phospholipids and proteins. The membrane facilitates and regulates the flow of material in and out of the cell. This membrane has the ability to adapt to the environment [36].

2.4.3.3 Nucleoid

The nucleoid is the region in the cytoplasm where chromosomal DNA is found. This is essential for cell reproduction [36].

2.4.3.4 Ribosome

Ribosomes are found in all cells. Their job is to take genetic code from nucleic acid in the DNA and to transform it to proteins. This happens through the process of transcription (DNA to messenger RNA) and translation (decoding of mRNA sequence to chains of polypeptides and proteins). Protein molecules are essential in most functions required by a cell to live [36].

2.4.3.5 Protein Structure

It is known that a cell will collapse and die above certain threshold temperatures. The simplest answer to why this occurs is that proteins are paramount to life [38]. Biophysicist, Professor Paola Picotti, conducted a series of experiments to determine the differences in protein stability and how that relates to the life of a cell [38].

To understand how proteins can become unstable, one must first understand how proteins are made. The proper conformation of a protein refers to a protein's 3-dimensional folded structure. Conformational stability refers to the various forces which keep a protein in its correct 3-dimensional shape [39][40].

There are four key levels of protein structure. The primary level consists of amino acids bonded together via peptide bonds. Multiples of these bonds form a linear sequence of polypeptide bonds [40].

The secondary level of protein structure refers to how the linear sequence folds up on itself and stabilises with hydrogen bonds. This can take the form of a coil called an alpha-helix or it could take

the form of a beta-sheet which can have parallel or anti-parallel polypeptides bonded together. This level is referred to as backbone interactions [40].

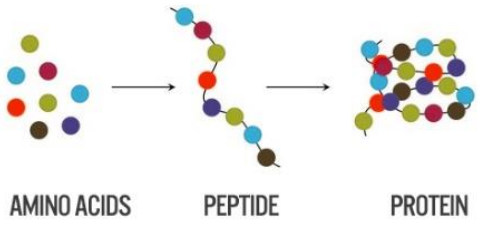

Figure 21 - How Protein is Formed [41]

The tertiary level of protein structure refers to a higher order of folding which is also stabilised with hydrogen bonds, along with Van der Waals interaction, hydrophobic packing and disulfide bonding. This level is referred to as distant group interactions [40].

The quaternary level of protein structure describes how individual protein sub-units interact with each other to create proper conformation of a protein. These interactions are stabilised in the same manner as the tertiary level [40]. Figure 21 above shows a basic understanding of what this might look like.

If any of the levels described above are disrupted, the protein will lose its shape and not function properly [39].

A fifth level which also aids in keeping proteins in their correct shape exists in the solution shell [39]. This concept is illustrated in Figure 22 below whereby a protein molecule inside a cell will be surrounded by a watery environment. The protein amino acids have a net positive charge and the water molecules surrounding them are polar. This means that the water molecules can orientate themselves in a way that stabilises the positively charged protein [39]. The red circles in the diagram show the positive negative coupling effect.

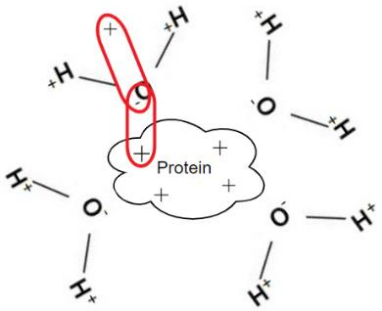

Figure 22 - Protein Interactions with Solution Shell

Picotti found that one of the clearest observations showed that not all the proteins unfolded with an increase in temperature. Picotti further stated that only a small sub-set of key proteins all collapsed very early. These proteins are essential to the life of the cell and without them, the cell will inevitably die [38].

Picotti also observed that heat resistant cells, which start to die around $90\ °C$, had protein structures that were very short when compared to that of *Escherichia coli* (*E. coli),* which starts to die around $40\ °C$ [38].

2.5 Sterilisation

Sterilisation is the process of removing or destroying all living microorganisms. This means that complete sterilisation will destroy yeasts, moulds, spores and bacteria [31]. This definition of sterilisation, however, may not actually be desirable in the food processing industry as not all microorganisms are harmful to humans. From this, it can be said that the key principle regarding sterilisation in the food industry is to ensure that the treated product is free from microorganisms which can cause food-poisoning in consumers or which can spoil the product before consumption [31].

2.5.1 Sterilisation Methods

Sterilisation can be achieved by various ways depending how the material to be treated reacts to the different methods. Some of the key methods used in sterilisation include heat treatment, filtration and sterilisation via chemicals.

2.5.1.1 Heat

Heat sterilisation is the most common form of sterilisation. There are multiple different ways in which a treatment sample can be heated. In broad terms, heat can be categorised as *wet heat* and *dry heat* [1].

Wet heat includes boiling and steaming [1]. Some boiling chambers such as a retort are used for in-package sterilisation [42] and some steaming chambers are called autoclaves. Autoclaves are commonly used to sterilise lab equipment [1].

Dry heat includes flaming, incineration, dry air ovens and radiation. Flaming and incineration are processes by which microorganisms are exposed to open flames to physically burn. Dry air ovens are sealed containers which circulate hot air for a desired amount of time at a specific temperature. Radiation treatments can be non-ionising (Microwave treatment) or ionising (X-rays and Gamma-ray treatments) [1].

2.5.1.2 Chemical

Chemical sterilisation techniques have a couple of desirable advantages over other sterilisation techniques. These include the ability for chemicals to kill heat-resistant organisms and can do so at low temperatures. This process, however, can take a long time and particular care must be taken to ensure that the chemical is able to contact the treatment sample completely. Another disadvantage is that some of the chemicals used are harmful to humans and thus strict safety procedures must be followed [1].

Ethanol can be used to sterilise tools and lab equipment as well as sterilise growth media from the lab so that it can be discarded safely [1]. Ethanol works by denaturing proteins. This is consistent with observations that the ethanol destroys the dehydrogenases of *E. coli. E. coli* can be destroyed in 10 seconds by a concentration of ethanol of $40\% - 100\%$. Furthermore, concentrations of ethanol between $60\% - 100\%$ are deadly to viruses like influenza and human immunodeficiency virus (HIV) [43].

Ethanol is not recommended for medical/surgical use alone. This is because ethanol does not kill spores and has difficulty penetrating protein rich materials [43].

2.5.1.3 Filtration

Filtration can prove to be a very successful mode of sterilisation with the benefit of being able to sterilise heat-sensitive materials. This is done with special bacterial filters, where the pore size is smaller than a single bacterial cell. This process can be extremely slow, especially when the filter

becomes blocked. Filtration of this type could be very costly and particular care must be taken to ensure no contamination occurs when filters are changed as this is when ruptures or leaks could occur at the seams [1].

2.5.2 Sterilisation in the Laboratory

The validity of all microbial growth experiments relies heavily on the ability to start experiments with as clean and sterile environment as possible. This not only means starting with a sterile environment but maintaining a sterile environment throughout the test. Lastly, it is important to leave the environment sterile once the experiment has been completed. This can be achieved by ensuring that all equipment used is autoclaved, keeping the air around the experimental set-up sterile and using uncontaminated media [44].

2.5.2.1 Autoclave Equipment

This is an application of wet heat as discussed in section 2.5.1. The reason this is done is to create sterile working equipment with the aim of not cross-contaminating or introducing microorganisms which are not part of the testing set-up [30][33].

All waste microbial material should be sterilised before being discarded. This is commonly done in the laboratory autoclave [44].

2.5.2.2 Laminar Flow Cabinet

Laminar flow describes the movement of a liquid or a gas which travels smoothly. This means that the individual particles do not really mix as everything travels in regular paths [45]. Figure 23 below shows how air flows through this cabinet.

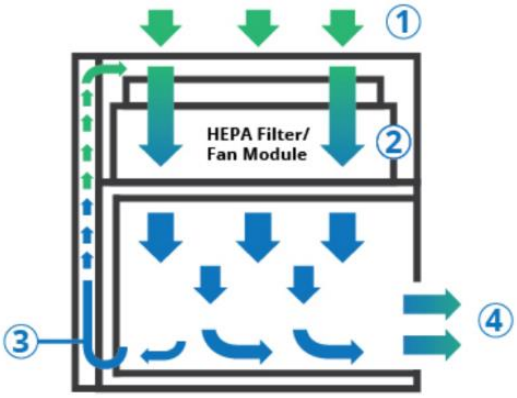

Figure 23 - Laminar Flow Cabinet Diagram (Side View) [46]

Position 1 in Figure 23 accepts external air which is then pushed through a filter at position 2 creating a steady downward laminar air flow. Position 3 allows some of the clean air to be recirculated (in a bid to extend the filters life expectancy). This is done by a process called “back plenum”. Position 4 has a steady stream of filtered air exiting the cabinet. This laminar flow doesn’t allow external unfiltered air to enter at position 4 [46]. Furthermore, the cabinet is sterilised before use with ultra violet (UV) light [1].

2.5.2.3 Ethanol

A 70% solution of ethanol should be used to wipe down all surfaces that are going to be used in the experiment. Once the surface has been wiped, it should be left to “air dry” and not be “wiped dry”. This will ensure that all microorganisms on the surface are destroyed [44]. Ethanol can also be sprayed on anything before it is placed in the sterile workspace, even the users’ gloves and forearms [1].

2.5.2.4 Ultrapure Water

Ultrapure water, also known as Milli-Q® water, has been purified by a process of reverse osmosis and de-ionised. This water is ideal for laboratory experiments as it does not contain any contaminants [1].

2.5.2.5 Bunsen Burner

Lighting a Bunsen burner and turning the flame to a blue cone is another good method to keep the air around the work environment sterile. The heat from the flame will create an updraft which will stop any contaminants from falling in the immediate work area. The Bunsen burner can also be used for flaming (discussed in section 2.5.1.1) the rims of containers which are opened and closed to further ensure no cross-contamination can take place [44].

2.5.2.6 Typical Experiment Environment

Figure 24 below shows a typical sterile working area in the laboratory.

Figure 24 - Lab Equipment Inside Laminar Flow Cabinet [1]

How calmly personnel move their physical body around the laboratory is also important. Sudden movements in the vicinity of the laminar flow cabinet could create a turbulent air flow inside the laminar flow cabinet negatively impacting the experiment within [44].

2.5.3 Sterilisation Standards

According to the World Health Organisation (WHO) and the Food and Agriculture Organisation (FAO), commercial sterility is defined as “the absence of microorganisms capable of growing in the food at normal non-refrigerated conditions at which the food is likely to be held during manufacture, distribution and storage” [47][48].

Sterilisation efficiency can be expressed as the number of decimal reductions in microbial populations. This arises because not all organisms will die all at the same time. This means that graphs can be created which assess the amount of organisms existing before treatment, and after various treatment times [48]. Figure 25 below shows what these graphs typically look like where N is the number of organisms present in the media before treatment.

The value of D is called the decimal reduction time and is the amount of time required to reduce N by 90% (one logarithmic reduction) [48]. The Z value is a measure of the amount of increase in temperature to alter the D value by a factor of one logarithmic unit [48].

Low acid foods are defined as having a pH greater than 4.6. This pH value is important for food processing because the organism *Clostridium botulinum* thrives in environments with this criterion and poses a significant public health issue if it not destroyed before consumption. This organism has

an acceptable level of sterilisation of 12 logarithmic reductions (1 in every 10^{12} products will contain no more than exactly 1 living spore) [31].

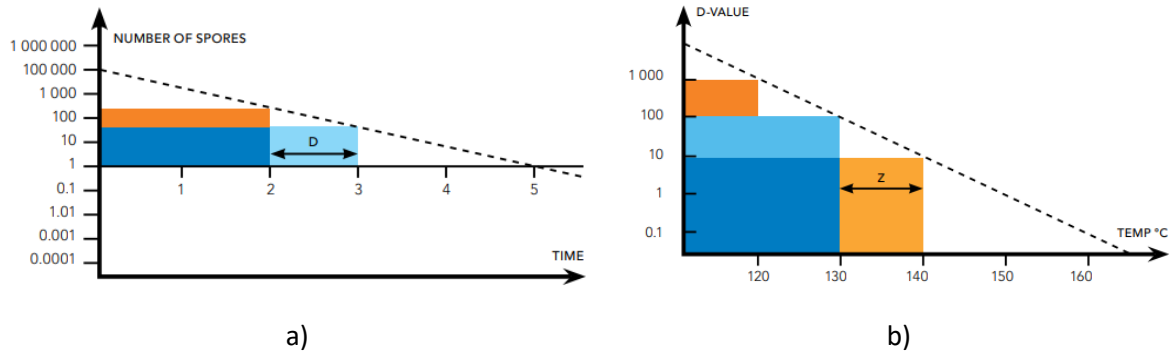

a) b)

Figure 25 - a) Number of Spores vs Time, b) D-Value vs Temperature

An organism responsible for food spoilage by mesophilic spore formers (spores which thrive at moderate temperatures) is PA 3679, which is a strain of *C. sporogenes*. This organism has an acceptable level of sterilisation of 5 logarithmic reductions. Thermophilic spore formers (spores which thrive at high temperatures) have an acceptable level of sterilisation of 2 logarithmic reductions [31].

Processing times always vary and, as a result, safety factors are built into all sterilisation set-ups which leads to food products being heated for longer than they need to be which increases the energy cost of sterilisation and decreases product quality [31].

2.6 Non-Thermal Microwave Effect

The non-thermal effect is a phenomenon which arises due to the fact that experimental results cannot be explained completely by thermal destruction alone. The term “non-thermal” is misleading and should actually be thought of as “microwave specific effects” [49].

The existence of the effect has been proposed by multiple authors. For example, Jacques Berlan [50] observed faster cycloaddition reactions when the medium was heated by microwave energy when compared to conventional heating techniques [51].

Further microwave specific effects can be seen in the sterilisation industry when *E. coli* was exposed to microwave radiation at $2.45\ \mathrm{GHz}$. The temperature was controlled from room temperature to $37\ ^{\circ}\mathrm{C}$. This test was repeated using conventional heating techniques for the same duration as the previous microwave test. The findings of this experiment showed that cell membrane modifications were present in the microwave test and not the conventional heating test [49]. Furthermore, the microwave test was conducted at different peak power levels. The results from this test showed that a power level of $200\ \mathrm{W}$ did not have an effect, however, power levels greater than $400\ \mathrm{W}$ did have an effect. It should also be noted that no real difference was observed for power levels between $400\ \mathrm{W}$ and $800\ \mathrm{W}$ [49].

In conclusion, these tests present compelling evidence that microwave heating is different to conventional heating and that “something” must be happening in the presence of microwave radiation. It is very difficult to isolate the thermal effects from the non-thermal effects. It is proposed that to gain the greatest insight into the understanding of the microwave specific effect is to stop measuring bulk solution temperatures and to rather find a way to measure individual molecules on a cellular level [49].

Chapter 3
Initial Investigation

3.1 Chapter Summary

This chapter aims to highlight the initial experiments which were conducted to gain a better practical understanding of potential system designs. Experiments were carried out with various TRIAC waveform switching strategies to ascertain whether the issue of the double transformer could be solved. A multimode cavity was analysed and used in the first sterilisation experiments. A single mode, batch experimental system was set up and used for the second sterilisation test. The second sterilisation test yielded important design information for this project moving forward.

3.2 Magnetron Power Control Experiments

Previous EHG works used conventional TRIAC control waveforms. However, the issue highlighted when doing this is that the filament in the magnetron is unable to get enough current to reach the required temperature to create the electron cloud discussed in 2.3.1. The solution to this problem was to introduce another transformer which remains uncontrolled to keep the filament at the designed temperature. The altered high voltage supply can be seen in Figure 26 below.

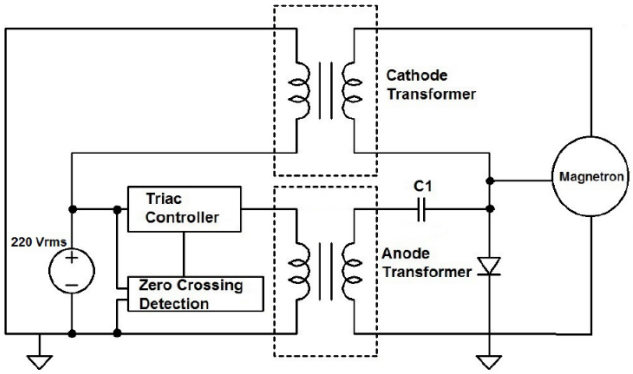

Figure 26 - Dual Transformer High Voltage Set Up [2]

The nature of the non-sinusoidal TRIAC current signal caused the anode transformer to heat up excessively. High levels of heat in a transformer could lead to insulation failure and subsequent failure of the entire transformer [2]. The solution to this problem may have been to buy a new, properly rated transformer for the non-sinusoidal signal, however, this could be prohibitively expensive. The alternative solution for this overheating problem was to reduce the input power by means of a fixed saturable control technique discussed in section 2.3.2.6. This solution lowered the transformer temperatures to an acceptable level.

3.2.1 TRIAC Control Experiments

The aim of this section was to implement various switching techniques to ascertain whether a single transformer could be used in conjunction with a TRIAC.

3.2.1.1 Switching Techniques

A conventional microwave was investigated to get a better understanding of how the oven regulates its output power. The investigation led to the result that the oven always outputs a maximum magnetron power peak on every negative half cycle. The switching is done by a mechanical timer

which turns the oven "on" for a set duration and then "off" for a set duration. The rate at which the switching is done is very slow (roughly $15\,s$ "on" and $10\,s$ "off") depending on the microwave setting.

The first switching technique created in the software was designed to mimic what the mechanical switch was already doing. This worked successfully, however, this form of duty cycle control would not work for sterilising applications (discussed in section 2.3.2.1).

The second switching technique implemented was to reduce both the "on" and "off" times of the first technique. The waveform for this technique can be seen in Figure 10 a). This caused the transformer to vibrate loudly and heat up rapidly.

The conventional microwave circuit was further studied. It was found that the high voltage capacitor, in conjunction with the diode, created a voltage doubling effect. This meant that on the positive half cycle the capacitor is charged to $2000\ \mathrm{V}$ and the negative half-cycle created a potential difference across the magnetron of roughly $-4000\ \mathrm{V}$ as the capacitor discharges. A third switching strategy was then designed to cut out the negative half cycle in a bid to not turn the magnetron on while maintaining enough current to keep the filament at the desired temperature. The wave form for this strategy can be seen in Figure 27 a) below.

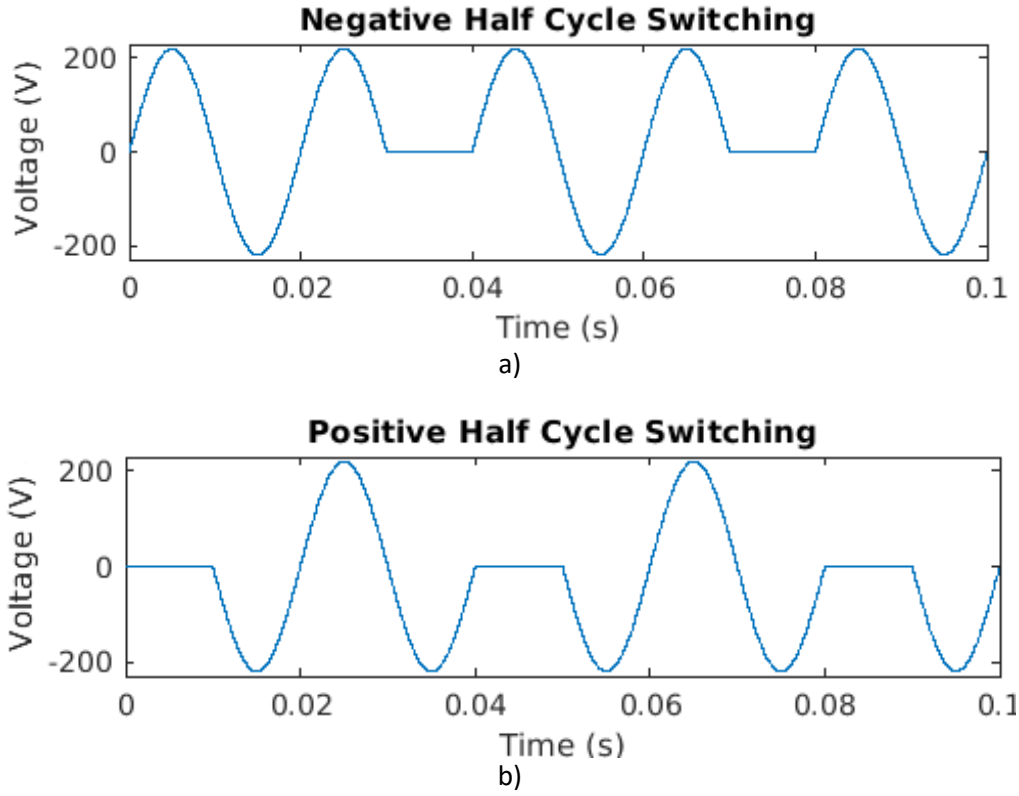

Figure 27 - a) Negative Half Cycle Switching b) Positive Half Cycle Switching

Switching strategy number three caused an $8\ \mathrm{A}$ safety fuse to break after only a couple of seconds. The experiment was further conducted by implementing the waveform seen in Figure 27 b) above, which also broke the protection fuse.

In conclusion, it was decided that the problem of the second transformer was not going to be solved by any forms of TRIAC switching techniques.

3.2.1.1 Magnetron Output Power Waveforms During TRIAC Switching

The literature provided in section 2.6 highlights that the non-thermal microwave effect may be attributed to the peak power levels supplied by the magnetron. The power pulses produced by the magnetron were viewed on an oscilloscope at various percentages of TRIAC power switching. The actual values of the signals are not important for this explanation. Figure 28 shows the observations made when conducting this experiment.

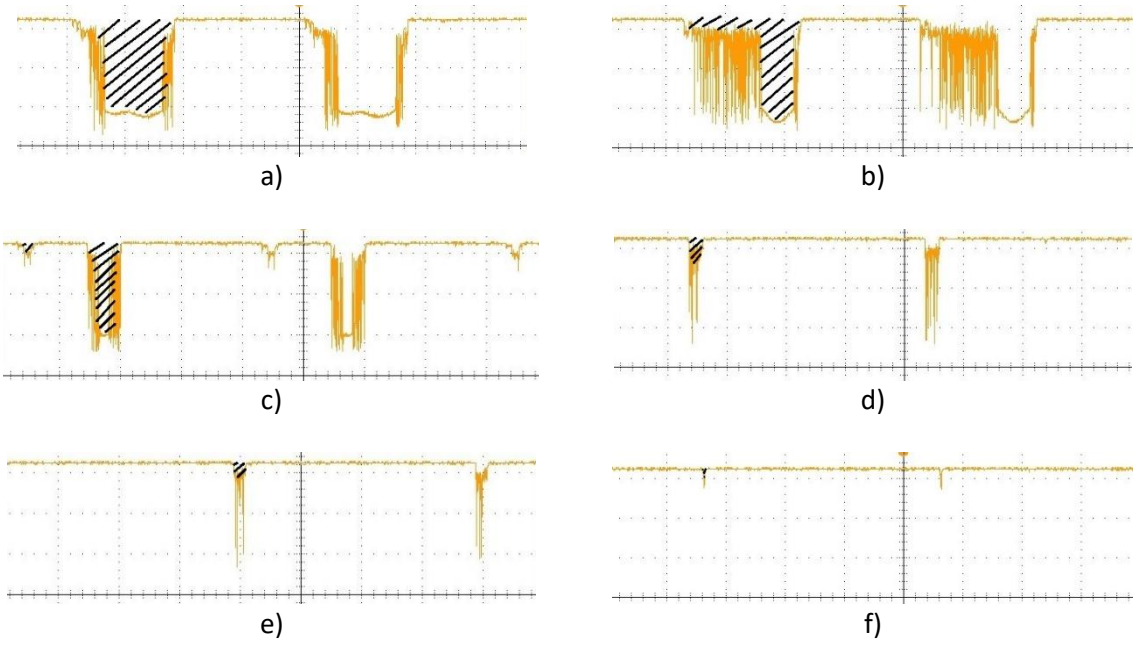

Figure 28 - Magnetron Output Power Waveforms During TRIAC Switching a) 100% Power b) 50% Power c) 35% Power d) 25% Power e) 20% Power f) 15% Power

The shaded areas depicted in each of the six pictures of Figure 28 represent the power level for every magnetron power pulse. The larger the area, the larger the power contained in that pulse. The areas of each pulse clearly decrease as the conventional TRIAC switching strategy is implemented to regulate the output power of the magnetron. A typical temperature fed control system using magnetron power control will therefore start by applying the waveforms seen in a) and b). However, when the target media reaches the required temperature, it is possible that waveforms c), d), e) or f) may be enough power to maintain the steady state temperature for the duration of the test. The pulses in this case are low power which may result in the system not reaping the benefits of the non-thermal microwave specific effect.

3.2.2 Variable Saturable Reactor Technique

This technique would rely on a variable capacitor. Variable capacitors are not manufactured for the voltage rating or even the capacitance values required by the conventional microwave circuit. A variable capacitor bank could be developed which used high voltage microwave capacitors and a mechanical switch to vary the capacitance across different series configurations of capacitors. This form of control has very similar drawbacks when compared to the variable transformer discussed in section 2.3.2.2. The variable capacitor bank route was not developed further.

3.2.3 Other Control Ideas

It is evident that a conventional microwave oven system is precisely designed for optimal use. This means that the best form of control may be to implement something which does not alter or effect the high voltage supply circuit. This could be done by changing the high voltage supply circuit

completely to a more efficient inverter type circuit (discussed in section 2.3.2.4), however, this would drastically increase the cost of the system.

Another idea to control the power would be to implement something which could reflect incoming power away from the media in the treatment chamber. This can be achieved with the use of a 3-stub tuner. An example of this device can be seen in Figure 29 below.

Figure 29 - 2.45 GHz 3-Stub Tuner [52]

These devices are used in a manner to reduce reflected power seen at the magnetron [52]. This device, however, could be repurposed to reflect power away from the media in the treatment chamber. The drawback to this method was that all the diverted power would be seen at the magnetron. This form of power control therefore was not considered feasible. Furthermore, this method does not use conventional microwave components and adds areas for mechanical failure in the system.

3.2.4 Variable Flow Rate Control

The last form of control investigated at the inception of the project was the use of a variable flow rate system. By introducing this, instead of creating a lower average power by turning the magnetron “on” and “off”, it was proposed that the magnetron remains permanently “on” while media moves “in” and “out” of the treatment chamber. This process could be made to occur faster or slower depending on whether the media needs to cool down or heat up. This solution allows the previously designed microwave circuitry, built by microwave oven companies, to operate as intended by the original designers. Although this form of control will require a liquid pump, which is not a conventional microwave oven component, the nature of the aqueous media in this project means that a pump would be required regardless of the control technique chosen.

3.2.5 Control Technique Conclusion

In conclusion, it is proposed that a motorised pump be acquired which can be controlled by means of a simple duty cycle control waveform. This form of control is pursued in this project as it solves the problem of the overheating high voltage transformer due to the TRIAC switching and promotes a design which incorporates the possibility of the non-thermal microwave specific effects seen in literature (section 2.6).

3.3 Baseline Sterilisation Experiment

The aim of this experiment was to investigate the time required to uniformly heat various substances in a conventional microwave oven. The experiments were conducted with closed glass Petri dishes. A Petri dish is a flat-bottomed circular plate used to “culture” or grow microorganisms.

3.3.1 Determining Potential Cold Spots

To get a good representation of how the microwave oven will interact with the Petri dish, a polystyrene disk was fitted with neon bulbs which glow in the presence of microwaves. This was used to find the optimum and most realistic place inside the microwave to place the Petri dish. Image a) in Figure 30 below shows the neon bulbs when the microwave is off. Image b) in Figure 30 shows that the Petri dish is not in an optimal place as standing waves cause areas of null energy which will lead to hot and cold spots forming in the Petri dish. Image c) in Figure 30 shows the Petri dish in the most optimal place as all the neon bulbs have lit up.

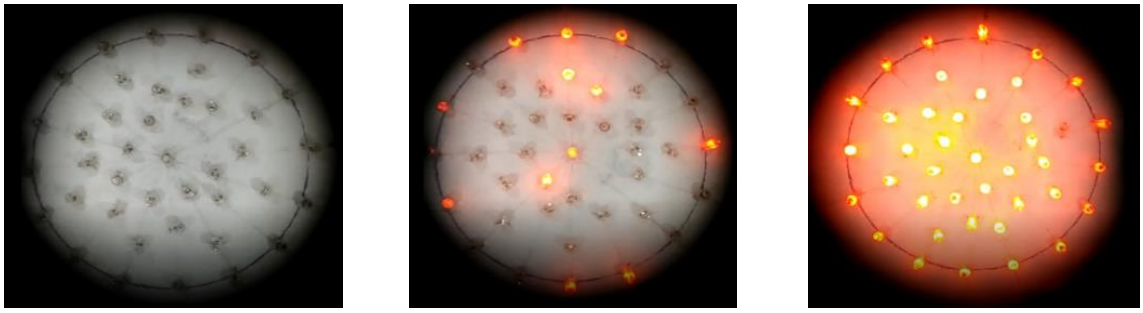

a) b) c)

Figure 30 - a) Microwave Off [53] *b) Microwave On-Bad Positioning* [53] *c) Microwave On-Good Positioning* [53]

3.3.2 Determining Treatment Time

The bottom of the Petri dishes were entirely covered by $10\ \mathrm{ml}$ of water. The method followed for determining the treatment times for various media was conducted by heating $10\ \mathrm{ml}$ of the media which was distributed uniformly on top of a closed Petri dish. The dish was then placed inside a microwave oven using the same place in the oven each time (a predetermined place was used so that each dish would be heated in the same way) to ensure consistency. The temperature was measured before and after cooking the dish in the microwave for various times using a thermal camera.

The use of the thermal camera is necessary to find potential cold spots and subsequently ensure that the Petri dish is heated uniformly.

The results of these experiments are documented in Appendix C. To summarise, the results show that a microwave oven can heat media rapidly to “lethal” temperatures for microorganisms. The results also show that all media behave differently in the presence of microwave radiation. The experiments showed that the precise location of “hot spots” are hard to predict inside the multi-mode microwave cavity.

3.3.3 The First Sterilisation Procedure and Results

Tests were done using *Lactococcus lactis*, suspended in $2\ \mathrm{ml}$ of saline solution. The samples were made at the Microbiology Department of Stellenbosch University. The samples were collected, processed and returned.

The processing consisted of applying microwave radiation to the samples for various periods of time. The microwave oven used was a $700\ \mathrm{W}$ $2.45\ \mathrm{GHz}$ Defy DMO 349. The samples were placed at the optimal location determined in section 3.3.1.

After the microwave treatment, the samples were taken back to the Microbiology Department for dilution and plating. This was done to give the surviving *Lactococcus lactis* a chance to grow and form colonies of bacteria. Once enough time had passed, the colonies on the plates could be counted, and the results visualised. The fundamental aspect for determining cell viability was used

that every colony of bacteria counted, started as a single bacterial cell. The results can be seen in Figure 31 below.

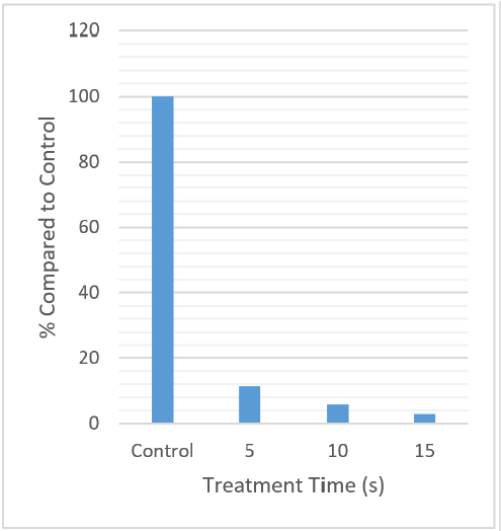

Figure 31 - Initial Sterilisation Results

The 15 second microwave treatment shows a 99% reduction in bacteria as compared with the control. This experiment gives the rest of the project a baseline to improve upon.

3.4 Experimenting with Single Mode Structures

The microwave cavities in previous EHG works all used multimode cavities. This makes it inherently difficult to predict and simulate interactions inside the microwave chamber. Waveguides can be used to create a single mode of operation which has predictable properties that can be simulated. This section aims to sterilise media in a single mode environment while also gaining important knowledge when working in the confined space of a waveguide. The experimental system can be seen in Figure 32 below.

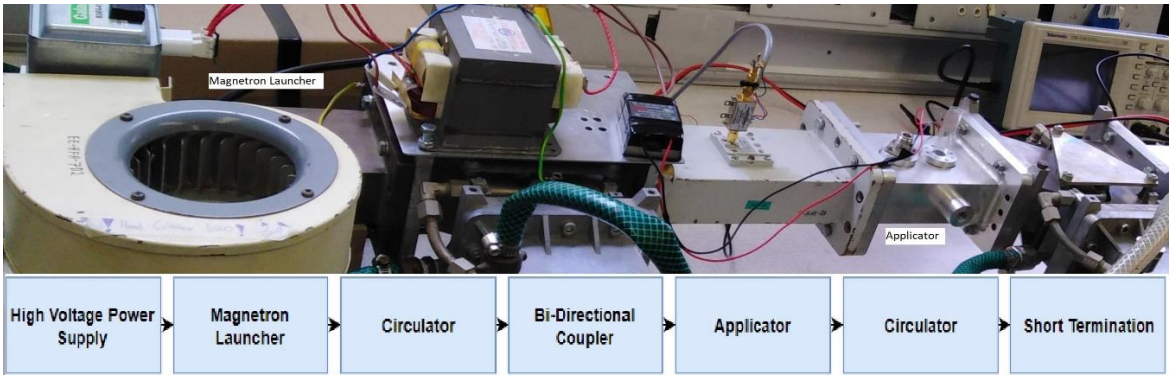

Figure 32 - Experimental System with Flow Diagram

The circulators (explained in section 6.2.4) are set up in such a way as to create a travelling wave between them. This was done to remove the need for a mode stirrer and/or sliding short. The travelling wave means that no matter where the treatment sample is placed, it will receive waves of maximum microwave energy.

The samples consisted of 3 ml of *Lactococcus lactis* suspended in saline solution. The samples were put into glass test tubes and lowered into the chamber through a carefully calculated non-radiating

hole in the applicator. The temperature of the samples was monitored by an infrared pyrometer, namely Optris CSLTv2.

The temperature of the sample was controlled by a simple proportional control system which altered the power with the TRIAC design from previous works. The results are tabulated in Table 1 below.

Table 1 - Single Mode Test Tube Sterilisation Results

Single Mode Test Tube Sterilisation Results						
	0 dilutions	2 dilutions	4 dilutions	6 dilutions	8 dilutions	
Control	n/a*	n/a*	574	7	0	$5.74x10^7$CFU/mL
T1 - 60 °C for 30 s	n/a*	687	2	0	0	$6.87x10^5$CFU/mL
T2 - 70 °C for 30 s	n/a*	39	0	0	0	$3.9x10^4$CFU/mL
T3 - 80 °C for 30 s	n/a*	358	1	0	0	$3.58x10^5$CFU/mL
T4 - 90 °C for 30 s	n/a*	158	1	1	0	$1.58x10^5$CFU/mL
*Too many colonies to count #CFU/mL = colony forming units/ mL						

The results of these tests were not good for sterilisation purposes. One can speculate that the results are non-optimal due to some of the media forming droplets on the inside walls of the test tube. This would appear to have resulted in the media not being fully sterilised as the droplets did not enter the treatment chamber. This is evident from the inconsistent results observed at the different temperatures (Table 1), as higher heat is expected to result in less viable bacteria. This can be seen in Figure 33 below.

Figure 33 - Test Tubes After Treatment

This experiment also showed that the infra-red camera reads the temperature of the surface of the media's container and not the media itself. This means that the change in media temperature is seen more slowly as the temperature change needs to first be conducted through the wall of the container.

3.5 Chapter Conclusion

The work illustrated in this chapter showed that the TRIAC power control technique was not going to fix the issue of the double transformer pair. The use of non-sinusoidal signals has too many inherent

losses when fed into a conventional microwave oven transformer. It is proposed that flow rate control strategies be used instead.

The baseline sterilisation test showed that it was very hard to predict the interactions inside a multi-mode cavity. This led to the necessity for a single mode system to be designed and simulated.

The single mode experiment yielded the results that IR temperature sensors should be replaced by sensors which can be placed inside the target media. This will allow the control system in the final design to be as fast and responsive as possible. Lastly, it is of the utmost importance to ensure that all the media receives microwave treatment.

Chapter 4
Simulations & Applicator Design

4.1 Chapter Summary

This chapter aims to show the evidence available when making design decisions with regards to the applicator. The chapter starts with a mathematical derivation intended to illustrate why different modal patterns exist. The modal patterns are then visualised through electromagnetic simulations. The interactions between the E-field and the target media is simulated and key concepts are learnt with regards to standing waves and travelling waves. Finally, the applicator used in this project is designed considering the important information learnt through coupled thermal and electromagnetic simulations.

4.2 Understanding Modal Patterns

In theory, there are an infinite number of ways in which EM waves can propagate inside an arbitrary waveguide. These ways are broken into three main subsections, namely: *Transverse Electromagnetic* (TEM), *Transverse Magnetic* (TM) and *Transverse Electric* (TE). TEM waves are categorised by having no $\mathbf{E}$ or $\mathbf{H}$ field in the direction of propagation (the z-direction in this project). TM waves subsequently have no $\mathbf{H}$ field in the z-direction and TE waves have no $\mathbf{E}$ field in the z-direction [54].

Since the EM waves provided by the magnetron are being used to heat up the media in this project, one needs to understand at which point these waves have the most energy. High energy points will have the greatest heating effect on targeted media. To understand EM waves, one can start with Maxwell's equations [54]:

$$\begin{aligned} \nabla \times \mathbf{E} &= -\frac{d\mathbf{B}}{dt}, \\ \nabla \times \mathbf{H} &= \mathbf{J} + \frac{d\mathbf{D}}{dt}, \\ \nabla \cdot \mathbf{D} &= \rho, \\ \nabla \cdot \mathbf{B} &= 0, \end{aligned} \tag{9}$$

where $\mathbf{E}$ is the electric field strength, $\mathbf{B}$ is the magnetic flux density, $\mathbf{H}$ is the magnetic field strength, $\mathbf{J}$ is the density of free currents (consisting of conduction current and convection current), $\mathbf{D}$ is the electric flux density and ρ is the volume density of free charges.

To understand the modal patterns, one needs to consider the behaviour of EM waves in a source-free region. This means that $\rho = \mathbf{J} = 0$. Essentially, one is interested in how the wave propagates and not how it originated. This means that, in the simplest case, where the wave is propagating in a linear, isotropic, homogenous non-conducting medium [54], Maxwell's equations can be reduced to:

$$\begin{aligned} \nabla \times \mathbf{E} &= -\mu\frac{d\mathbf{H}}{dt}, \\ \nabla \times \mathbf{H} &= \varepsilon\frac{d\mathbf{E}}{dt}, \\ \nabla \cdot \mathbf{E} &= 0, \\ \nabla \cdot \mathbf{H} &= 0, \end{aligned} \tag{10}$$

where μ is the permeability and ε is the permittivity. These equations are first order differential equations comprised of both $\mathbf{E}$ and $\mathbf{H}$ [54]. They can become second order differential equations of a single variable by taking the curl and considering the identity:

$$\boldsymbol{\nabla} \times \boldsymbol{\nabla} \times \mathbf{A} = \boldsymbol{\nabla} \cdot (\boldsymbol{\nabla} \cdot \mathbf{A}) - \boldsymbol{\nabla}^2 \mathbf{A}\,, \tag{11}$$

where $\mathbf{A}$ is an arbitrary vector interchangeable with $\mathbf{E}$ and $\mathbf{H}$.

The second order differential equations are:

$$\begin{aligned} \boldsymbol{\nabla}^2 \mathbf{H} - \varepsilon\mu \frac{d^2\mathbf{H}}{dt^2} &= 0\,, \\ \boldsymbol{\nabla}^2 \mathbf{E} - \varepsilon\mu \frac{d^2\mathbf{E}}{dt^2} &= 0. \end{aligned} \tag{12}$$

Equations in (12) can be further simplified by considering the identity in Equations (13 a).

$$\begin{aligned} \mathbf{A}(x,y,z,t) = Re[\mathbf{A}(x,y,z)e^{j\omega t}] \qquad & \frac{d}{dt}\mathbf{A}(x,y,z) = j\omega\mathbf{A}(x,y,z) \quad \text{(a)} \\ \mathbf{A}(x,y,z,t) = Re[\mathbf{A}^0(x,y)e^{(j\omega t - \gamma z)}] \qquad & \frac{d}{dz}\mathbf{A}(x,y,z) = (-\gamma)\mathbf{A}^0(x,y) \quad \text{(b)} \end{aligned} \tag{13}$$

Which reduces (12) to:

$$\begin{aligned} \boldsymbol{\nabla}^2 \mathbf{H} + k^2 \mathbf{H} &= 0\,, \\ \boldsymbol{\nabla}^2 \mathbf{E} + k^2 \mathbf{E} &= 0\,, \end{aligned} \tag{14}$$

where $k = \omega\sqrt{\varepsilon\mu}$ and is known as the wave number [54].

Equations in (14) are homogenous vector Helmholtz's equations. The variable ∇^2 is 3-dimensional and can be broken into the addition of two parts:

$$\boldsymbol{\nabla}^2 = \boldsymbol{\nabla}_{u1u2}^2 + \boldsymbol{\nabla}_z^2\,, \tag{15}$$

where $\boldsymbol{\nabla}_{u1u2}$ represents the cross-sectional coordinates, and $\boldsymbol{\nabla}_z = \frac{d}{dz}$ represents the longitudinal coordinates [54]. For an infinitely long rectangular waveguide using rectangular coordinates with width a , height b and $a > b$ seen in Figure 34 below.

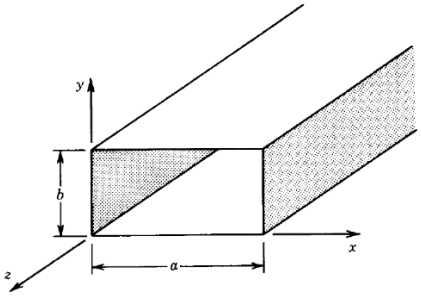

Figure 34 - Rectangular Waveguide with Coordinate System [55]

Substituting Equation (15) and considering the identity in Equation (13 b), Equations in (14) reduce to Equations in (16):

$$\nabla_{xy}^2 H_z + h^2 H_z = 0\,, \qquad \text{(a)}$$
$$\nabla_{xy}^2 E_z + h^2 E_z = 0\,, \qquad \text{(b)} \tag{16}$$

where $h^2 = \gamma^2 + k^2$. The values for h which have solutions are called the characteristic values or eigenvalues [54].

For transverse electric (TE) waves $E_z = 0$, which leaves Equation (16 a) to be solved for H_z and we can write that:

$$H_z(x, y, z) = H_z^0(x, y)e^{-\gamma z}\,, \tag{17}$$

where $H_z^0(x, y)$ must satisfy the second order partial differential equation highlighted in Equation (16 a), which can be rewritten in Equation (18) below [54]:

$$\left(\frac{d^2}{dx^2} + \frac{d^2}{dy^2} + h^2\right) H_z^0(x, y) = 0\,. \tag{18}$$

The solution for $H_z^0(x, y)$ must satisfy the boundary condition presented in

Table 2 below:

Table 2 - Boundary Conditions for TE waves in a Rectangular Waveguide [54]

$\boldsymbol{x}$-direction ($\boldsymbol{E_y = 0}$)	$\boldsymbol{y}$-direction ($\boldsymbol{E_x = 0}$)
$\boldsymbol{\frac{dH_z^0}{dx} = 0 \quad at\ x = 0}$	$\boldsymbol{\frac{dH_z^0}{dy} = 0 \quad at\ y = 0}$
$\boldsymbol{\frac{dH_z^0}{dx} = 0 \quad at\ x = a}$	$\boldsymbol{\frac{dH_z^0}{dy} = 0 \quad at\ y = b}$

$H_z^0(x, y)$ thus, has a solution given by Equation (19) below:

$$H_z^0(x, y) = H_0 \cos\left(\frac{m\pi}{a}x\right) \cos\left(\frac{n\pi}{b}y\right), \tag{19}$$

where m and n are real integers (i.e. 1,2,3…) and either m or n could be zero, but not at the same time. The eigenvalue h also has the relationship provided by Equation (20) below:

$$h^2 = \left(\frac{m\pi}{a}\right)^2 + \left(\frac{n\pi}{b}\right)^2. \tag{20}$$

Other field components can be solved and are presented in Equations (21) below:

$$\begin{aligned} E_x^0(x,y) &= \frac{j\omega\mu}{h^2}\left(\frac{n\pi}{b}\right) H_0 \cos\left(\frac{m\pi}{a}x\right)\sin\left(\frac{n\pi}{b}y\right), \\ E_y^0(x,y) &= -\frac{j\omega\mu}{h^2}\left(\frac{m\pi}{a}\right) H_0 \sin\left(\frac{m\pi}{a}x\right)\cos\left(\frac{n\pi}{b}y\right), \\ H_x^0(x,y) &= \frac{\gamma}{h^2}\left(\frac{m\pi}{a}\right) H_0 \sin\left(\frac{m\pi}{a}x\right)\cos\left(\frac{n\pi}{b}y\right), \\ H_y^0(x,y) &= \frac{\gamma}{h^2}\left(\frac{n\pi}{b}\right) H_0 \cos\left(\frac{m\pi}{a}x\right)\sin\left(\frac{n\pi}{b}y\right), \end{aligned} \tag{21}$$

where:

$$\gamma = j\beta = j\sqrt{\omega^2\varepsilon\mu - \left(\frac{m\pi}{a}\right)^2 - \left(\frac{n\pi}{b}\right)^2}. \tag{22}$$

Equations in (19) and (21) can be used to sketch the shapes of various modal patterns inside the waveguide [54]. These shapes can be seen in Figure 35 below. The red arrows show areas of high energy and the blue areas show areas of low energy.

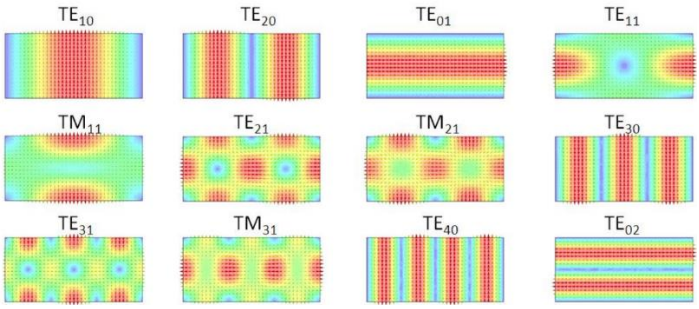

Figure 35 - The First 12 Modes in a Rectangular Waveguide [56]

Similar derivations can be done in cylindrical coordinates to show the shapes of the TE or TM modes in circular waveguides, shown in Figure 36 below.

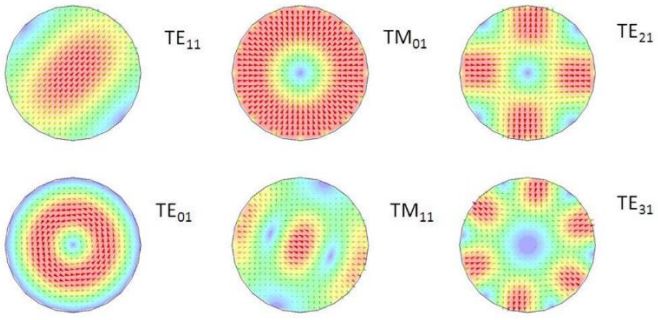

Figure 36 - The First 6 Modes in a Circular Waveguide [56]

Simulation packages like CST Studio Suite®, a 3D EM analysis software package, can be used to show the 3-dimensional modes and can save a lot of time when trying to visualise equations. CST Studio Suite will be used for further design of the applicator structure.

4.3 Electromagnetic Simulations

The derivation shown in Section 4.2 relies on a very simple set-up inside the infinitely long waveguide structure. The system built in this project is not an infinitely long waveguide and is instead a finite length waveguide cavity. This means that the boundary conditions in

Table 2 change which, in turn, leads to the modal patterns changing. This section illustrates the 3-dimensional modal patterns and behaviours for a finite length waveguide cavity through simulation.

4.3.1 Empty Waveguide

Figure 37 below shows the fundamental mode (TE_{10}) for a rectangular waveguide. This is the mode with the lowest cut-off frequency. The simulation shows that the electric field is oscillating and that a standing wave exists within the waveguide.

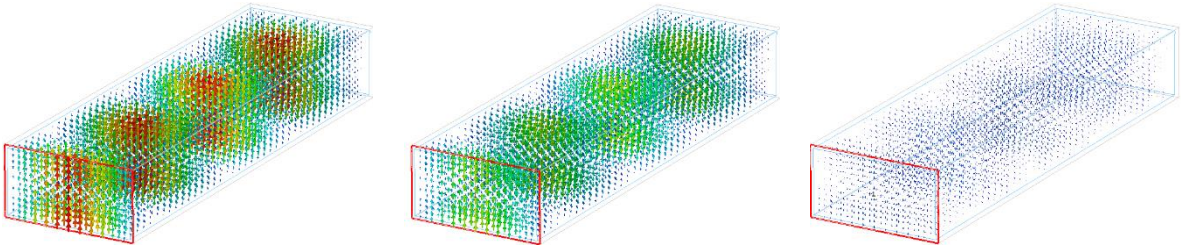

Figure 37 - Fundamental Mode for Rectangular Waveguide Shown in 3-D a) Phase Angle = 0° b) Phase Angle = 45° c) Phase Angle = 90°

Starting from Figure 37 a), the E-field has maximum energy. Close inspection shows that the magnitude of the E-field decreases to a minimum seen in c). The magnitude of the E-field then increases to a maximum again from a phase angle 90 ° to 180 °(where a phase angle of 180 ° looks like that in a) however the direction of the E-field has “flipped”).

Similarly, Figure 38 shows the fundamental mode (TE_{11}) for a circular waveguide.

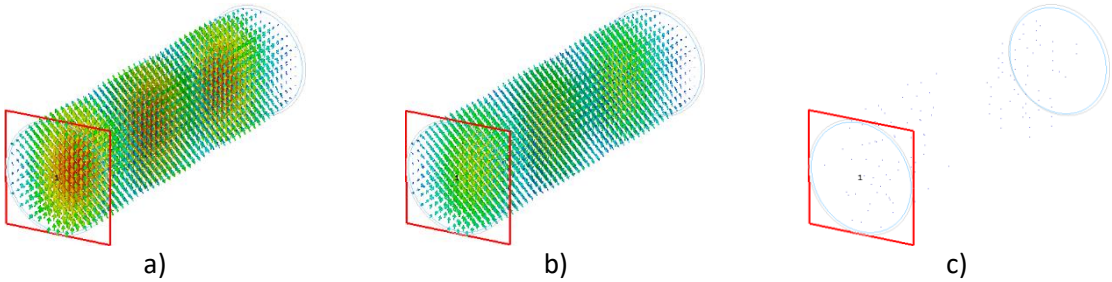

Figure 38 - Fundamental Mode for Circular Waveguide Shown in 3-D a) Phase Angle = 0° b) Phase Angle = 45° c) Phase Angle = 90°

The simulations above were conducted with vacuum filled waveguides and the structures were made from perfect electrical conductors (PEC). The simulations consisted of a single port radiating

into a waveguide which is terminated by a short circuit. This is the definition of the perfect case for simulations which speeds up the solving time.

4.3.2 Changes in Field State due to Dielectric (Water)

The simulation software is able to make graphical representations of what is happening inside the waveguide and visually demonstrate the interactions between EM fields and the dielectric medium placed inside the waveguides. Figure 39 shows what happens to the E-fields when a coiled water tube is placed into the "perfect" conditions seen in section 4.3.1.

a) b)

Figure 39 - E-field Interactions Inside Waveguides with Water Coils a) Rectangular Waveguide b) Circular Waveguide

The E-fields behave drastically differently when compared with the previous empty waveguide case. Figure 39 a) and b) should be comparable to Figure 37 a) and Figure 38 a) respectively as the phase angle in these images are the same. The dielectric inside the waveguides causes additional reflections, which change the shape of the E-fields.

4.4 Coupled Thermal and Electromagnetic Simulations

CST Studio Suite can couple EM simulations with thermal simulations. This means that one can see exactly how a dielectric will heat up directly due to the microwave source. This section focusses on the different heating patterns produced by rectangular and circular waveguides for different dielectric shapes. The waveguides simulated in this section both have the same length in the z-direction and both hold the same volume of dielectric water in the same relative position inside the waveguide structure. The structure dimensions are consistent with the dimensions used at a frequency of $2.45\ \mathrm{GHz}$.

4.4.1 Thin Flat Sheet of Water

Figure 40 shows how EM energy can heat up a thin, flat water sheet within the respective waveguides.

a) b)

Figure 40 - Thin Flat Sheet of Water a) Rectangular Waveguide b) Circular Waveguide

The heating patterns show that the rectangular waveguide heats this water shape more evenly than that of the circular waveguide. It is interesting to note that the E-field patterns for the rectangular waveguide structure were comparable with Figure 37 a) whereas the E-filed for the circular waveguide structure were not comparable with Figure 38 a).

4.4.2 Thin Rod of Water

Figure 41 shows how EM energy can heat up a thin rod of water placed in the centre of the respective waveguides.

a) b)

Figure 41 - Thin Rod of Water a) Rectangular Waveguide b) Circular Waveguide

Both E-fields in Figure 41 a) and b) are comparable with the E-fields seen in Figure 37 a) and Figure 38 a) respectively. The similarity produced was speculated to be because the volume of the water present inside the waveguide was not great enough to influence the E-field. Closer inspection of the water rod seen with the simulation software shows that when the E-field behaves in this manner, “hot-spots” are formed in the areas of maximum E-field strength.

4.4.3 Thin Cylindrical Sheet of Water

Figure 42 shows how EM energy can heat up a thin cylindrical sheet of water within the respective waveguides.

a) b)

Figure 42 - Thin Cylindrical Sheet of Water a) Rectangular Waveguide b) Circular Waveguide

Both E-fields in Figure 42 a) and b) are comparable with the E-fields seen in Figure 37 a) and Figure 38 a) respectively.

4.4.4 Thin Parallel Sheets of Water

Figure 43 shows how EM energy can heat up two, parallel, flat thin water sheets within the respective waveguides.

a) b)

Figure 43 - Thin Parallel Sheets of Water a) Rectangular Waveguide Vertical Water Orientation b) Rectangular Waveguide Horizontal Water Orientation c) Circular Waveguide Vertical Water Orientation d) Circular Waveguide Horizontal Water Orientation

Both E-fields in Figure 43 a) and b) are comparable with the E-fields seen in Figure 37 a) and Figure 38 a) respectively. It is interesting to note that although the E-fields are in a predictable form, the heating characteristics differ between a) and b) for the rectangular waveguide structures whereas the circular structure seen in c) and d) produced heating patterns which were similar to each other.

This result was not expected because the maximum E-field intensity from Figure 37 a) lies in the central plane, directly passing through the dielectric media in Figure 43 b) whereas the media in Figure 43 a) tends to lie on the outskirts of the maximum E-field. This simulation suggests that maximum heating of a dielectric media does not occur at the point of maximum E-field intensity.

4.4.5 Asymmetric Water Experimental Shapes

Figure 44 shows how EM energy can heat up various asymmetrical water shapes within the respective waveguides. The purpose of this simulation was intended to find a dielectric shape which promotes homogenous heating patterns by forcing the “perfect” modal patterns to reflect due to the asymmetry of the dielectrics.

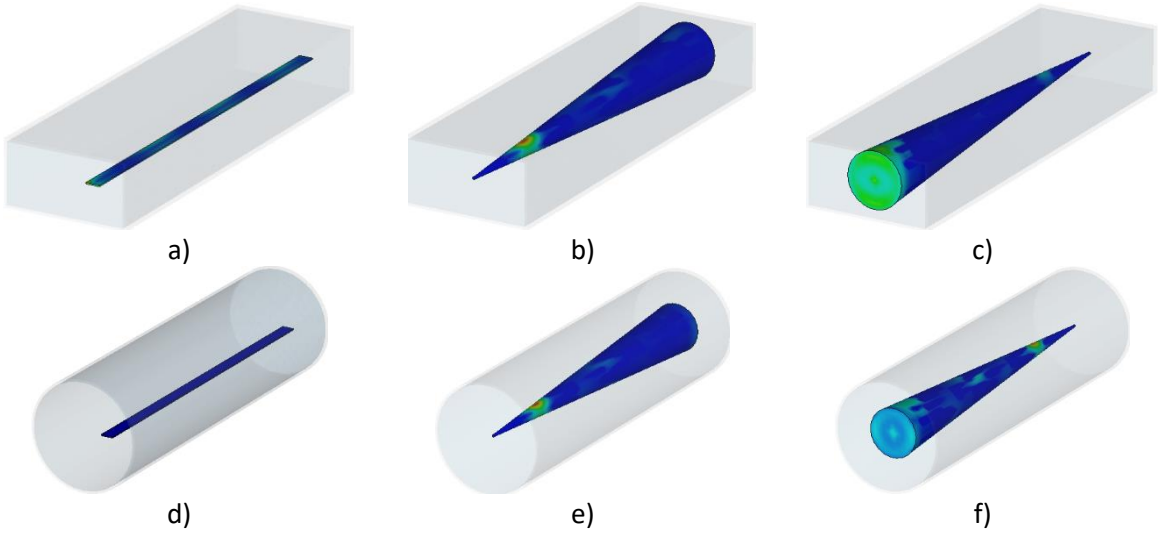

Figure 44 - Asymmetric Water Experimental Shapes a) Rectangular Waveguide with Offset Thin Water Sheet b) Rectangular Waveguide with Solid Water Ascending Cone c) Rectangular Waveguide with Solid Water Descending Cone d) Circular Waveguide with Offset Thin Water Sheet e) Circular Waveguide with Solid Water Ascending Cone f) Circular Waveguide with Solid Water Descending Cone

It is important to note here that the interaction between the E-field and the water medium is not predictable. The heating patterns in a) and d) were very feint and not homogenous. These experiments were also conducted to try and find a shape which minimised the reflected power

returned to the magnetron within the waveguide. No significant decrease in reflected power was observed for these shapes.

4.5 Moving Media Simulations

This type of simulation would result in the ability to simulate the entire system process designed in this thesis. These simulations took too long to run and caused the program to become unresponsive. Due to time constraints, this simulation model was never completed or refined further in this project.

4.6 Applicator Design

The details in this section motivate the design decisions made for the waveguide applicator used in this project. The waveguide shape, length and other design specifications are discussed.

The first design decision for the applicator is that a coiled tube should be used inside the applicator to promote secondary flow for the media. Secondary flow is a process by which fluid inside the pipe "swirls" inside the pipe causing the media to mix. This mixing will distribute heat evenly through the media and helps reduce the chances of hot-spot formation [1]. Figure 45 below shows the thermal heating observed through simulation for a) rectangular waveguide structures, b) circular waveguide structures.

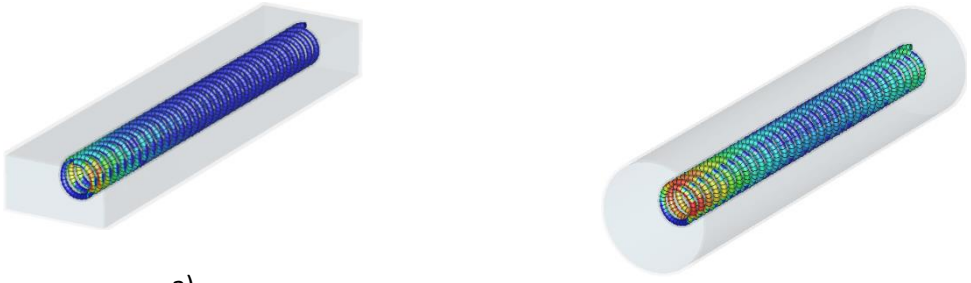

a) b)

Figure 45 - EM Thermal Coupled Simulation for Coiled Pipe a) Rectangular Waveguide b) Circular Waveguide

The circular waveguide clearly heats the water in the coiled pipe more efficiently than the rectangular waveguide structure. The greater heat seen in b) is a result of the water in the circular waveguide being in a more optimal relative location to absorb more EM power. Figure 46 below shows the S_{11} parameter over the operating frequency for the EM thermal coupled simulation seen in Figure 45.

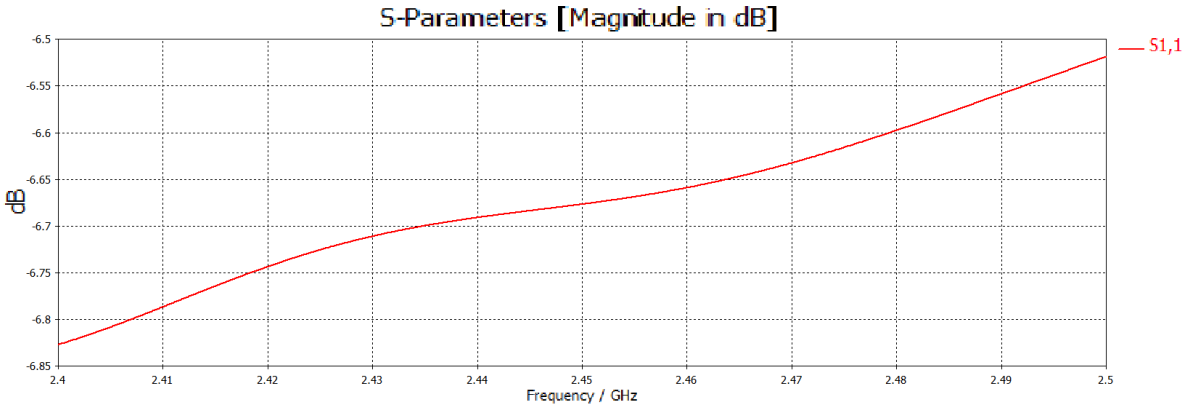

a)

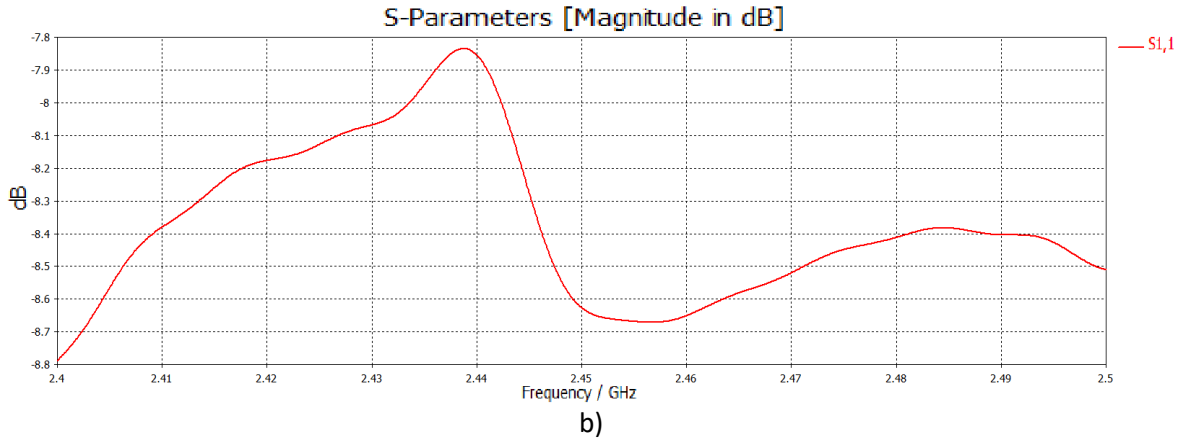

b)

Figure 46 - S_{11} Graphs for EM Thermal Coupled Simulation a) Rectangular Waveguide b) Circular Waveguide

S_{11}, also known as the reflection coefficient, is a measure of how much power leaves a radiating source compared to reflected radiated power. This means that if $S_{11} = 0$ dB it would translate to full reflection from the source. This means that no power was absorbed by the system and all the radiating power can be seen at the source. Similarly, $S_{11} = -\infty$ dB, represents full absorption by the water in the waveguide. Figure 46 a) show $S_{11} = -6.655\ dB$ and at b) shows $S_{11} = -8.625\ dB$ at 2.45 GHz.

4.6.1 Choosing a Waveguide Shape

The choice of waveguide shape is limited to the two options of either a rectangular or circular shape. Table 3 attempts to quantify the advantages and disadvantages of either the rectangular or circular waveguide shapes. This means the decision for the applicator is not solely driven by the heating patterns observed by simulations.

Table 3 - Quantifying Pros and Cons for Waveguide Shapes

No.	Point of Interest	Importance	Rectangular	Circular
1	Waveguide Inside Volume Larger	2		✓
2	Waveguide Less Bulky	2	✓	
3	Other Waveguide Component Shapes Needed	5	✓	
4	Less Modal Interference	1	✓	
5	Fabrication of Waveguide Shape Easier	3		✓
6	Fabrication of Inlet and Outlet Microwave Chokes Easier	4	✓	
7	Attenuation in Transmission Minimal	1		✓
8	Magnetron Launching Easier	3	✓	
9	Thermal Heating on Coiled Pipe Better	4		✓
10	Total Importance	25	15	10

The quantifying process can be explained by saying that points 4 and 7 have the importance value of $\frac{1}{5}$. This is because the modal interference cannot be fully simulated as the final design dimensions may differ from the perfectly simulated design structure. Similarly, the difference in attenuation of the transmission signal is negligible since the waveguides are not transporting important information from one place to another.

Points 1 and 2 get an importance value of $\frac{2}{5}$. This is because although the most compact solution is preferred, the smaller inside cross-section means the rectangular waveguide will be longer than the circular waveguide.

Points 5 and 8 receive an importance value of $\frac{3}{5}$. This is because these points directly affect the performance of the system designed. The cost value for these points is also relatively low when compared to the other costs of the system.

Points 6 and 9 show an importance value of $\frac{4}{5}$. This is because the potential sterilisation efficiency of the system may be affected. Furthermore, the cost of manufacturing custom shaped inlet and outlet attenuators greatly increases the cost of manufacturing the applicator.

Point 3 gets an importance factor of $\frac{5}{5}$. This is because the applicator is only one aspect of the entire system and needs to interface with other components. Previous systems worked with rectangular waveguide structures (e.g. rectangular bi-directional couplers for power detection). This means that if a circular waveguide were to be chosen, special circular to rectangular transitions would need to be designed. This could dramatically add to the cost of the design whilst also potentially decreasing the efficiency of the design.

4.6.2 Design Specifications

The design specifications used when designing the applicator in this project were:

- Rectangular waveguide to be used.
- The applicator will receive roughly 900 W power peaks (seen in Figure 95).
- The applicator will receive 350 W of average power.
- The applicator should reflect less than 100 W.
- A coiled pipe needs to be used for the media transport to promote secondary flow.
- Multiple temperature sensors required along the length of the pipe.
- Leakage radiation must conform with the Food and Drug Administration (FDA) guidelines.

4.6.3 Applicator Length

The applicator length can be determined by the amount of media required inside the treatment chamber. Section 2.3.3.3.3 highlighted the minimum amount of media required with respect to power. Accordingly, the minimum volume of required media for 350 W of power would be 87.5 ml. Furthermore, previous works of the EHG showed that an inner pipe dimension between 4 mm and 6 mm should be used. The reason for this is that larger diameters lead to the formation of air bubbles inside the pipe. Air bubbles are not desirable as they may cause uneven heating within the target media. Smaller diameters lead to pressure build up in the system causing seals to rupture [1].

The waveguide used had inside dimensions of 86.36 mm by 43.18 mm. This means that the outer diameter of the coil will need to be less than 43.18 mm.

Therefore, if we consider a circular coil with an outer diameter of 40 mm and an inside pipe diameter of 5 mm. We can calculate the rough volume of a single turn in the coil. This volume is found to be 2.467 ml. This means that 35.47 turns will be required to satisfy the minimum volume of 87.5 ml. The outside pipe diameter is roughly 7 mm, however, it is more realistic to assume that each turn of the coil will take up 10 mm of space in the z-direction. This means that the applicator length needs to be at least 360 mm long in order to accommodate the 36 turns required. The applicator length design in this project is 400 mm.

4.6.4 In and Out Waveguide Microwave Choke

The nature of the project specifications dictates that the liquid media needs to continuously flow through the system. This means that the liquid media will need to flow through a pipe. The pipe utilised will ultimately need to enter and exit the waveguide in order to expose the liquid media to microwave energy. The only way this will be possible is if a slot or a hole is introduced into the wall of the waveguide structure.

Introducing a slot or a hole in the wall of a waveguide is often done to create a radiating waveguide antenna. This means that the energy can escape from the waveguide and radiate. This system, however, needs to retain the energy so that it can be used to heat up the liquid media. Furthermore, leakage radiation could be harmful to individuals. This means particular care must be taken when placing slots or holes to ensure no radiation occurs [57].

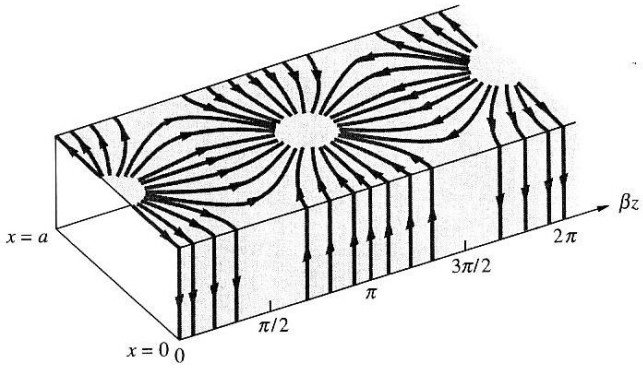

Figure 47 - Surface Currents for TE_{10} Mode [54]

Radiation occurs when the surface currents seen in Figure 47 are forced to change direction and "go around" the slot or hole [57]. The holes in this project are constrained by practical factors such as the outer width of the pipe. This means that the dimensions of the holes are likely to cause surface currents to meander around the holes, which will result in radiation.

The FDA has regulated the manufacture of microwave ovens since 1971 [58]. A Federal Standard (21 CFR 1030.10) [58] states that a microwave oven should not radiate with more power than $5\ \mathrm{mW/cm^2}$ when measured from about $5\ \mathrm{cm}$ from the ovens structure [58].

This standard means that any radiated power needs to be attenuated to an acceptable level. Adding a small circular waveguide cylinder over the hole will create a transition junction from the rectangular waveguide to a circular waveguide. The aim of this junction is to attenuate the signal so that it cannot escape the waveguide structure. The attenuation of a signal propagating in a waveguide below the cut-off frequency is large.

4.6.4.1 Mathematical Approach

The attenuation constant is derived by Abe and Yamaguchi [59] which states:

$$\alpha_{c11} = \frac{15.99}{a}\sqrt{1-\left(\frac{f}{f_c}\right)^2}\left[1-\frac{\delta}{2a}\frac{1+\left(\frac{f}{f_c}\right)^2/2.391}{1-\left(\frac{f}{f_c}\right)^2}\right], \tag{23}$$

where α_{c11} is the attenuation constant for a cylindrical waveguide, f is the propagating frequency, f_c is the cut-off frequency, δ is the skin depth and a is the radius of the waveguide ($5\ \mathrm{mm}$ in the final design).

The cut off frequency for a circular waveguide can be obtained from [60] to be:

$$f_c = \frac{1.8412\, c}{2\pi a}, \tag{24}$$

where c is the speed of light.

The skin depth obtained from [61] is:

$$\delta = \sqrt{\frac{\rho}{\pi f \mu_r \mu_0}}, \tag{25}$$

where ρ is the resistivity, μ_r is the relative permeability, and μ_0 is the permeability of free space.

For a waveguide made from aluminium, a value of $3166.7\ {}^{\mathrm{dB}}/_{\mathrm{m}}$ is obtained for α_{c11}.

To convert Watts into a value relating to dB, Equation 26 is used:

$$P_{dBm} = 10log_{10}\left(\frac{P_W}{1mW}\right), \tag{26}$$

where P_{dBm} is the power in dBm and P_W is the power in Watts.

The input power peak $900\ \mathrm{W}$ is rounded up to $1\ \mathrm{kW}$ for the calculation to add a safety margin on the calculation. This value for the peak can be converted to $60\ \mathrm{dBm}$. The power seen at exit of the attenuator can be assumed to be the $5\ \mathrm{mW}$ attained from the standards set by the FDA, which can be converted to roughly $7\ \mathrm{dBm}$. This means that the input power needs to be attenuated by $53\ \mathrm{dB}$ through the circular waveguide choke.

Since the unit for $\alpha_{c11}$is per unit length, the following relationship must hold true:

$$\alpha_L = L\alpha_{c11}\,, \tag{27}$$

where α_L is the attenuation for the value L and L is the length of the circular waveguide.

Using the relationship above, a value of $16.7\ \mathrm{mm}$ is obtained for L. This value is practically realisable. Further optimisation was achieved through simulation.

4.6.4.2 Simulation Approach

The simulation procedure below aims to confirm the mathematical results obtained above. The simulation tool was also used to investigate other microwave choke waveguide geometries. The geometries explored are circular and square; they are seen in Figure 48 below.

a) b)

Figure 48 - Simulation Objects a) Circular Choke b) Square Choke

The structures above were simulated with various lengths ranging from $10\ \mathrm{mm}$ to $60\ \mathrm{mm}$. The S-parameter, S_{21}, gave an indication of the attenuation which takes place in the system. The results can be seen below. A result of $S_{21} = 0\ dB$ means that all the power entering the waveguide is exiting the waveguide. A result of $S_{21} = -\infty\ dB$ means that none of the power entering the waveguide is making it to the exit of the waveguide.

Table 4 - S_{21} Values for Broad Optimisation Simulation

Attenuator Length (mm)	Circular S_{21}(dB)	Rectangular S_{21}(dB)
10	-32	-28
20	-62	-62
30	-92	-92
40	-128	-108
50	-151	-138
60	-180	-157

A finer variable sweep between $10\ \text{mm}$ and $20\ \text{mm}$ was then simulated to find the length which results in a $S_{21} = -53\ \text{dB}$. The length required for the circular waveguide microwave choke is $16.1\ \text{mm}$. The length required for the square microwave choke is $18.4\ \text{mm}$. The simulation confirms the result obtained in section 4.6.4.1 and demonstrates that a circular attenuator is preferable to a square attenuator.

4.6.5 Media Transport Simulation

The coiled water in the simulated model of Figure 45 a) will need to be encapsulated by a silicone pipe (discussed in section 6.3.3). A simulation model for an air-filled silicone coiled pipe with the same dimensions as the water was created to assess the material design decision. The purpose of the simulation is to ascertain whether or not the material truly is “invisible” to microwave energy. The model can be seen in Figure 49.

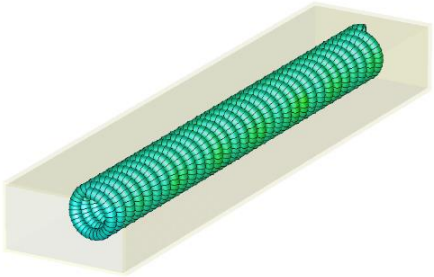

Figure 49 - Air Filled Silicone Coil Tube Model

The E-field pattern observed for the model were comparable to Figure 37 a). This suggests that the coil itself does not interact with the E-field causing a change in the modal pattern. The S_{11} behaviour can be seen in Figure 50 below.

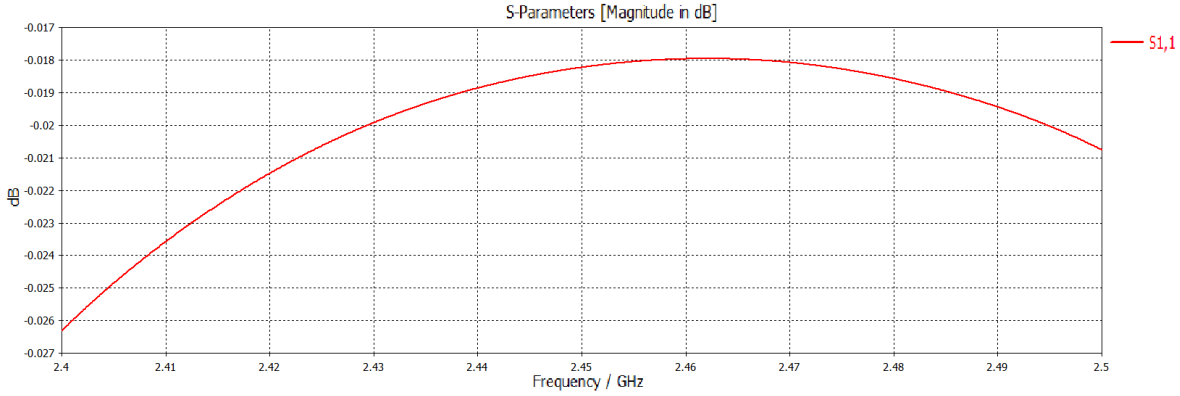

Figure 50 - EM Thermal Coupled Simulation for Silicone Coil

The expected S_{11} should be as low as possible and this is confirmed to be $-0.0182\ \text{dB}$ at $2.45\ \text{GHz}$.

4.6.5 CAD Design of Applicator

The applicator designed in this project looks like the model in Figure 51 below:

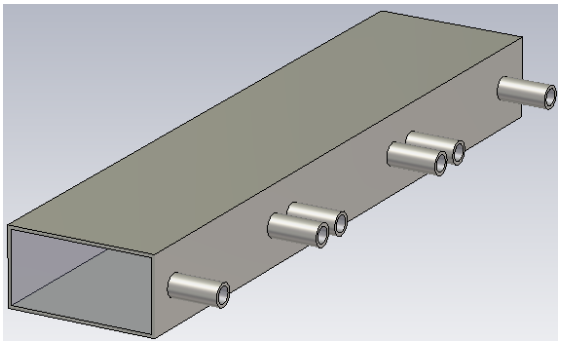

Figure 51 - Proposed Applicator Design

The coiled pipe is assembled in three equal sections. Each section of pipe exits the waveguide so that the temperature of the media can be read. The pipe will subsequently re-enter the waveguide after passing through the temperature sensor.

4.7 Chapter Conclusion

The simulation software used greatly increases the ability to understand how different EM fields interact with the target media. The size and location of the target media is very important if uniform heating is to be achieved. Observations regarding the E-field suggest that homogenous E-field patterns yield homogenous heating patterns in the target media.

The applicator geometry chosen was rectangular due to the quantitative analysis of the qualitative advantages and disadvantages shown in Table 3.

The reflected power in the design specification is achieved because an incoming forward power of $350\ \mathrm{W}$ translates to roughly $55.441\ \mathrm{dBm}$. The reflection seen in the rectangular waveguide is subsequently $48.745\ \mathrm{dBm}$ which translates to $75.6\ \mathrm{W}$. The reflection seen in the circular waveguide is $46.775\ \mathrm{dBm}$ and translates to $48.0\ \mathrm{W}$. This means that both waveguide shapes would satisfy the design specifications.

The silicone tube simulation suggests that $1.44\ \mathrm{W}$ is absorbed by the tube from an input power of $350\ \mathrm{W}$ which is less than 1%. This confirms that the silicone tubing is effectively “invisible” to microwave energy.

The applicator length was designed to be $400\ \mathrm{mm}$ long. This length holds enough coil turns to ensure the volume of media inside the applicator reaches the minimum suggested by literature.

The shape of the “in-out” waveguide microwave choke was chosen to be circular because it performed better than the square shape simulated. The length of this microwave choke was calculated to be $16.7\ \mathrm{mm}$ and simulated to be $16.1\ \mathrm{mm}$. Therefore, a length of $20\ \mathrm{mm}$ was used in the fabrication of the physical applicator to ensure a good safety margin. The diameter of the microwave choke used was $10\ \mathrm{mm}$.

The theoretical design proposed in this section conforms with the design specifications set out in section 4.6.2.

Chapter 5
Experimental System Overview

5.1 Chapter Summary

This chapter aims to illustrate all the different aspects of this project in relation to one another. The block diagrams in this chapter specifically encapsulate the entire experimental system designed in this project and shows how each hardware category interacts with other hardware categories. The block diagrams also demonstrate how various software categories interact with other software categories in this project. Finally, the block diagrams also show how hardware and software interact with each other.

5.2 Key System Subsections

Figure 52 below shows the most basic interactions between hardware and software.

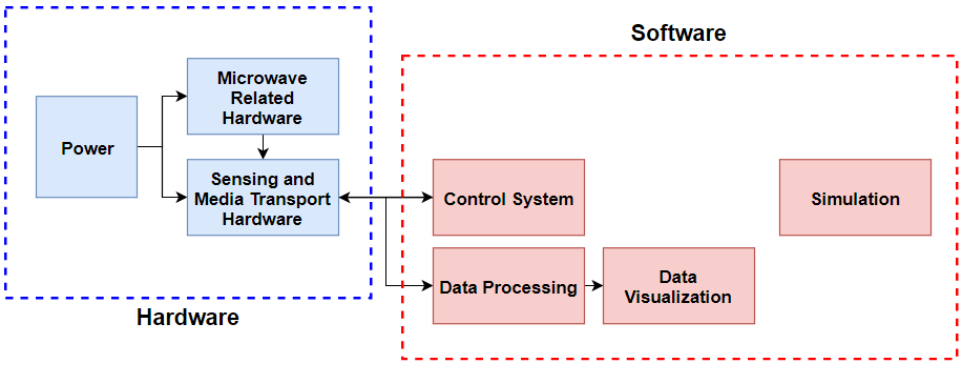

Figure 52 - Key System Subsections

The link seen between the sensing hardware and the data processing software is not required for the system to operate correctly.

5.2.1 Hardware Overview

Figure 53 below shows an expanded hardware setup and categorises the types of hardware.

The power block utilises the main supply provided by Eskom and interfaces with the electronics block through a controllable AC relay to provide power to the system. The microcontroller block is the heart of the system providing automation through a hybrid control system developed in this thesis.

The waveguide hardware used has dimensions consistent with WR340 microwave structures promoting the propagation of a single mode and was chosen in order to move away from complex multi-mode structure previously studied by the EHG.

The media transport hardware was designed with the aim of keeping the system closed to external microbiological cross-contamination. Additionally, the hardware and materials chosen attempted to remain “invisible” to microwave heating effects so that the treatment media can be specifically targeted inside the system.

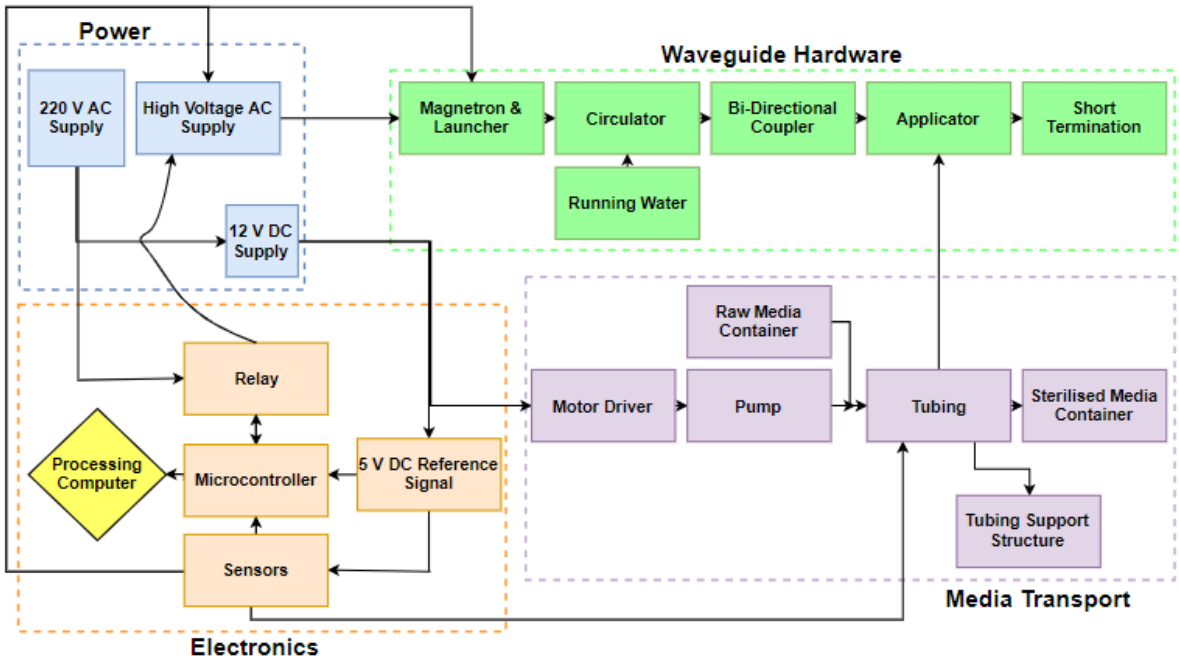

Figure 53 - Hardware Overview

The microcontroller which contains the proportional-only control system interfaces with the motor driver block (not explicitly shown in Figure 53.

5.2.2 Software Overview

Figure 54 below shows an expanded software setup and categorises the types of software and their roles in the system.

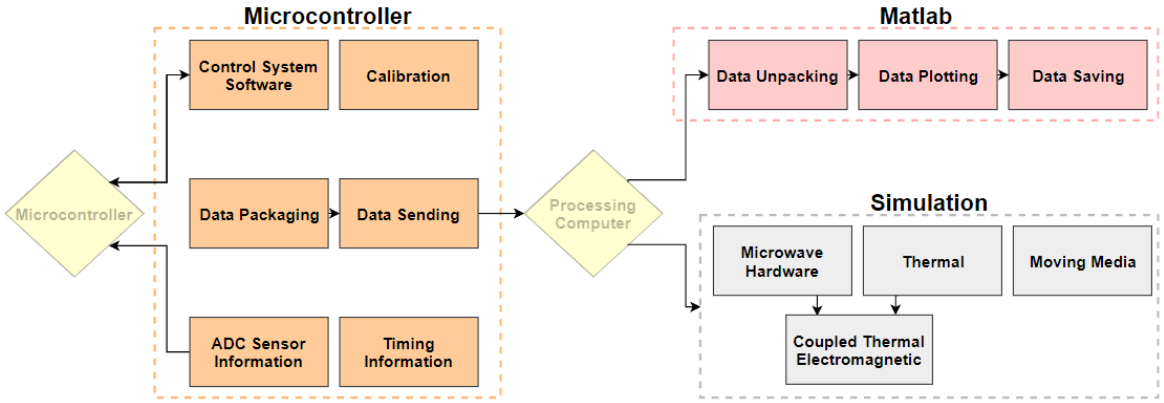

Figure 54 - Software Overview

The microcontroller in this project was responsible for reading all the information provided by the sensors. The microcontroller implements various software calibration techniques in order to ensure the data understood by the system is as accurate as possible.

5.2 Photos

This section shows two photos of the physical system designed. The first show the experimental system which was used in microbial tests and the second show a few expensive components which can be removed.

5.2.1 Physical Experimental Hardware

Figure 55 shows a labelled photo for the experimental system.

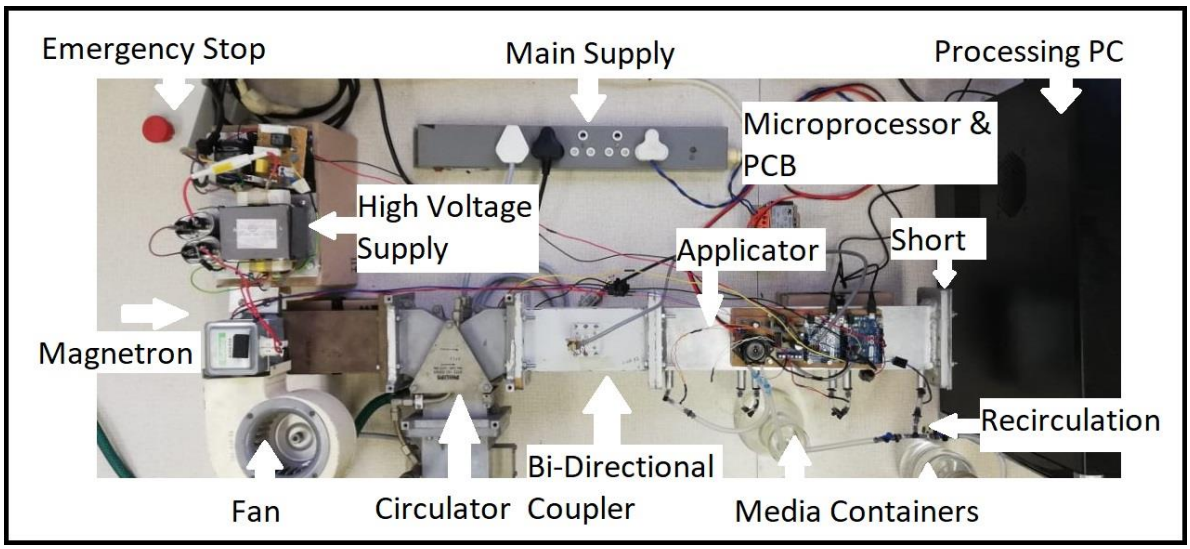

Figure 55 - Physical Experimental System Hardware

5.2.2 Physical Reduced Hardware Solution

Figure 56 shows a labelled photo for the minimum viable solution.

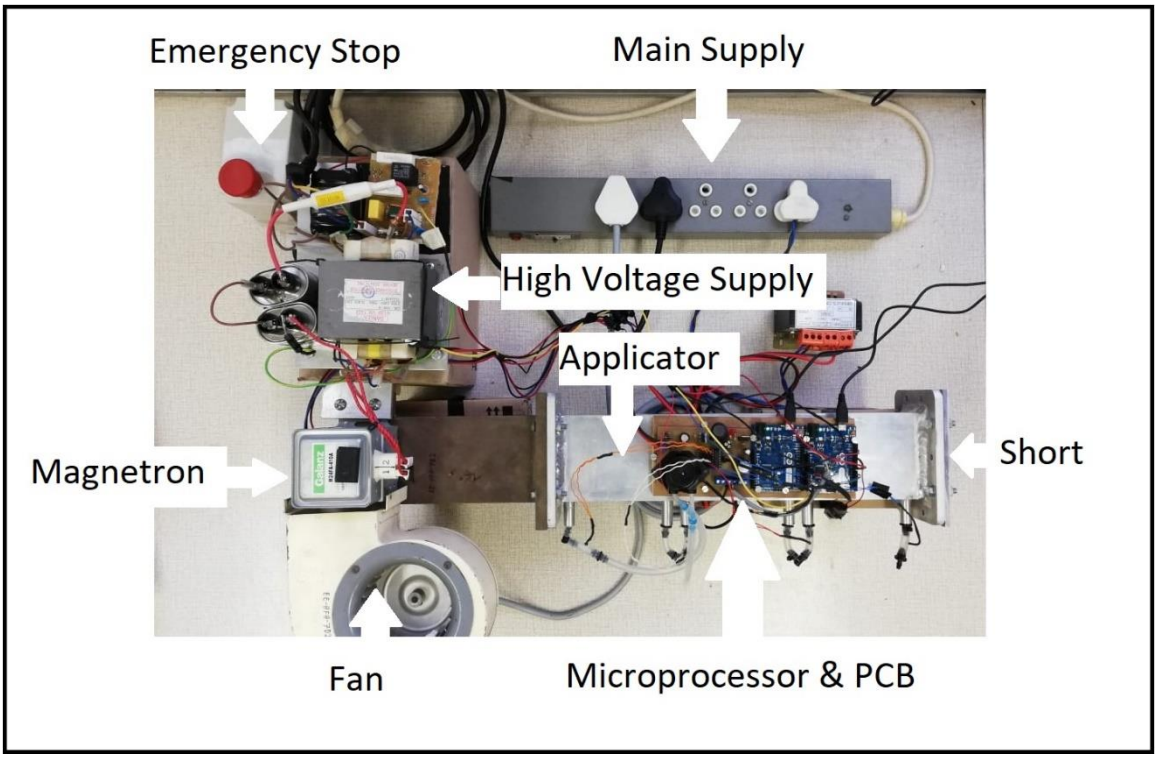

Figure 56 - Physical Reduced Hardware Solution

Chapter 6
Hardware

6.1 Chapter Summary

The hardware in this project was designed in a modular component style. This means that different components can be added or removed from the system with ease, without influencing other surrounding hardware. This style of design allows one to achieve a project prototype relatively quickly.

This chapter shows the design decisions undertaken for hardware in this project. The microwave hardware consists of the magnetron and launcher, protective circulator, bi-directional power coupler, applicator and waveguide termination. The media transport hardware consists of a motor driver, pump, tubing and media containers. The power supplies shown are the main AC supply, high voltage AC supply and low voltage DC supply. The electronics used in this project refer to the relay, temperature sensors, voltage reference, microprocessors, main processing computers and the PCB designed for this project.

6.2 Microwave Energy Hardware

A waveguide is a dielectric filled hollow structure used to propagate high frequency signals. Waveguides are used in communication and radar applications as well as any other high frequency designs [62]. The geometry of a waveguide is important with regards to the frequency which can propagate inside the waveguide. The general rule of thumb is that the cross-sectional area of the waveguide should be large enough to fit a single complete wavelength of the high frequency signal.

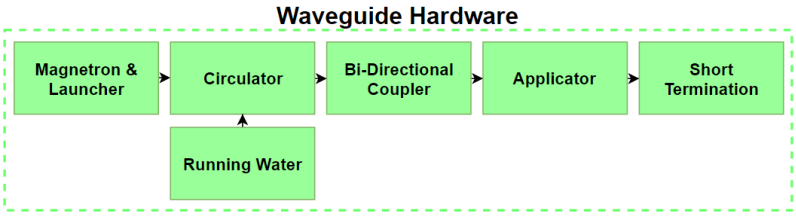

Figure 57 - Waveguide Hardware Block Diagram

For a frequency of $2.45\ \text{GHz}$, a rectangular waveguide called WR340 should be used. This waveguide has a width of $86.36\ \text{mm}$ and a height of $43.18\ \text{mm}$ and has a cut-off frequency of $1.736\ \text{GHz}$ [62]. Figure 57 above shows the modular components of the waveguide structure in this project. It is important to ensure that the individual waveguide components line up perfectly when they are connected. Imperfect connections will lead to ridges inside the waveguide structure which will cause unwanted reflections of microwave energy. This is shown in Figure 58 below.

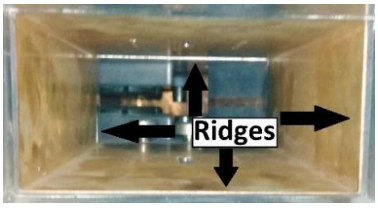

Figure 58 - Inside Waveguide Showing Unwanted Ridges

6.2.1 Magnetron and Launcher

A microwave launcher is a device used to couple microwave energy to the waveguide system. This type of device can take on many shapes and configurations. Ridged and tapered waveguide launchers are used to gradually match the impedance of transmission with that of the media load inside the waveguide applicator. This type of design leads to lower microwave reflections and higher order coupling [63].

For this project, only the fundamental mode is required to propagate. This can be achieved by mounting the magnetron antenna through a hole located on the "top" of a rectangular waveguide. This can be seen in Figure 59 below.

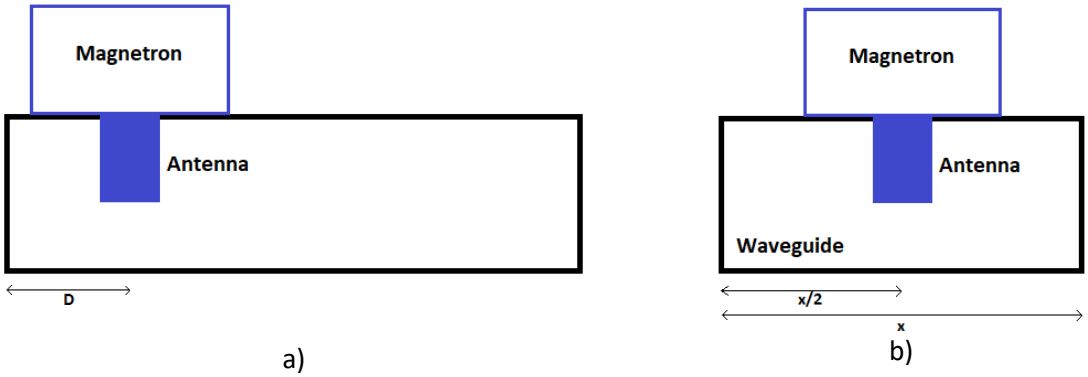

Figure 59 - a) Side View of Microwave Launcher b) Front View of Microwave Launcher

The distance D can be calculated from a magnetron coupling datasheet to be $\frac{\lambda}{4}$ [64], however, modern launchers on the market appear to have a distance D of $\frac{\lambda}{8}$ [65]. The variable, λ, is the wavelength for the frequency of propagation and the variable, x, is $86.36\ \mathrm{mm}$.

The launcher in this project has a D value of $\frac{\lambda}{4}$ and was chosen as it was available in the lab and was previously proven to work in JP van der Merwe's design.

The magnetron discussed in section 2.3.1 is a high-power device, which although very efficient, still dissipates a large amount of heat energy. This means that magnetron protection schemes should be put in place [22]. The magnetron in this project is air-cooled and has a temperature sensor attached to the heat sink. The temperature sensor is designed to turn the magnetron off if a threshold safety temperature is exceeded.

6.2.2 Circulator

Reflected power from the system could cause the magnetron to heat up undesirably. The purpose of the circulator is to negate any reflected power from the system returning to the magnetron.

The circulator in this project is a three-port waveguide component. The magnetron launcher is connected to port 1, the bi-directional coupler is connected to port 2 and a circulating water bath is connected to port 3. The basic operation of a circulator is to pass a signal entering port 1 to port 2. Furthermore, a signal entering port 2 will be passed on to port 3 whilst a signal entering port 3 is passed back to port 1 [22]. The circulator achieves this by having a ferrite rod near the centre of the component that is magnetised by a permanent magnet. The effect of this configuration results in any signal entering any port to be rotated by a set phase. The geometry of the accepting port will be aligned with this newly acquired phase of the signal. The water bath connected to port 3 is designed to absorb the reflected power entering port 2 and thus no power can be reflected out of port 3 to port 1 [22].

6.2.3 Bi-Directional Coupler

A directional coupler is a device which harnesses a pre-determined amount of EM power from a high-powered main transmission line into a secondary, lower power, transmission line. The power in the secondary transmission line is low enough to be measured by a sensing circuit and gives an indication of the forward travelling power in the main transmission line [66]. A bi-directional coupler is, in essence, two directional couplers orientated back-to-back. This configuration allows measurement of the forward travelling power as well as the reflected, backward, travelling power.

A directional coupler is a 4-port device which has the generic schematic symbol seen in Figure 60 below. The input, transmitted, coupled and isolated ports are commonly referred to as the incident, received, forward and back ports respectively [67].

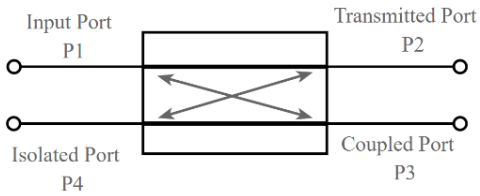

Figure 60 - Directional Coupler Symbol [66]

6.2.3.1 Ideal Characteristics of Directional Couplers

- All terminations are matched to the ports [67].
- Power travels from port 1 to port 2 with a small portion going to port 3 (none to port 4) [67].
- Similarly, for bi-directional couplers, power travels from port 2 to port 1 with a small portion going to port 4 (none to port 3) [67].
- If power were to travel through port 4, a portion will be seen at port 2 (none at port 1) [67].
- If power were to travel through port 3, a portion will be seen at port 1 (none at port 2) [67].
- Ports 1 and 4 are completely decoupled [67].
- Ports 2 and 3 are completely decoupled [67].

6.2.3.2 Calibration

A Muegge bi-directional coupler, type MW-7071-0070, was used in this project as it was available in the laboratory. This component is said to measure -60 dB of the input power from port 1 at port 3. A signal generator and spectrum analyser were used to measure the exact coupling factor for this device. Figure 61 shows the ports on the physical bi-directional coupler.

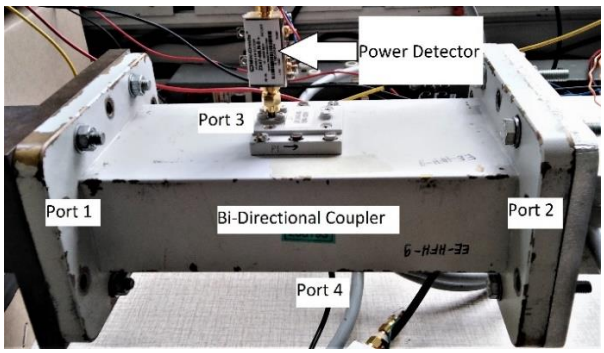

Figure 61 - Muegge Bi-Directional Coupler

The measuring process starts by calibrating the spectrum analyser with a waveguide WR340 calibration kit. The spectrum analyser has on screen prompts which are followed by configuring the required “through”, “short” and “$50\ \Omega$ load termination” and clicking “calibrate” for each.

The next step in calibration involves measuring the power lost in the cables used to connect to the spectrum analyser and signal generator respectively. The two cables are connected, with one end connected to the signal generator which outputs $0\ \text{dBm}$ at $2.45\ \text{GHz}$ and the other connected to the spectrum analyser. The loss in power can be read to be $-1.75\ \text{dBm}$.

The bi-directional coupler was then set up for calibration. Port 1 is connected to the signal generator through a waveguide to coaxial transition. Port 2 is terminated by an absorptive $50\ \Omega$ waveguide structure. Port 3 is connected to the spectrum analyser and port 4 is terminated by a $50\ \Omega$ load. The signal generator was again set to output $0\ \text{dBm}$. The measurement for port 3 read $-62.19\ \text{dBm}$. Port 3 was then terminated by the $50\ \Omega$ load and then port 4 measured. The signal generator power needed to be increased to $16\ \text{dBm}$ to measure a value of $-75.42\ \text{dBm}$.

The bi-directional coupler was turned around and the same procedure described above was followed. Port 3 (previous port 4 now seen as the coupling port for the new configuration) measured $-59.97\ \text{dBm}$. Port 4 measured $-79.55\ \text{dBm}$.

Table 5 - Calibrated Bi-Directional Coupler Characteristics

	Reverse Coupler	**Forward Coupler**
Coupling Factor	$-60.44\ \text{dB}$	$-58.22\ \text{dB}$
Isolation Factor	$-89.67\ \text{dB}$	$-93.80\ \text{dB}$

Table 5 above shows the calibrated results for the Muegge bi-directional coupler used in this project after considering the loss from the cables and the increased power to get a useable reading for the respective isolation ports. The ports were then labelled to ensure the correct orientation in the final system.

6.2.4 Applicator

A vector network analyser (VNA) is used to verify the simulated characteristics of the applicator designed in Chapter 4. The applicator contains the silicone tube coil and polystyrene support structures. The VNA set-up calibration is completed for both measuring ports before measurements are taken. These ports are then connected to either side of the applicator structure through waveguide to coaxial transitions. Figure 62 shows the response observed when no media is present in the coiled tube.

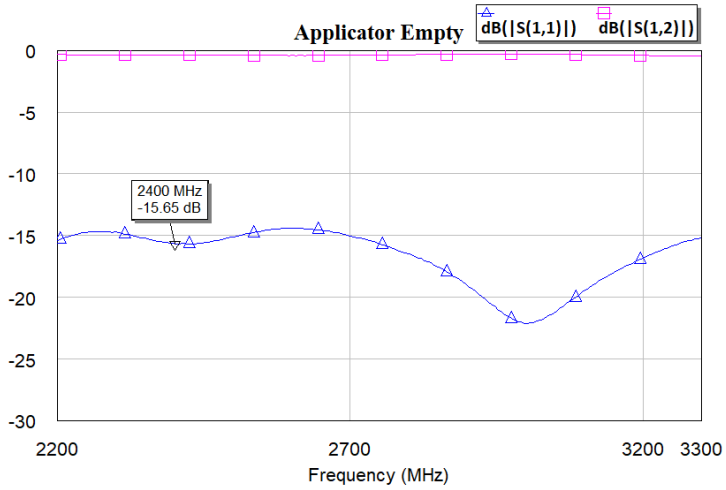

Figure 62 - Empty Applicator S-Parameters From VNA

The S_{12} line on Figure 62 has a value of -0.3494 and suggests 27 W will be absorbed by the silicone and polystyrene structures inside the applicator. This equates to roughly 8% of the 350 W input in the final system. The simulation in section 4.6.5 did not account for the polystyrene tube support. PTFE could be used to lower the relative amount of power absorbed by the media transport hardware inside the waveguide structure.

The S_{11} line on Figure 62 yields no significant information. This is because all the microwave energy is absorbed into port 2 through the antenna in the waveguide to coaxial transition and is not reflected to port 1 as designed in this thesis.

The coil inside the applicator was then filled with water and measured again. The results can be seen in Figure 63 below.

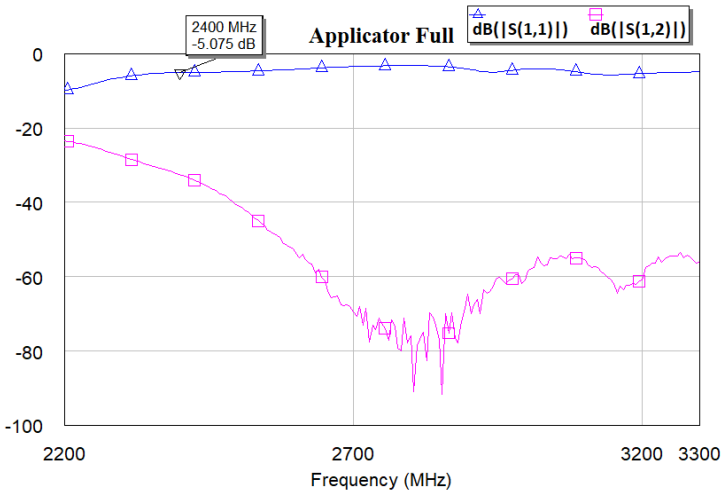

Figure 63 - Full Applicator S-Parameters From VNA

The S_{11} line on Figure 63 shows that some of the microwave energy is reflected to port 1. Since port 2 is said to be absorbing any microwave energy which reaches it, the reflected power seen at port 1 is a result of the water load. The S_{11} value suggests that 108.8 W will be reflected from an input of 350 W. This means that reflected power is roughly 31 %. This result differs from the simulation in section 4.6 and is attributed to incorrectly modelling the system for simulation. The coil in the physical design moves in and out of the applicator and the simulated design considers a perfect coil.

The S_{12} line has a value of $-36.2\ \mathrm{dBm}$ resulting in 0.0839 W seen at port 2 from the 350 W input at port 1. The amount of power absorbed by the water load after considering the power reflected to port 1 by the full coil structure and the power absorbed by the silicone and polystyrene, 214.9 W is absorbed directly by the water. This means the water load absorbs roughly 61% of the input power to the system and 0.024% is seen at port 2.

6.2.5 Waveguide Termination

The energy propagating needs to be stopped from radiating out of the waveguide structure, after it has interacted with the target media. The termination of a waveguide structure is described as either absorptive or reflective.

6.2.5.1 Absorptive Termination

Absorptive terminations occur when the impedance of the waveguide structure matches that of the termination. This type of termination maintains the characteristics of a travelling wave inside the waveguide structure. This can be achieved using a resistive load matched to the impedance of the waveguide structure. This resistive load can be created in three different ways. The first method is to fill the termination with a graphite-sand mixture, the second method is to place a resistive rod inside the termination and the third method is to place a resistive wedge inside the termination. These configurations can be seen in Figure 64 a), b) and c) respectively [68].

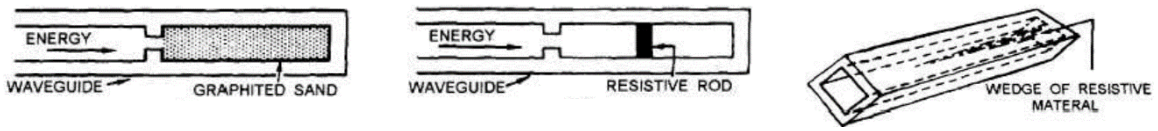

a) b) c)

Figure 64 - Absorptive Waveguide Terminations [68]

The configuration in a) absorbs EM radiation because the E and H-fields enter the termination and induce currents in the mixture. The configuration in b) is set up in the centre of the E-field which induces current in the resistive rod. The configuration in c) has the resistive material perpendicular to the H-field forces which subsequently induce currents in the resistive material. The result of these currents is the absorption of energy which is released in the form of heat [68].

6.2.5.2 Reflective Termination

Reflective terminations occur when the impedance of the waveguide structure does not match that of the impedance of the termination [68]. Reflective terminations are also referred to as “a short circuit termination” [69]. This type of termination causes standing waves inside the waveguide structure as the forward travelling wave interacts with the backwards travelling wave [68].

The easiest way to create a reflective termination is to attach a flat metal plate to the end of the waveguide structure system [68]. Alternative solutions exist which are designed to combat the standing waves created in the system. Sliding shorts, seen in Figure 65, move the termination plate a desired distance [69].

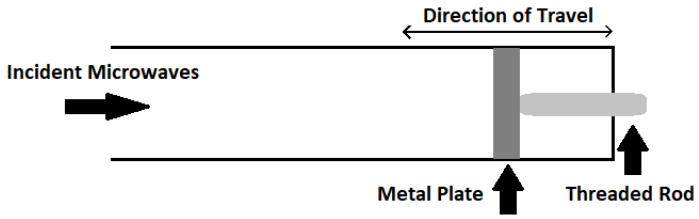

Figure 65 - Sliding Short Diagram

The configuration will result in the standing waves moving up and down along the length of the waveguide structure. Sliding shorts, however, can be very expensive and add a mechanical component to the system which is subject to wear and tear.

6.2.5.3 Waveguide Termination Design Decision

It was decided that the power seen at port 2 should be re-introduced to the system with a reflective termination. This decision is motivated by the fact that the power will get a "second chance" to heat the media as opposed to heating the termination.

A flat metal plate was chosen as it could be attached to the flange of the applicator in the same manner as all other waveguide components in the system.

6.3 Media Transport Hardware

This section describes and shows the design decisions for the hardware related to moving the media through the waveguide structures. The components include the motor driver, pump, tubing and support structures as well as the media containers. A flow diagram of these components can be seen in Figure 66.

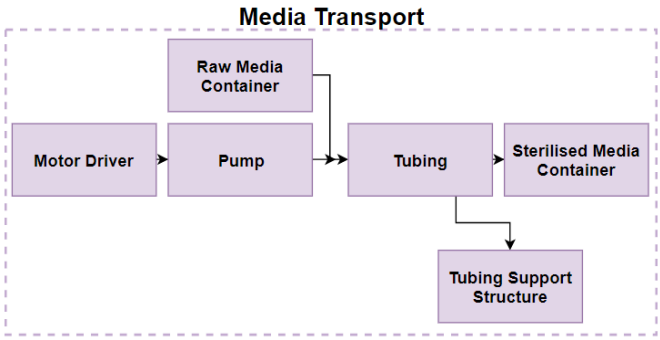

Figure 66 - Media Transport Block Diagram

6.3.1 Motor Driver

A motor driver is an electronic device used to interface microcontrollers with motors. Motor drivers are necessary because the voltage and current produced by a microcontroller is not sufficient to operate a motor properly. There are two main types of motor driver circuits considered in this project. The first is "Transistor Based DC Motor Driver Circuit" and the second is "H Bridge Circuit" [70].

The "Transistor Based DC Motor Driver Circuit" is very simple with very few components. The drawback to this design is that it is only suitable for applications where the motor is only required to operate in a single direction [70].

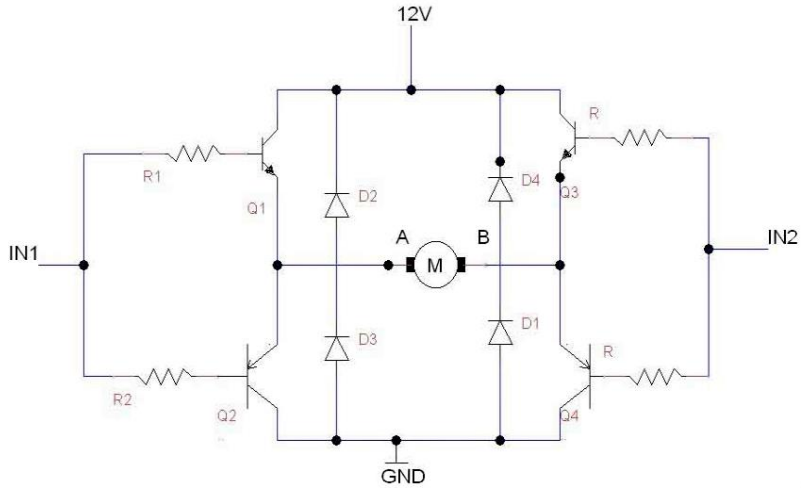

Figure 67 - H Bridge Circuit Schematic [70]

The circuit in Figure 67 shows that the "H Bridge Circuit" solution and has more components compared to the single transistor model. The advantage of this solution, however, is that the motor being driven by this circuit has the capability of moving in both the forward and reverse modes of operation [70].

6.3.2 Pump

A pump is a device used to create flow and movement of media which, in this project, can be directed through a tube. There are many different categories of pumps on the market. One category of pump is referred to as "centrifugal". These pumps are usually used in fast flow rate applications where the media has low viscosity (e.g. water). Another category of pumps commonly used are referred to as "positive displacement pumps". These pumps operate at a lower flow rate and can handle media with a higher viscosity [71][72].

Positive displacement pumps work by having an expanding cavity near the inlet side, and a contracting cavity on the outlet side. This configuration creates a pressure difference inside the pump causing the inlet to "suck" media into the pump at the inlet and expels media at the output. These types of pumps generally have two different configurations that are of interest. The first is called reciprocating and the second is referred to as rotary [71].

Reciprocating pumps have a piston which moves back and forth making an internal media chamber larger and smaller. The piston action coupled with one-way valves ensure that the media flow is in a single direction. An example of a reciprocating pump can be seen in Figure 68 below and is called a diaphragm pump [71].

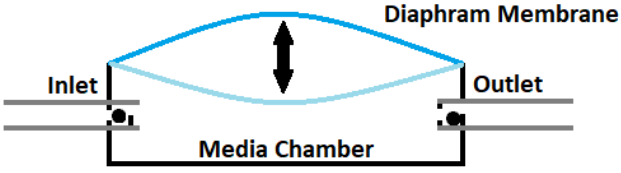

Figure 68 - Diaphragm Pump Diagram

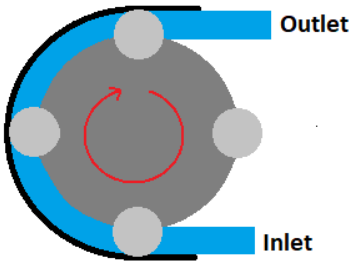

Figure 69 - Peristaltic Pump Diagram

Rotary pumps operate using a spinning gear. The spinning motion accepts media at the input and "pushes" the media out the outlet. An example of a rotary pump is called a peristaltic pump and can

be seen in Figure 69 above [71]. Peristaltic pumps have the benefit of operating in both forward and reverse directions (i.e. the inlet and outlet are interchangeable). Peristaltic pumps also have the advantage that media can remain in a closed system as the rotating gear compresses the tube carrying the media. Operating within a closed system is desirable for the sterilisation industry as the risk of cross-contamination is reduced because the pump cannot "leak" [72]. Table 6 below highlights some of the key features of two shortlisted pumps for this project.

Table 6 - Comparison Between Shortlisted Diaphragm and Peristaltic Pumps

	Diaphragm Pump	**Peristaltic Pump**
Price	R 776.88	R 355.00
Flow Rate	$9\ {}^{litres}/_{hour}$	$6\ {}^{litres}/_{hour}$
Bi-directional	No	Yes
Temperature Range	0-100 °C	0-40 °C
Pressure	1 bar	1 bar
Variable Flow Rate	Yes	Yes

The complete datasheet/product information for the diaphragm and peristaltic pumps can be found at [73] and [74] respectively.

6.3.3 Tubing and Support Structure

The tubing in this project was required to be moulded into a coil which could be held in place inside the applicator. Particular care must be taken when selecting the materials be used. Section 2.3.3.3.1 shows that the dissipation factor ($tan\delta$) can indicate how much microwave energy will be absorbed by a material. The tubing and support structures should therefore have an ideal dissipation factor which is as small as possible.

The dissipation factor of a material is both temperature and frequency dependant. Table 7 below shows values for dissipation factor for relevant materials at a temperature of $25\ °C$ and a frequency range of $1 - 10\ \mathrm{GHz}$ [75].

Table 7 - Dissipation Factor for Relevant Materials

Item/Material	**Can be Used as Tubing**	**Can be Used as Support**	**Dissipation Factor ($tan\delta$)**
PTFE (Teflon)	Yes	Yes	0.0001 - 0.0002
Polystyrene	No	Yes	0.0002 - 0.0003
Borosilicate Glass	Yes	Yes	0.001 - 0.002
Silicone	Yes	No	0.01 - 0.05
Water*	No	No	0.1 - 1.0
*Presented in this table as a comparison			

PTFE appears to be the obvious choice for the material to be used for both the tubing as well as the supporting structure according to the dissipation factor. PTFE, however, has a much higher cost when compared to silicone and polystyrene. The ideal inside tube diameter is between $4 - 6\ \mathrm{mm}$. Experiments were conducted in the lab with a small length of PTFE tubing. The experiments ascertained that the PTFE tubing is not particularly malleable and as a result cannot bend in a tight enough coil without kinking. Similar experiments were conducted on silicone tubing and the results

showed that the correctly sized coiled structure could be built from it. This can be seen in Figure 70 below.

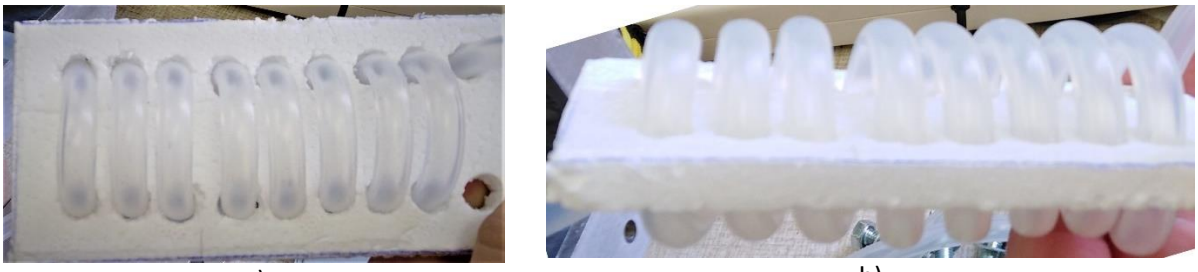

a) b)

Figure 70 - Coiled Pipe Configuration a) Top View b) Side View

Polystyrene support structures were used to hold the tube in the required coiled shape; the material was considered adequate as polystyrene can hold its own physical shape, as well as having a very low dissipation factor.

6.3.4 Media Containers

The media containers in this project, by necessity, have to be easy to transport and need to withstand a laboratory autoclave. This is to ensure sterility before media is put into the container. It is important that steps be taken to avoid cross-contamination when testing the system.

Schott bottles were selected, and their lids modified to allow the tube to enter the media container. The modified lids, seen in Figure 71 a) and b), have dedicated breather holes which are stuffed with cotton wool. This configuration ensures the system remains closed to the influences of outside elements as far as possible and ensures that no pressure can build up in the system.

a) b)

Figure 71 - a) Input/Output Media Container b) Media Container Lid

The input media container lid, seen in Figure 71 a), has a third hole to allow the possibility of recirculating the output media back to the input container until the desired target output temperature is achieved.

6.4 Power Supplies

This section highlights the various electrical signals required by this project.

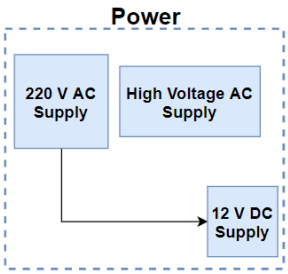

Figure 72 - Power Block Diagram

Figure 72 above, illustrates that the main AC supply is used to create the high voltage AC supply required by the magnetron. The main supply is also used to create the low voltage DC supply required by the motor in this project.

6.4.1 AC Supply - 220 V_{rms}

The main power supply in this project is provided by Eskom and has a rated voltage of $230\ \mathrm{V} \pm 10\%$ at 50 Hz [76].

6.4.2 High Voltage AC Supply

The schematic for the high voltage supply can be seen in Figure 9. The components for this was salvaged from a conventional microwave oven and adapted using saturable reactor control (discussed in section 2.3.2.6) by introducing an additional identical high voltage capacitor in series with the $0.95\ \mu\mathrm{F}$ capacitor seen in the voltage doubling block. This configuration results in halving the net value for the high voltage capacitor which, in turn, roughly halves the output power produced by the magnetron. Figure 73 shows the high voltage supply used in this project.

Figure 73 - Modified High Voltage Supply

The output power can be further reduced with the addition of a third high voltage capacitor.

6.4.3 DC Supply - 12 V

The $12\ \mathrm{V}$ supply in this project is required to power the pump motor and serve as an efficient step-down pre-regulator for a linear voltage regulator. The $12\ \mathrm{V}$ supply makes use of a LM2576 switching regulator which has a wide input voltage range and an adjustable output voltage. Figure 74 below shows the schematic design for this regulator and component values and can be found in Appendix A.

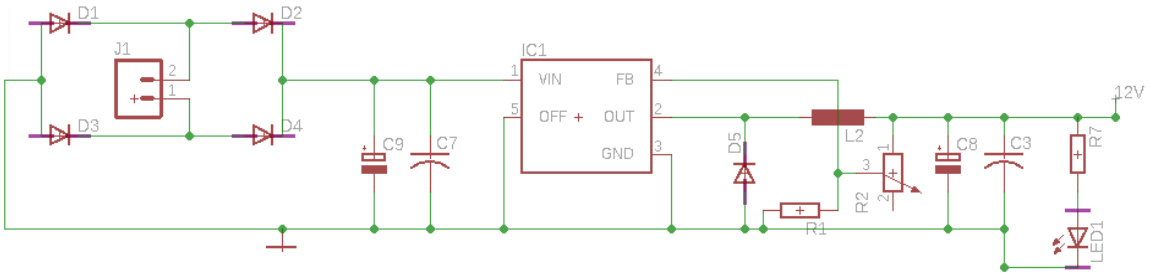

Figure 74 - 12 V DC Supply Schematic

A switching regulator was chosen as they are more efficient and produce less heat when large differences are present between the input and regulated output voltages.

Figure 75 below shows the oscilloscope measurement for the 12 V supply.

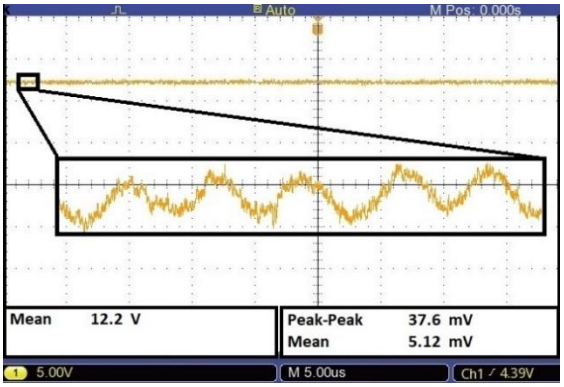

Figure 75 - Oscilloscope Measurement for 12 V DC Supply (LM2576)

The ripple voltage seen on the signal is less than 1% and deemed satisfactory.

6.5 Electronics

The electronics in this section focus mainly on sensing important information about the system so that it can be analysed by a microprocessor. Sensing information is crucial so that the microprocessor can make decisions on how to best control the system.

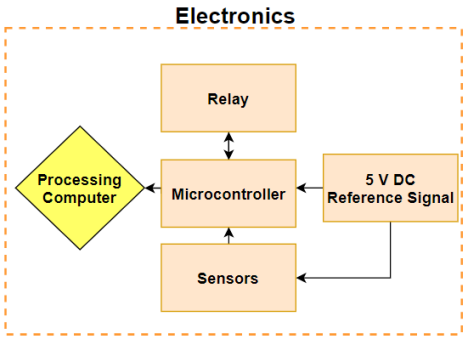

Figure 76 – Electronics Block Diagram

Figure 76 above summarises this section and the electronics include a power relay, microprocessor, temperature sensors, DC reference voltage, waveguide power detectors and a processing computer.

6.5.1 Relay

The position of the relay in this project can be seen in Figure 9. The primary role for this relay is to turn the main supply to the high voltage magnetron supply "on" and "off". This is necessary as the magnetron must only be powered "on" once the sterilisation process has been set to "start". Additionally, this relay will turn the main supply "off" if the magnetron or high voltage transformer reach an undesirable temperature during operation.

The component selected for this is a $10\ \mathrm{A}$, optically isolated, ESR500 series solid state relay. This relay has zero-crossing detection built in to minimise electromagnetic interference (EMI) when switching and operates in the frequency range between $47\ \mathrm{Hz}$ and $63\ \mathrm{Hz}$. This relay further boasts low power consumption and low turn on current control ($15\ \mathrm{mA}$ maximum) which is perfect for a microprocessor to directly control.

Due to the zero-crossing detection switching capabilities, this relay can implement switching strategy 1 discussed in section 3.2.1. Although this switching strategy is deemed not viable for sterilisation purposes, a control strategy may be developed where the flow of media is halted in the "off" periods.

6.5.2 Microprocessor

The microprocessor used in this project was an Arduino Leonardo which is based on the ATmega32u4 microcontroller. This device has a $16\ \mathrm{MHz}$ crystal oscillator, provides 10-bit resolution for analogue readings and operates with $5\ \mathrm{V}$ logic level ($5\ \mathrm{V}$ seen as a binary 1 and $0\ \mathrm{V}$ seen as a binary 0). This microprocessor was programmed through the Arduino integrated development environment (IDE) and the coding language used is C++. This device communicates with the processing computer using a universal serial bus (USB) COM port.

The final prototyped design in this project required the use of two Arduino Leonardo's running in parallel. This configuration was necessary because a single Arduino Leonardo could not perform all the sensing and data sending fast enough, simultaneously, to capture the waveforms produced by the power detection circuitry as well as the control system software. This means that the first Arduino Leonardo board is dedicated to temperature sensing and the control system software and the second Arduino Leonardo is dedicated to the power sensing circuitry and the sending of this data to the processing computer.

6.5.3 Temperature Sensors

Temperature sensors in this project are crucial for the control software and overall safety of the system. Four temperature sensors are used to measure the temperature of the target media and two temperature sensors are used to monitor the magnetron and high voltage transformer.

Section 3.4 notes an issue with regards to infra-red temperature modules. In addition to this issue, infra-red modules can be very expensive when compared to other temperature sensors on the market. A type of temperature sensor which can be place in-line with the flow of the target media is called a thermistor. A thermistor is a type of resistor whose resistance value changes depending on the temperature of the component. Many thermistors, however, are not suitable for immersion in a fluid as this may cause the component to short circuit. This can happen when the component leads are exposed to the fluid creating a different conducting path along which the electrical signals travel.

A negative temperature coefficient (NTC) thermistor was acquired with special insulated leads. The insulation on the leads is an ochre-coloured epoxy layer. The datasheet for this component highlights that the thermistor can be placed in-line with the target media and has a response time of

0.7 s in oil. The thermistor has an operating temperature range of -40 °C to 125 °C and an accuracy of $\pm$ 0.5 °C between 25 °C and 85 °C [77].

Figure 77 below shows how the resistance of the thermistor changes with respect to temperature.

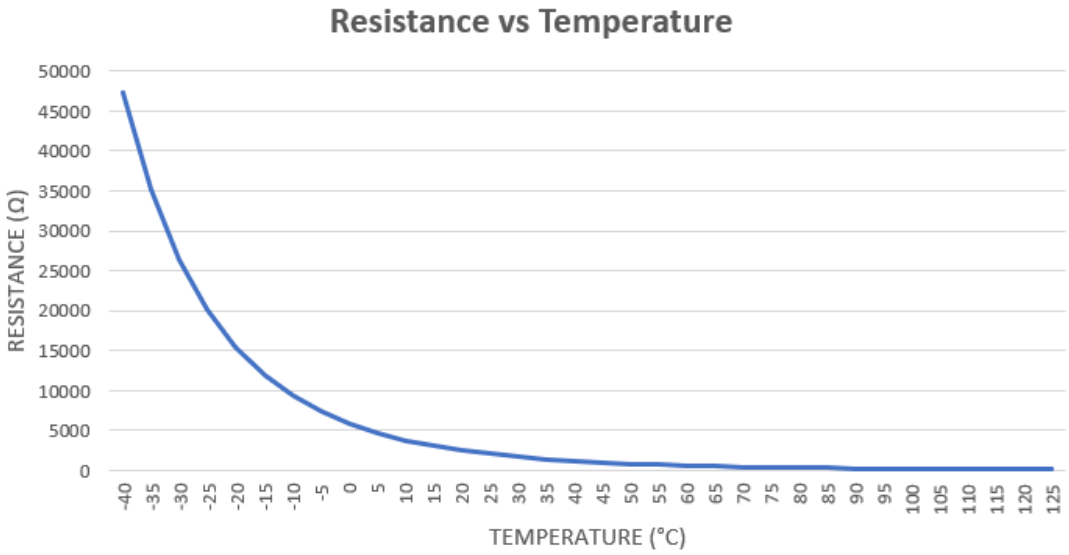

Figure 77 - Vishay® NTC Thermistor Resistance vs Temperature

Figure 78 shows the voltage divider circuit used with the thermistor.

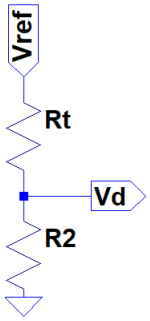

Figure 78 - Voltage Divider Schematic

$$V_d = \frac{V_{ref} * R_2}{R_t + R_2} \tag{28}$$

Equation 28 shows the mathematical relationship for the circuit in Figure 78. V_d is the divided voltage which is measured by the microprocessors ADC. V_{ref} is the reference voltage in section 6.5.4, R_t is the resistance of the thermistor shown in Figure 77 and R_2 is a fixed resistor which needs to be selected. The design objective in the selection of R_2 was to get a linear relationship between temperature and the voltage V_d for an operating temperature range between 20 °C and 100 °C. Figure 79 shows the relationship between V_d and temperature with the data extracted from Figure 77 for R_t and various values for R_2.

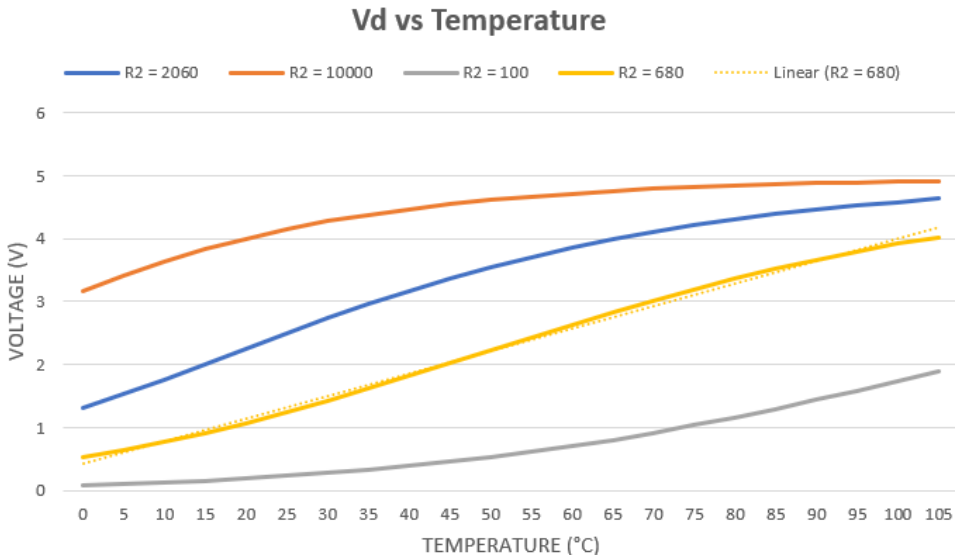

Figure 79 - V_d vs Temperature

Common resister values were chosen for R_2 and a linear response is observed for a value of $680\ \Omega$.

6.5.4 DC Reference Voltage - 5 V

The 5 V supply in this project is required to provide a steady reference voltage for the Arduino Leonardo's ADC as well as the temperature sensing circuitry. The 5 V supply makes use of a LM7805 positive voltage regulator which has a fixed output voltage. Figure 80 below shows the oscilloscope measurement for the 5 V supply.

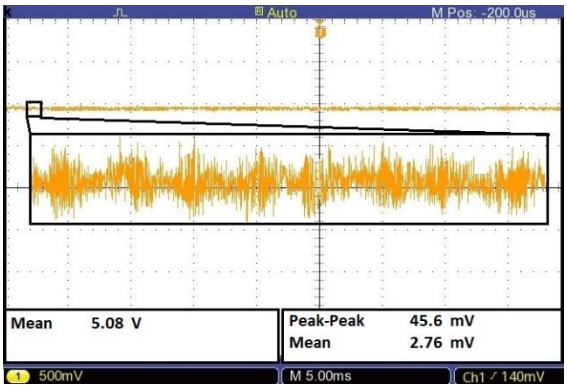

Figure 80 - Oscilloscope Measurement for 5 V DC Supply (LM7805)

The ripple voltage seen on the signal is less than 1% and deemed satisfactory.

6.5.5 Power Detectors

The power detectors in this project measure the forward and reverse power seen at the relevant ports of the bi-directional coupler discussed in section 6.2.3. The components used are Mini Circuits® power detector series ZX47-40LN-s+ which have a wide bandwidth, temperature stability and require a 5 V supply. The components have a measuring range between -40 dBm and 20 dBm over a frequency range of 10 MHz to 8 GHz.

The datasheet for these devices shows that the detectors output a specific voltage with reference to the input power received. The output voltage heavily relies on the temperature of the component, the frequency being received, and the output load connected to the component.

The power detectors in this project were calibrated in an air-conditioned room at $22\,°C$ at a frequency of $2.45\,GHz$ and an output load of $1000\,\Omega$. The results of this calibration process can be seen in Figure 81 below.

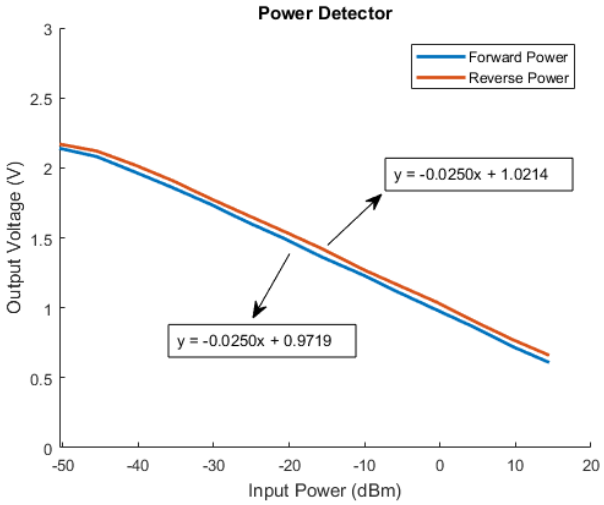

Figure 81 - Power Detector Calibration Graph

The forward and reverse calibration lines are not identical, and this is because the reverse power detector cannot be attached directly to the bi-direction coupler due to physical constraints. The result of this is that the power detector is connected through an extension cable.

The output from the power detectors was measured on an oscilloscope while the magnetron was "on". The waveform can be seen in Figure 82 below.

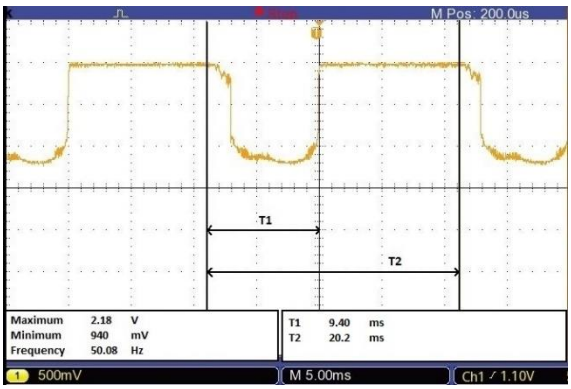

Figure 82 - Power Detector Output Waveform During System Operation

Figure 82 shows that the conventional magnetron in this project outputs homogenous high-power pulses of microwave energy. Section 7.2.5.3 shows how this signal was captured in software and section 7.3.2.2 shows how the captured signal can be mathematically manipulated to find the peak and average power.

6.5.6 Processing Computer

The processing computer in this project is a stand-alone desktop personal computer (PC) running Microsoft Windows 10. Both Arduino Leonardo's are connected to this PC through two separate dedicated USB cables.

6.5.7 PCB Design

The PCB designed in this project contains the circuitry for the $12\ \mathrm{V}$ supply, $5\ \mathrm{V}$ reference signal, temperature sensing circuitry, motor driver and motor mount. The schematic, parts lists and PCB can be found in Appendix A.

6.6 Chapter Conclusion

This chapter presented some of the design decisions when considering various hardware components in this project.

A waveguide size called WR340 was used as the dimensions are a standard for the single mode propagation of EM waves at $2.45\ \mathrm{GHz}$. The magnetron antenna is placed at a distance of $\lambda/4$ from the launcher's reflective termination. The magnetron is air cooled and has a safety temperature attached to the heatsink. A circulator was implemented during the development stage of this project to protect the magnetron from reflected EM power. The EM power in the system is measured using a bi-directional coupler paired with Mini Circuits® power detectors. The waveguide system is terminated with a simple reflective flat metal plate.

The media transport hardware decisions included the use of a peristaltic pump. This was introduced to keep the system isolated from the surrounding environment as far as possible in order to lower the risk of cross-contamination. The pump motor is driven by an H-bridge so that bi-directional control of the pump motor can be achieved. Silicone tubing was used to construct the coil as the ideal PTFE tubing was not malleable enough to bend into the required coil dimensions to fit into the applicator. Polystyrene tubing support structures were used as the material is cheap and readily available in the laboratory as well as having the benefit that the dissipation factor is similar to that of PTFE. Schott bottles with modified lids were used for sterilisation experiments as the containers may be placed in an autoclave. The modified lids were designed to reduce the risk of cross-contamination during testing and transportation of the media between departments.

The power supplies in this project make use of Eskom's main supply and powers the high voltage supply, $12\ \mathrm{V}$ supply and $5\ \mathrm{V}$ reference signal. The transformer from the high voltage supply has a safety thermistor attached to the transformer core housing.

Two Arduino Leonardo microprocessors are run in parallel: one for temperature sensing and control and the other to capture the power detectors output waveform signal. The Arduino's directly interface with the processing computer used in this project.

NTC thermistors with insulated leads are placed at four different points along the silicone coil.

Chapter 7
Software

7.1 Chapter Summary

This chapter discusses the software used in this project. The software includes scripted code written to perform required tasks and highlights other software packages used during this project. Software calibration of hardware techniques are shown and discussed.

Figure 83 below briefly outlines important key software features in this project.

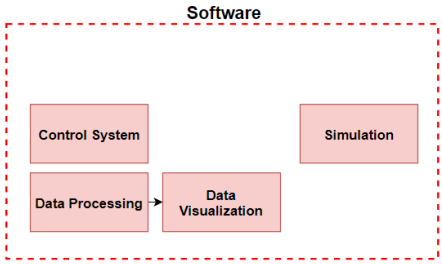

Figure 83 - Software Overview

This chapter illustrates how various coded scripts operate and communicate using flow diagrams.

7.2 Microcontroller Software

The microcontrollers in this project are used to gather information about the system, control the system and subsequently send the information to the processing computer.

Figure 84 illustrates key functions of the software for the microcontrollers in this project.

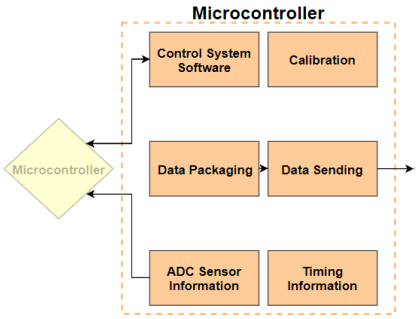

Figure 84 - Microcontroller Software Block Diagram

The microcontroller ADC's, temperature sensor information, power detector information and software run times are calibrated to yield accurate results. A data packing strategy was discussed to achieve an acceptable program loop time.

7.2.1 ADC Calibration

Good calibration of a system requires the calibration of every step in a system. The first step to calibration starts at the point where information is converted to a useable form for the microprocessor. For this project, the ADC's on the microcontroller are used.

ADC's work by creating a number between 0 and 1023 depending on the voltage supplied to the ADC input pin on the microcontroller. An ADC value of 0 should represent 0 V and a value of 1024 should represent the reference voltage supplied to the microcontroller.

The method used to calibrate the ADC's in this project involves attaching all the ADC's together to a common node (the same reference point). This node is then grounded (0 V) and measurements are recorded. This method of recording values is repeated by changing the value of the node connected to the ADC's with an external variable power supply. The voltage is changed by half-volt increments and the ADC values noted until an ADC value of 1023 is observed. The results are shown in Table 8.

Table 8 - ADC Calibration Values

ADC#	**Voltage (V)**											
	0	0.5	1	1.5	2	2.5	3	3.5	4	4.5	5	5.05
0	0	100	211	301	407	507	608	711	820	917	1017	1023
1	0	100	212	301	407	507	607	710	821	917	1017	1023
2	0	101	213	302	407	507	608	711	820	917	1017	1023
3	0	100	213	301	408	507	608	711	821	917	1017	1023
4	0	100	212	301	407	507	608	711	821	916	1016	1023

In an ideal environment, all the ADC's should produce the exact same value because they are all connected to the same node at the same time.

Figure 85 shows that all the ADC's follow a linear trend and have no major discrepancies between each other. Equation 29 (shown below Figure 85 on this page) shows the relationship between ADC value and the voltage seen at the ADC. It is used when converting the ADC values to voltages in software.

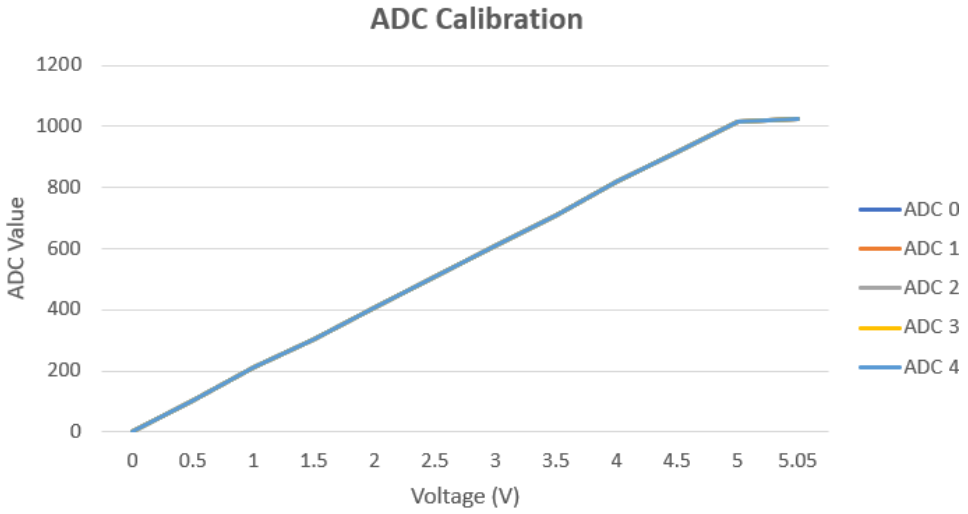

Figure 85 - ADC Calibration Graph

$$y = 203.77x - 1.85 \tag{29}$$

A possible reason for the slight differences seen in Table 8 may be due to the program running on the microcontroller sequentially. This means that each ADC is read one by one and not at the exact same time. This slight time change between readings means that the voltage "ripple" on the signal

may change between readings. The calibration process not only defines the linear relationship between ADC value and voltage but shows that ADC's produce results which are accurate relative to each other.

7.2.2 Calibrating Media Temperature Sensors

The calibration method used for the temperature sensors involved placing a digital temperature measuring probe in-line with each individual thermistor used in the system. The media was heated using the magnetron to various controlled temperatures. The voltage produced by the sensing circuit was then recorded with the corresponding digital temperature achieved. Figure 86 shows the data generated.

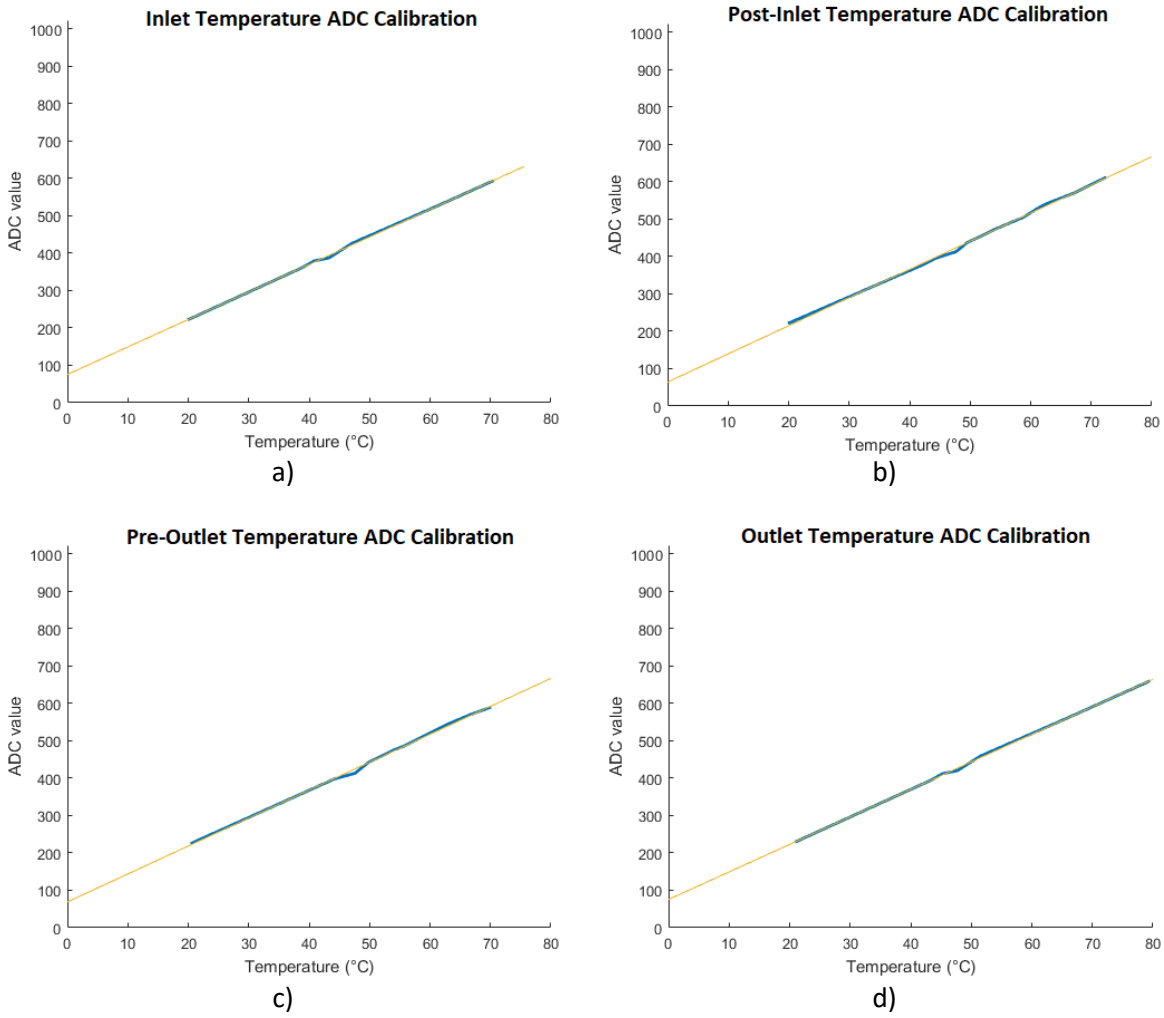

Figure 86 - Temperature Sensor Calibration a) Inlet Sensor b) Post-Inlet Sensor c) Pre-Outlet Sensor d) Outlet Sensor

The data produced shows that a linear equation can be fitted to each sensor which relate ADC value to temperature. Equations 30 – 33 show the relationship used in software.

a) $$y = 7.3295x + 75.355 \quad (30)$$

b) $$y = 7.5329x + 64.127 \quad (31)$$

c) $$y = 7.4716x + 68.989 \quad (32)$$

d) $$y = 7.3627x + 75.439 \quad (33)$$

7.2.3 Arduino Data Types

When programming a microcontroller, it is important to understand variable data types. A data type is a format in which data is stored. Different data types have different ranges of values which they represent [78]. Understanding data types and their assignation is crucial because if the microcontroller attempts to store a value which exceeds the value range of an assigned datatype, errors are likely to occur, and the code will not behave as intended. Table 9 represents all the variable data types available in the Arduino IDE.

Table 9 - Arduino Data Types

Data Type	Bytes Required	Variable Range		
byte	1	0	to	255
char	At least 1	0	to	255 or more
unsigned char	1	0	to	255
int	2	-32768	to	32767
unsigned int	2	0	to	65535
short	2	-32768	to	32767
long	4	-2147483648	to	2147483647
unsigned long	4	0	to	4294967295
double	4	-3.4028235E+38	to	3.4028235E+38
float	4	-3.4028235E+38	to	3.4028235E+38

A data type not represented in Table 9 is the data type “string”. The string data type is defined by an array of “char” characters ended by a null termination identifier (“\0”). The termination character is required so that the microcontroller understands when the string is complete [79].

7.2.4 Control System Arduino Leonardo

The control system code oversees reading ADC information, converting the data to a temperature value and then implementing the proportional control designed in Chapter 8. Figure 87 shows a flow diagram depicting how the code operates within the microcontroller. The temperature response in the system behaves differently depending on whether or not the coil is partially filled versus completely filled. This means that a hybrid control strategy had to be developed in order to control the media temperature at all stages of operation. Table 10 describes the meanings of the words used in the flow diagram.

Table 10 - Flow Diagram Word Meanings

Flow Diagram Word	Meaning
serialUp	Is there a valid serial connection between the Arduino Leonardo and the processing computer?
byteAv	Is there a byte available on the serial line to read?
isRun	Is the program run flag set for the motor to start pumping and turn the magnetron “on”?
T3	Outlet temperature sensor
T2	Pre-Outlet temperature sensor
T1	Post-Inlet temperature sensor
conSig	Pulse Width Modulation (PWM) control signal used to drive the pump with duty cycle control
relayFlag	The flag which tells the system that the power to the magnetron should be turned “off”
isButP	Is the button pressed which by-passes the system and sets the pump at maximum flow rate?

The hybrid control strategy works by monitoring the post-inlet, pre-outlet and outlet temperature sensors. The proportional control characteristics for each sensor is defined in code. The code will choose to control the dominant sensor until the output temperature is finally controlled and maintained. The dominant sensor in the code is defined as the sensor which is closest to the output and above $35\ ^{\circ}\mathrm{C}$.

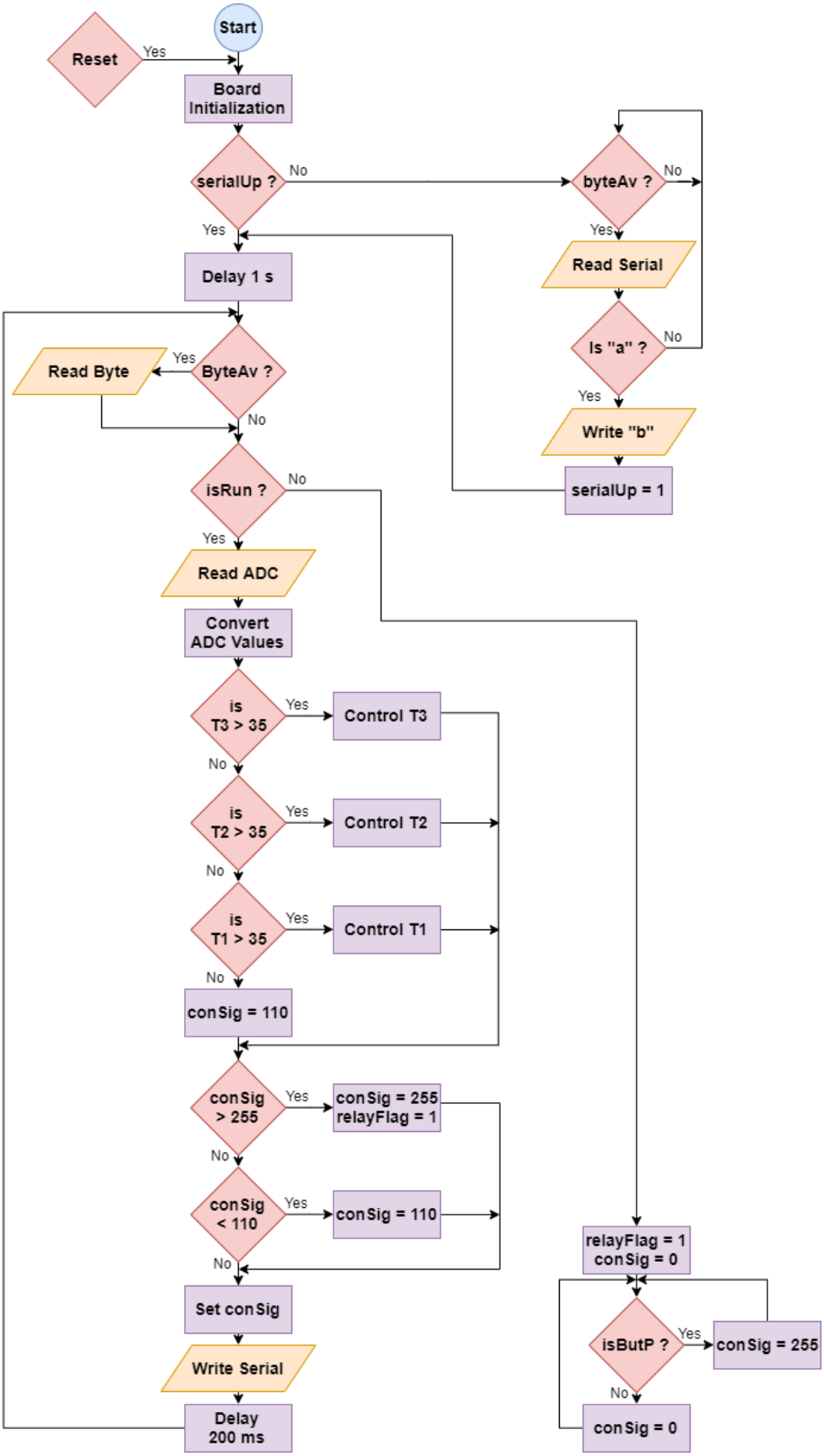

Figure 87 - Control System Flow Diagram

7.2.4.1 Data Packing and Sending

Each loop cycle in code gathers ADC information, this information is converted to a useable form for the control system algorithm. The information is then sent over the serial connection to the processing computer. Figure 88 shows the format in which information is sent.

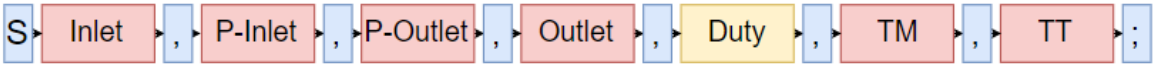

Figure 88 - Control System Arduino Data Protocol

The blue blocks represent the data type “char” and are intended to show the start and end of a data section as well as separating the different sensor readings. The red blocks represent temperature readings and are data type “int”. The orange block represents the PWM control signal used to control the speed of the pump and is of type “int”. TM represents the temperature of the magnetron and TT represent the temperature of the transformer.

The serial line on the Arduino Leonardo is set to run at a baud rate of 57600 bps (bits per second). Serial information is configured to “send 1 start bit” and “1 stop bit with no parity bit”. This means that for every byte of information that is transferred, 10 bits are required. The transmission in Figure 88 contains 22 bytes which is expected to take $3.82\ \text{ms}$ to transfer over the serial line.

7.2.4.2 Calibrating Timing Information

The time between serial samples of data is required by the processing computer so that graphs can be generated to portray the information accurately. The time between each sample can be calculated by Equation 34:

$$T_s = T_d + T_r\ , \tag{34}$$

where T_s is the time between samples, T_d is the delay time in the program loop and T_r is the run time of the loop before the delay.

7.2.5 Power Detection Arduino Leonardo

The power detection software runs simultaneously with the control system software and has the goal of looping and reading data samples from the ADC’s as fast as possible. This microcontroller only reads from two ADC’s and the information gathered is the forward power waveform and the reverse power waveform.

7.2.5.1 Data Packing and Sending

Data is sent similarly to section 7.2.4.1 and Figure 89 shows the format in which information is sent for the power detector software. The ADC produces a number between 0 and 1023. This means that initial implementation required the use of the “int” data type to represent the forward and reverse sensor information, this resulted in a calculated serial send time for 7 bytes of $1.22\ \text{ms}$. This means that the waveform seen in Figure 82 would be tracked by 16 data points.

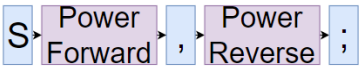

Figure 89 - Power Detector Arduino Data Protocol

The 16 data points did not, however, track the signal with enough accuracy. The solution to this problem was to understand that the power detector would not output a voltage greater than $2.1\ \text{V}$ and would not produce a value less than $0.9\ \text{V}$. The ADC value for a voltage of $2.1\ \text{V}$ from Equation 29 yields an ADC value of 426.067. Similarly, a voltage of $0.9\ \text{V}$ yields an ADC value of 181.543. Subtracting the one from the other produces a result of 244.524. The significance of this allows for

the ability to use the “byte” data type instead of the “int” data type. This results in only sending 5 bytes down the serial line to the processing PC which is calculated to take 0.868 ms. This means that the waveform seen in Figure 82 would now be tracked by 23 data points. The software on the processing PC then adds the 181.543 to the data it receives. This solution tracked the power detector signal with an acceptable level of accuracy seen in the comparison of Figure 82 and Figure 90.

7.2.5.2 Calibrating Timing Information

Similarly, to section 7.2.4.2, Equation 34 can be used to calculate the time that elapses between samples. The difference in this case is that T_d is set to zero as the loop in code is required to run as fast as possible. Software timers were implemented to record the time between sample sends. The value of T_r was recorded to be 0.661 ms.

7.2.5.3 Capturing Power Detector Waveform

Figure 90 shows that the power detection sensor waveform seen on the oscilloscope reading in Figure 82 can be tracked.

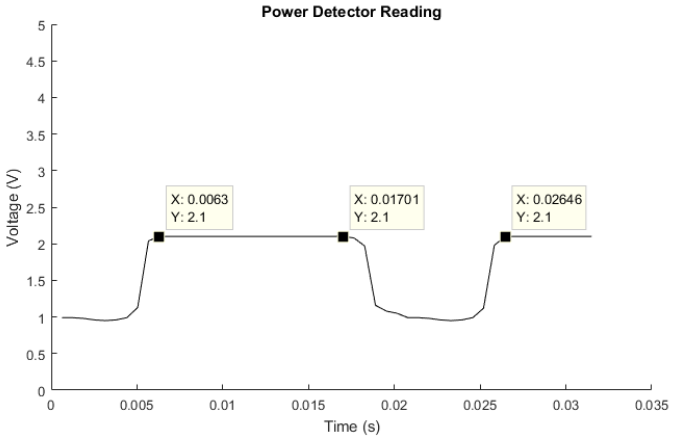

Figure 90 - ADC Power Detector Data Plot

The oscilloscope reading shows a signal wavelength time of 20.2 ms and the ADC data shows a signal wavelength of 20.16 ms. The width of the power pulse seen on the oscilloscope is 9.4 ms and the power pulse from the ADC data shows 9.45 ms.

7.3 Processing Computer Software (MATLAB)

The processing computer was mainly used to save the data produced by the system and to plot the data in a visual format. The software used to do this MathWorks® MATLAB & Simulink.

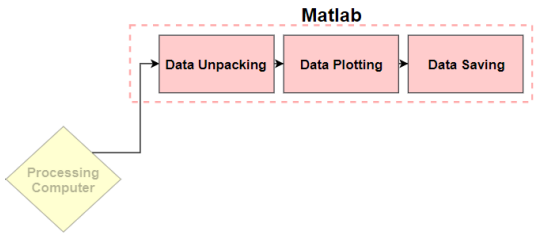

Figure 91 - MATLAB Block Diagram

Figure 91 summarises the role MATLAB software plays in this project.

7.3.1 Data Unpacking and Saving

The processing software creates data files for the information received from the microcontrollers and sets up a serial connection for each microcontroller simultaneously. Figure 92 shows a flow diagram illustrating how data is received and then saved.

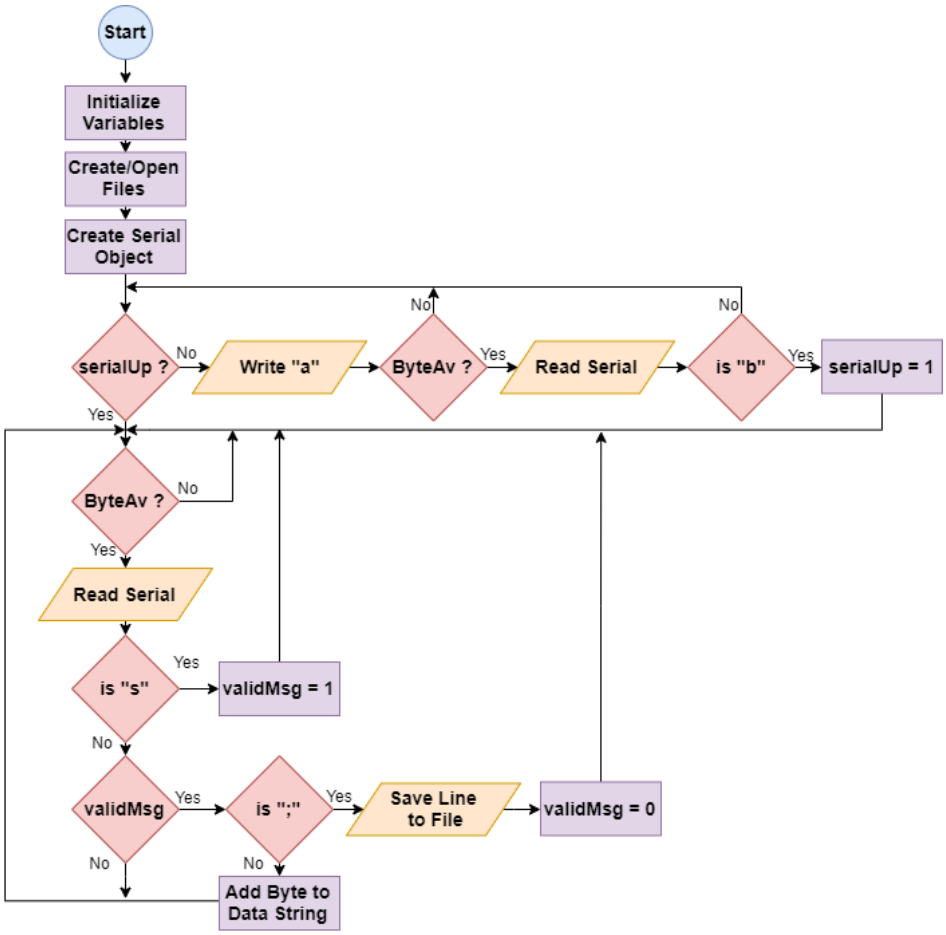

Figure 92 - Data Saving Flow Diagram

The code rejects any messages on the serial line which do not start with the character “s”. Once the character “s” is received, the code sets a valid message flag “high” and data bytes received are added to a character string until the character “;” is seen. After the character “;” is seen, the character string is written as a new line to a file. The file is dedicated to the data which is received from the current active test. This means that a new file is created each time a new test is conducted.

7.3.2 Data Plotting

The information received from the microcontrollers may be viewed as the “y” coordinates in a Cartesian axis. This means that when the function is called to plot the data saved in the file, an array is created which has the same number of elements as there are lines in the file. Starting from zero, each consecutive element increases by the T_s value obtained from Equation 34. This timing array represents the “x” coordinates in a Cartesian axis.

7.3.2.1 Temperature Sensor Data

The data from the files is read line by line and each sensors data is sorted into its own dedicated array. Upon the completion of reading all the data from the file, the file is closed and the data is plotted. Figure 93 shows the code required to plot the data in the arrays.

```
figure(1);
hold all
plot(timeArr, inTemp, 'r');
plot(timeArr, postInTemp, 'g');
plot(timeArr, preOutTemp, 'b');
plot(timeArr, outTemp, 'y');
ylim([0 110]);
title('Temperature Response');
xlabel('Time (s)') ;
ylabel('Temperature (°C)');
legend('Inlet','Post-Inlet','PreOutlet','Outlet');
drawnow
```

Figure 93 - MATLAB Graph Plotting Code

The graphs generated by the MATLAB code can be seen in Figure 94.

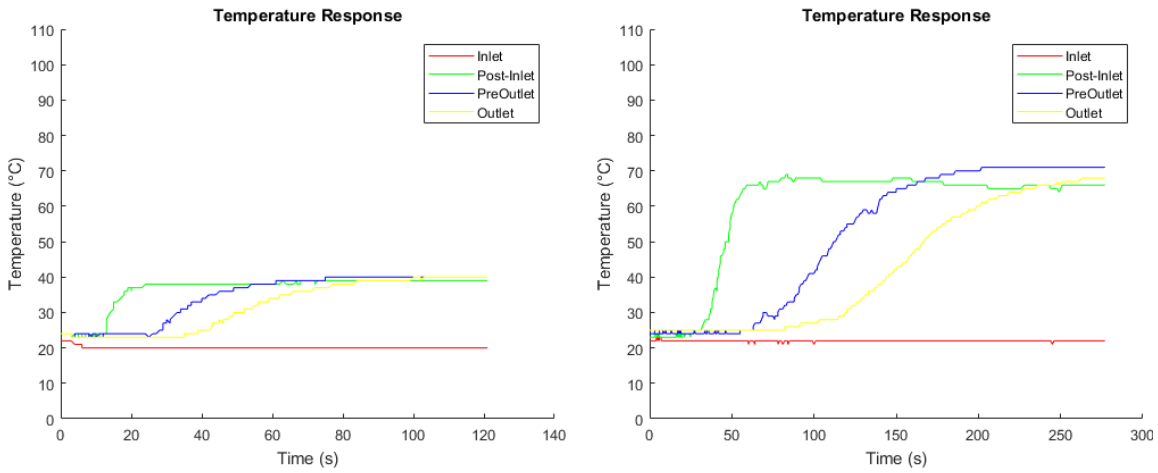

a) b)

Figure 94 - MATLAB Temperature Data Graph Examples a) 3 Capacitor Power Supply, Fast Flow Rate b) 3 Capacitor Supply, Slow Flow Rate

The timing information for the graphs was considered accurate because the experiment seen in Figure 94 a) was set to run for 2 minutes.

7.3.2.2 Power Detector Data

The data which is saved for the power detectors are offset ADC values. The goal is to mathematically convert the data into a useable format so that the average power for the system can be realised. The coding steps followed to achieve this goal are performed as follows:

1. Convert the character array read from the file line by line to a decimal datatype (similar to the double and float data types seen in Table 9).
2. Add the offset ADC value discussed in section 7.2.5.1.
3. Apply Equation 29 to convert the data values to voltage values.
4. Apply equations seen in Figure 81 respectively creating data values with the unit dBm.
5. Add the bi-directional coupler reduction values discussed in section 6.2.3.2.
6. Convert data to Watts using the relationship seen in Equation 35 below.

$$P_{Watt} = \frac{10^{\frac{P_{dBm}}{10}}}{1000} \tag{35}$$

Figure 95 represents the power pulses in Watts which exist during the operation of the system.

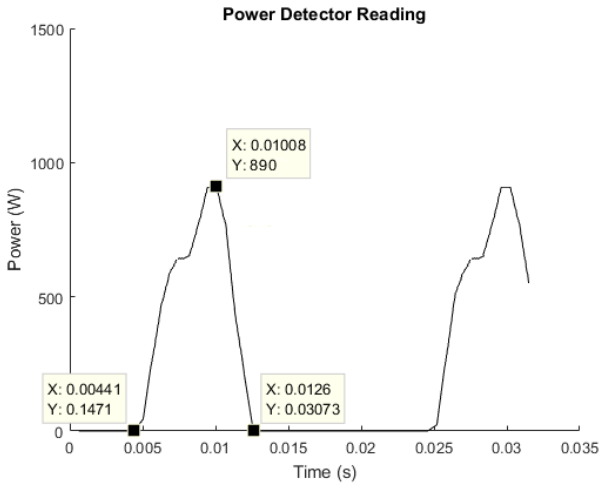

Figure 95 - Power Detector Pulses in Watts

The average power in the system is equivalent to the area "underneath" the pulses seen in Figure 95. The area for each pulse is calculated by multiplying each data point by the sampling time ($661\ \mu s$) and adding the results together for each pulse. The results of this operation can be seen in Figure 96 below.

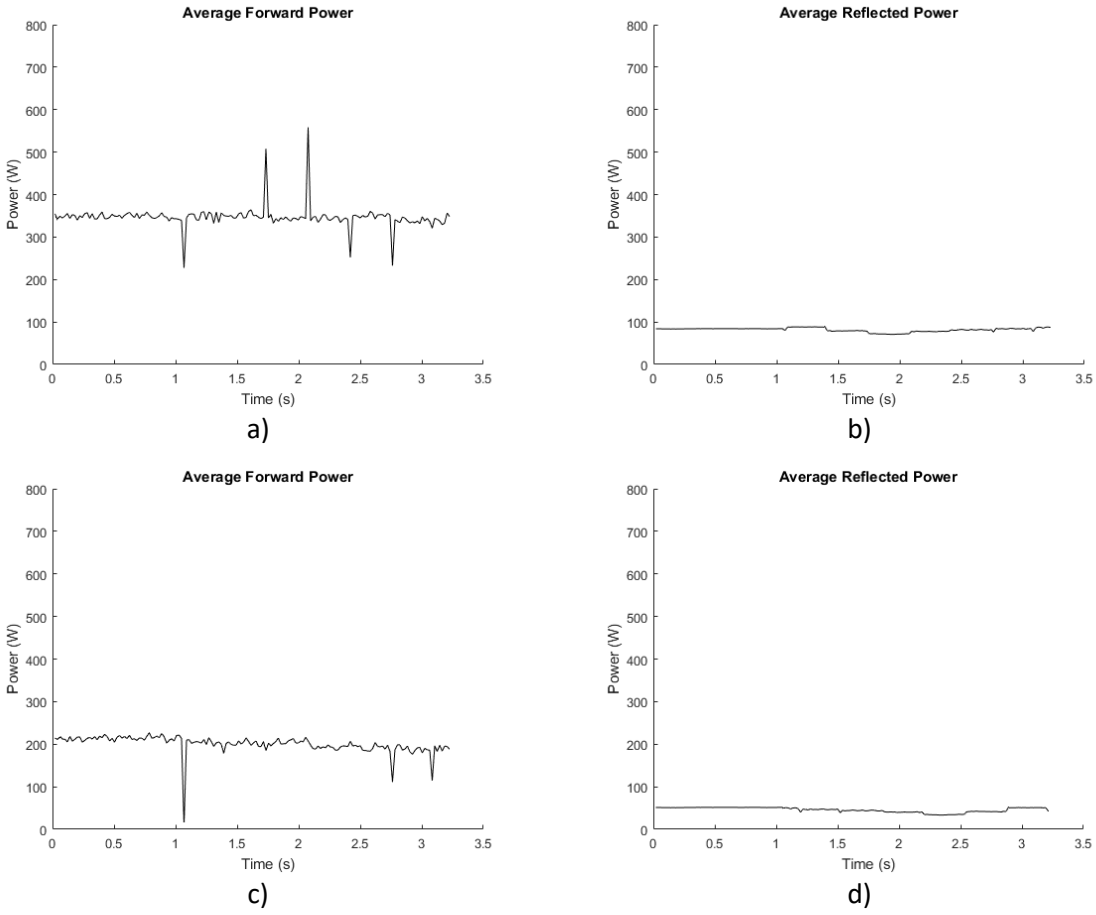

Figure 96 - Average Power Measurements a) 2 Capacitor Power Supply Forward Power b) 2 Capacitor Power Supply Reverse Power c) 3 Capacitor Power Supply Forward Power d) 3 Capacitor Power Supply Reverse Power

The average forward power seen in Figure 96 a) and c) are consistent with the forward power seen in Figure 16 which has a similar power supply set up and considered accurate. The average reflected power seen in Figure 96 b) shows a value of roughly 90 W.

7.4 Other Software Used

7.4.1 CST Studio Suite®

Used for EM modelling and applicator design.

7.4.2 AWR Microwave Office

Used to plot the data obtained from the VNA.

7.4.3 Autodesk Eagle

Used to create the schematics and PCB layouts in this project.

7.4.4 Autodesk Inventor Professional

Used to create 3D printable parts for mode stirrers and motor attachments (not discussed in this project).

7.4.5 Draw.io

Online software package used for all block diagrams and flow charts in this thesis.

7.4.6 MS Paint

Used to illustrate some concepts as well as edit and overlay text on images in this thesis.

7.5 Chapter Conclusion

The software in this project highlighted that using a single Arduino Leonardo was not the ideal microprocessor for the project, however, it was too late in the design cycle to change. The solution to the issue involved running two Arduino Leonardo's in parallel.

The software calibration techniques used were deemed successful because the power detector data, timing information and temperature sensor information were all accurate and repeatable.

The desired linear temperature sensor response designed in the hardware section was considered successful as the temperature response from the system was linear.

The message protocol designed was considered successful. This was due to the fact that before its implementation, faulty data caused the processing computer software to crash. After the implementation, the code stopped crashing and no faulty data was present in the data file.

The control software was designed as a stand-alone component, which does not need to be connected to the processing computer for the system to operate successfully. If the processing computer is not connected however, no data will be saved.

The reflected power in the system was measured to be below 100 W, seen in Figure 96 b).

Chapter 8
Control System

8.1 Chapter Summary

This chapter starts with a short literature study which defines what a control system is, as well as, listing ideal characteristics, types of control systems, types of available controllers and shows some basic controller transfer functions. The control system for this project was then designed and began by identifying and deriving a mathematical model for the system. The control system specifications are stated. The designed control system was simulated and altered to meet the system requirements. Finally, the control system is implemented in a live test.

8.2 Control Literature Review

A control system is a component in a system which regulates the desired output of a complete system by altering output signals of other components in the full system. Control systems mathematically relate input and output signal relationships either linearly or non-linearly [80]. The requirements for a good control system include:

- Accuracy – The measuring tolerance on sensors effects the tracking error which determines control system performance [80].
- Sensitivity – Changes in the environment can be unpredictable and a control system should be able to react in the correct manner [80].
- Noise – The control system should be able to reject unwanted input signals [80].
- Stability – A rough definition of control system stability states that with bounded input signals, the output signal should also be bounded (not increasing out of control) [80].
- Speed – Good control systems reach an acceptable level of stability in an appropriate time [80].
- Oscillation – Control systems are considered stable if minimal oscillations occur or if a constant oscillation is maintained [80].

There are two main types of control systems. The first is called “open loop control” and the second is called “closed loop control”. Open loop control states that the control action is independent from the output signal. An example of this is a domestic bread toaster. The toaster will run for a predetermined time no matter how toasted or untoasted the bread is. The nature of this type of control means that any change in the system cannot be controlled automatically and instead the system can be altered after the output product (bread) is assessed and treatment time can either be increased or decreased for the next treatment. Closed loop control states the control action is dependent on the output produced by the system. An example of this can be seen in air-conditioning units (air-con). An air-con turns “on” and “off” depending on the desired room temperature. This form of control necessitates automation in a system. Open loop control systems can be converted to closed loop control systems with the addition of a feedback loop. The feedback loop contains information about the output signal and can be used to alter the input signal accordingly [80].

There are three basic types of closed loop controllers, they are: proportional, integral and differential controllers. These controllers can be used individually or together in combination [81].

Proportional (P) control creates an output which can be correlated to an error signal. An error signal in many cases is the difference between the desired output signal (the input signal) and the current output signal. This can be seen in the block diagram in Figure 97 below.

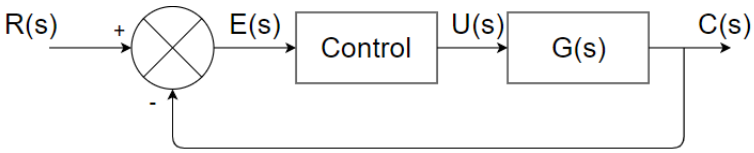

Figure 97 - Negative Feedback Loop Control Block Diagram

$R(s)$ represents the input signal, $E(s)$ represents the error signal, $U(s)$ represents the controlled signal, $G(s)$ represents the dynamics of the system which is to be controlled and $C(s)$ represents the output signal.

Derivative (D) control creates a control output ($U(s)$) which can be correlated to the derivative of the error signal. Integral (I) control creates a $U(s)$ which can be correlated to the integral of the error signal [81].

Common combinations of these controllers include: P, PD, PI and PID [82].

- P controllers are used in systems which require fast response and are useful when the error and importance of the measured signal is not too great. This type of control can only be used for first order systems and has one coefficient of control [82].
- PD controllers are used in systems with moving objects because this type of control attempts to predict the error signal in order to improve stability of the system. This type of control has two coefficients of control [82].
- PI controllers are used in systems which can afford slow reactions. This makes this type of controller insensitive to disturbance signals and produces zero control error. This type of system has two coefficients of control [82].
- PID controllers are used in systems which require all the advantages brought forward by the basic controllers. This type of control has three coefficients of control and can be difficult to tune its parameters to achieve the desired output signal specifications [82].

The transfer function of the control block in Figure 97 is represented by the relationship $\frac{U(s)}{E(s)}$ and derived in Table 11 below. Starting with the time domain expression for the input error signal to the control block and its proportionality to the output of the control block.

Table 11 - Basic Control Component Transfer Functions [81]

P	D	I
$\boldsymbol{u(t) = K_P * e(t)}$	$u(t) = K_D * \frac{de(t)}{dt}$	$u(t) = K_I * \int e(t)dt$
Applying Laplace transforms on both sides of the equation yields:		
$\boldsymbol{U(s) = K_P * E(s)}$	$U(s) = K_D * s * E(s)$	$U(s) = K_I * \frac{1}{s} * E(s)$
Rearranging the equations, the transfer functions can be found to be:		
$\boldsymbol{\frac{U(s)}{E(s)} = K_P}$	$\frac{U(s)}{E(s)} = K_D * s$	$\frac{U(s)}{E(s)} = K_I * \frac{1}{s}$

The effects of changing the constant coefficients K_P, K_D and K_I can be seen in Table 12 below.

Table 12 - The Effects of Changing Control Coefficients

Parameter	Speed of Response	Stability	Accuracy
Increasing $\boldsymbol{K_P}$	Increases	Deteriorates	Improves
Increasing $\boldsymbol{K_D}$	Increases	Improves	No Change
Increasing $\boldsymbol{K_I}$	Decreases	Deteriorates	Improves

The transfer function for combinations of controllers is simply the addition of the transfer functions for each basic controller. For example, the control block for a PID controller takes the form seen in Equation 36.

$$\frac{U(s)}{E(s)} = K_P + K_D * s + K_I * \frac{1}{s} \tag{36}$$

8.3 Control System Design

The method used to design the control systems in this project is summarised by Figure 98 below.

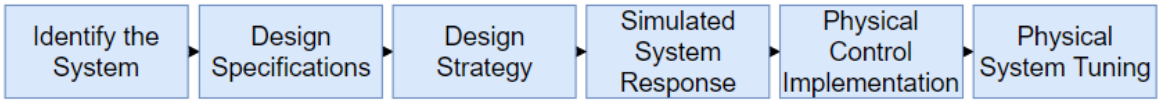

Figure 98 - Control System Design Steps

Proportional control was selected for this system as a starting point for control. This type of control is the simplest form and is incorporated in all the other strategies discussed in section 8.2. The performance of the system was then analysed to see if this form of control is suitable on its own.

8.3.1 Identifying the System

Before the implementation of any control, the system is seen as an open loop system and can be represented by Figure 99 below.

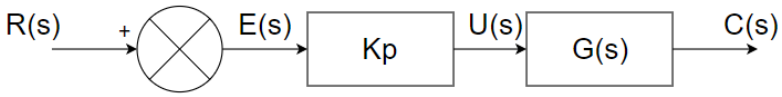

Figure 99 - Open Loop Control Block Diagram

The transfer function of this block diagram is represented by Equation 37 below.

$$\frac{C(s)}{R(s)} = G(s) * K_P \tag{37}$$

The variable function $G(s)$ is known as the plant and K_P represents the gain of the constant flow rate controller. This system can be compared to the toaster discussed in Section 8.2 because the power in the system remains constant and the flow rate of the media is kept constant. Experimental observations allow the tweaking of K_P between tests to alter the output target temperature.

The open loop response of the system can be used to determine the characteristics of $G(s)$ to create a mathematical relationship which can be simulated. The open loop response for this system is analysed in two ways for this project. The first response is recorded by setting the flow rate of the pump to a maximum and maintain the input power. The second type of response is recorded by setting the flow rate of the pump to a minimum while maintaining input power.

8.3.1.1 Maximum Flow Rate

The maximum flow rate represents the response in the system where the output temperature will be the lowest. This is because the faster the media moves through the applicator, the less time the media is interacting with the microwave energy. Section 2.3.3.3 highlights that dielectric properties effect microwave heating. This project has no direct application and as a result, the media to be sterilised in this system is unknown. This means the dielectric properties of the media cannot be assessed before designing the control system. The approach to designing the control element of the system was to obtain the open loop responses for tap water, distilled water and saline water at the three different power levels available from saturable reactor control discussed in Section 2.3.2.6.

The method used was to pump tap water through the system while the magnetron was “off”. The purpose of this was to cool the system between experiments so that all the sensors can start at the same temperature. The system is then drained and the appropriate media for each experiment is primed to be fed into the system, the magnetron is powered “on” as the media enters the chamber and the results then being sent to the processing computer. Figure 100 shows that the response for each media type is similar in shape, however, settle at different output temperatures.

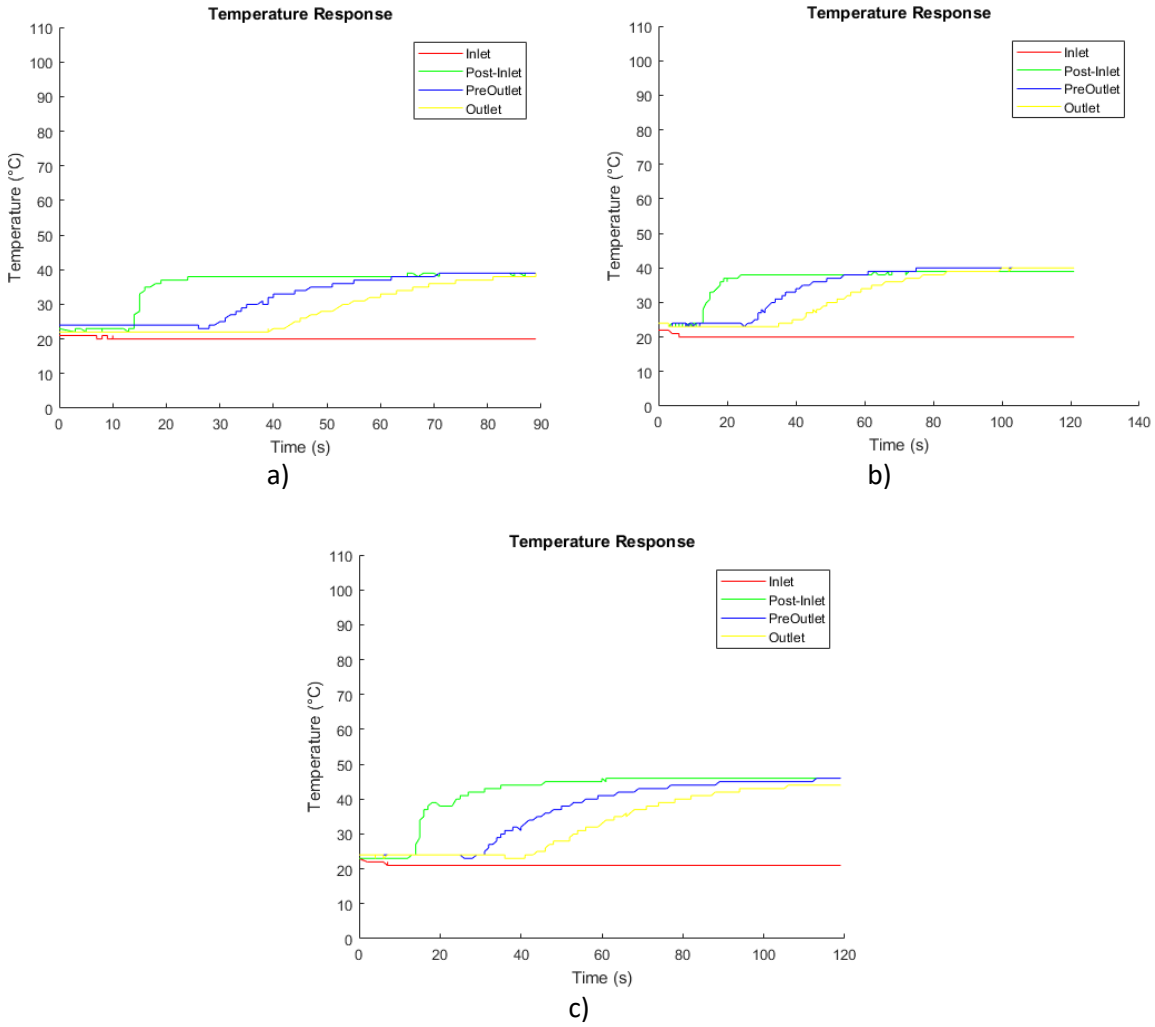

Figure 100 - Open Loop Response, Fastest Flow Rate, 3 Capacitor Power Supply for a) Distilled Water b) Tap Water c) Saline Water

Table 13 below shows summarised results for the nine open loop experiments conducted for the maximum flow rate response.

Table 13 - Maximum Flow Rate Response Summary

Number of capacitors in power supply	**Output Temperature (°C)**		
	Distilled Water	*Tap Water*	*Saline Water*
3	37	39	44
2	46	49	60
1	81	86	*Boiling
*Boiling caused the media flow rate to become unusable			

8.3.1.2 Minimum Flow Rate

The flow rate of the pump can be controlled using square pulses at a set duty cycle. The square pulse signal is supplied by the microcontroller in the form of a PWM signal. The minimum flow rate for the pump was determined experimentally by altering the duty cycle until the pump stops pumping at a steady continuous flow rate. The initial lowest duty cycle signal required maintain continuous flow was found to be around a 30% duty cycle (the square pulse is high for 30% of the time and of for 70% of the time). This signal however was not great enough to start the pump from an "off" state. One of the reasons for this is that the motor is connected to the peristaltic pump which squeezes the silicone pipe. The coefficient of static friction is speculated to be much higher than that of the coefficient of dynamic friction. This results in the pump requiring more power at start up to overcome the static friction. The lowest duty cycle required to turn the pump "on" from "off" state was found to be around a 45% duty cycled signal.

The open loop response at a 45% duty cycled signal produced unreliable results. Through further experimentation it was found that the lowest duty cycle which could be used for the system and still produce reliable results was a 55% duty cycle signal. Similarly, to the previous section, the nine open loop responses are summarised in Table 14 below.

Table 14 - Minimum Flow Rate Response Summary

Number of capacitors in power supply	**Output Temperature (°C)**		
	Distilled Water	*Tap Water*	*Saline Water*
3	71	70	85
2	79	80	95
1	*Boiling	*Boiling	*Boiling
*Boiling caused the media flow rate to become unusable			

8.3.1.3 Experimental Discussion and Conclusion

The number of capacitors in the high voltage magnetron power supply is required to stay fixed in the system. The control system will only be able to control the output temperature range between the temperatures produced by the maximum flow rate and the minimum flow rate. Common sterilisation practices often don't sterilise media below 60 °C. The media used in this project is suspended in saline solution. For these reasons, the two-capacitor configuration was chosen for this project giving the system a controllable range for saline water between 60 °C and 95 °C.

8.3.1.4 Modelling $G(s)$

There are two main states in the system which require temperature control. The first state is the "start-up" case and the second state being the "continuous operation" case. The states behave differently because the start-up state has large delay periods before data can be measured since the media needs to reach the sensors in the system. The start-up state is relatively unimportant because it lasts for approximately $40\ s$ whereas the continuous state can last for hours.

The project design for the start-up case was mainly determined through experimental observation until a flow rate was identified which heated the target media to $60\ °C$ by the first temperature sensor. At this stage the control system takes control of the flow rate using the data obtained from the first temperature sensor. As the system fills up, the control system logic switches to the pre-outlet temperature sensor, and once full, switches to controlling the outlet temperature as and when valid data is received by the system (valid data in this design is defined by a temperature reading greater than $35\ °C$). The system dynamics for each temperature sensor was designed and an appropriate control algorithm for each sensor applied in software.

This section shows the system identification process for the continuous case which only controls the outlet temperature sensor. Figure 101 below shows the step responses obtained for the continuous case. The coiled pipe was completely full before the magnetron was turned "on".

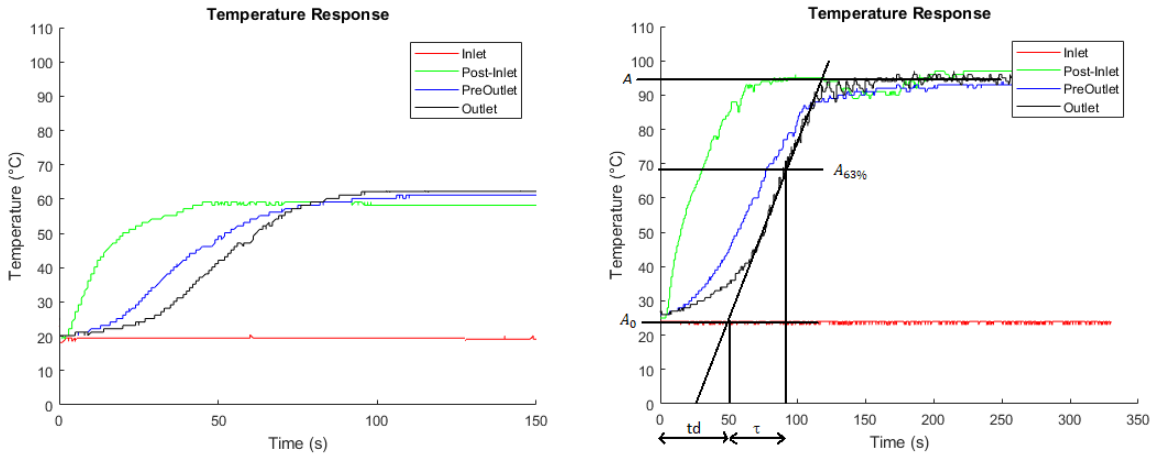

Figure 101 - Open Loop Step Response (Continuous Case) a) Maximum Flow Rate b) Minimum Flow Rate

The response of the outlet data line is $G(s)$ and can be modelled by a standard transfer function seen in Equation 38 below:

$$G(s) = \frac{(A - A_0)e^{-st_d}}{\tau s + 1}, \tag{38}$$

where A is the maximum steady state temperature, A_0 is the starting temperature, t_d is the delay time and τ is the time taken to reach a temperature 63% of A. The variables in Equation 38 are illustrated in Figure 101 b). The exponential term e^{-st_d} can be removed from $G(s)$ through an approximation seen in Equation 39 below.

$$G(s) = \frac{(A - A_0)\frac{2}{t_d}}{(\tau s + 1)(s + \frac{2}{t_d})} \tag{39}$$

The approximated G(s) is then plotted to verify the model is correct and can be seen in Figure 102.

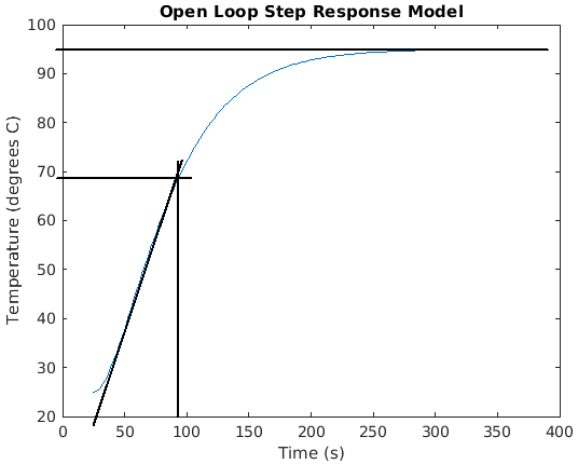

Figure 102 - Open Loop Approximated G(s)

Comparing Figure 101 b) and Figure 102, the approximated mathematical model was considered accurate.

8.3.2 Control Specifications

The specifications for the control system in the design should be that an overshoot of 5% at 90 °C. This will result in a maximum overshoot of 4.5 °C. A higher overshoot will cause the media to boil causing the flow rate to be unpredictable. Previous works of the EHG state that some media as the potential to "caramelise" at higher temperatures [1].

The design should also have a steady state tracking error smaller than 2 °C.

8.3.3 Control Design

Figure 97 shows the closed loop control block diagram which incorporates negative feedback. The chosen control system in this design is proportional only control, thus making the control blocks transfer function K_p. The closed loop transfer function for the system can be seen in Equation 40.

$$\frac{C(s)}{R(s)} = \frac{K_p G(s)}{K_p G(s) + 1} \tag{40}$$

A root locus plot of the approximated model for $G(s)$ can be used to find a K_p value which satisfies the overshoot specification and is seen in Figure 103 below.

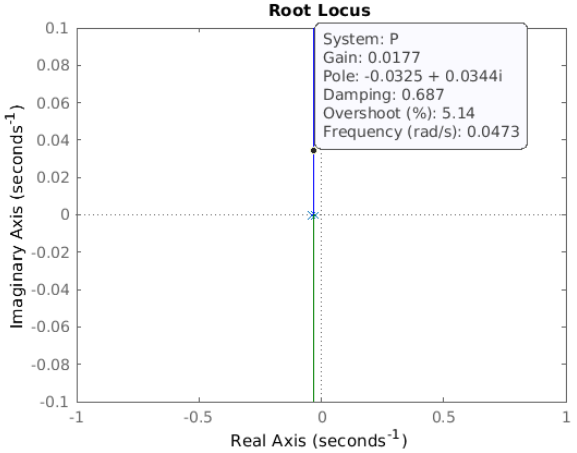

Figure 103 - Root Locus Plot for Approximated G(s)

The root locus suggests that a K_p value of 0.0177 will satisfy the control design specification of a 5% overshoot.

8.3.4 Control Simulation

The closed loop response of the system is plot using Equation 40.

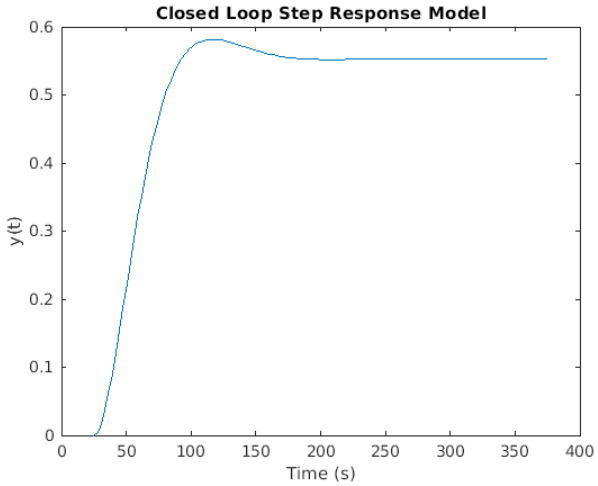

Figure 104 - Closed Loop Response with K_p = 0.0177

The closed loop response is expected to settle around a $y(t)$ value of 1. The simulated closed loop response can be altered by varying K_p.

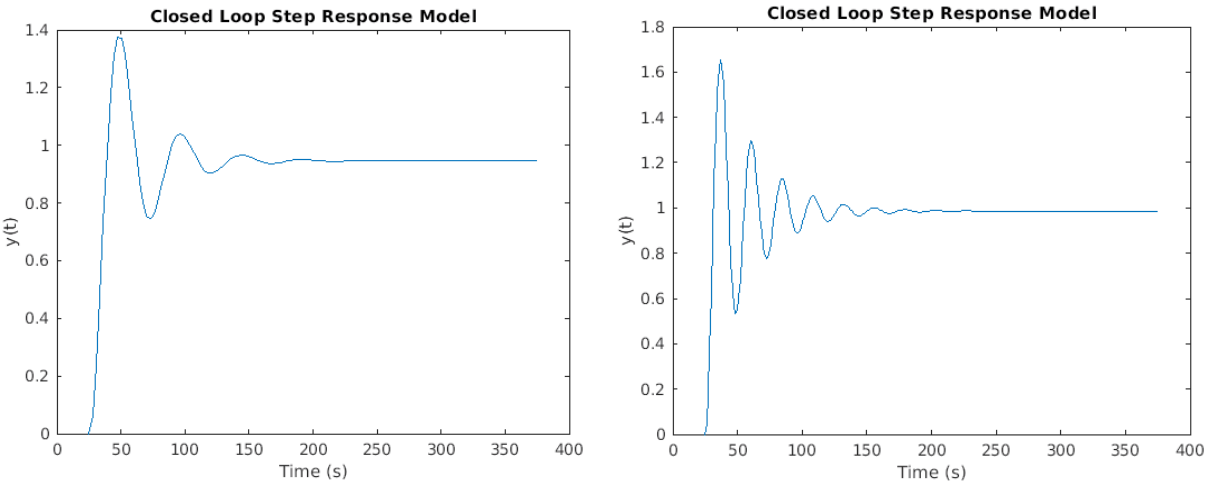

Figure 105 - Closed Loop Response a) K_p = 0.25 b) K_p = 1

Increasing K_p changed the overshoot designed by the root locus as expected. Achieving the steady state tracking error, however, takes precedence over the temporary overshoot since increasing K_p does not make the system unstable.

A K_p value of 1 is simulated with a reference input to control to 65 °C and 90 $℃$ respectively. The results can be seen in Figure 106 below.

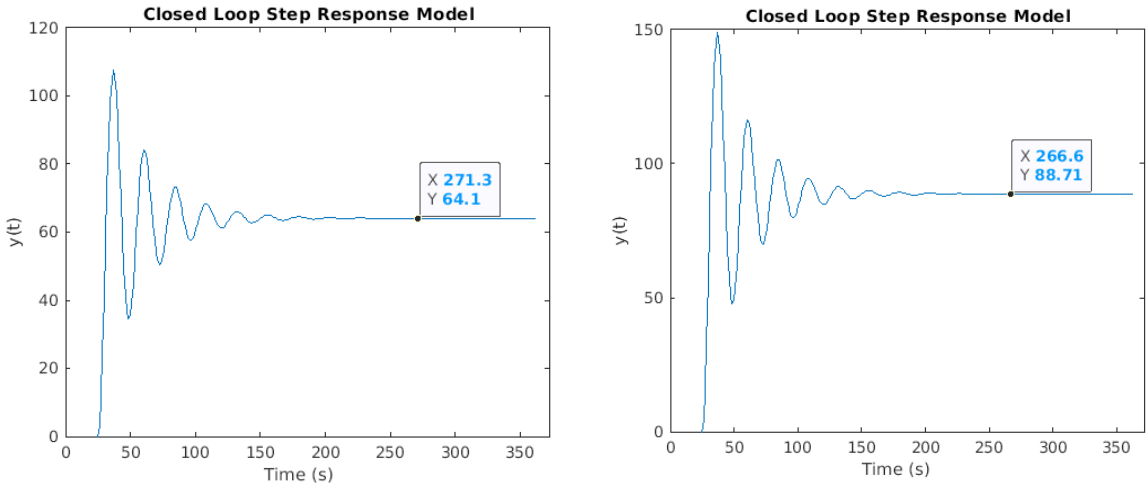

a) b)

Figure 106 - Simulated Control a) 65 °C b) 90 °C

Figure 106 a) and b) both show that a steady state tracking error of less than 2 °C is realisable with the designed control system.

8.3.5 Control Implementation and Conclusion

The control system was implemented in software with $K_p = 1$ and the results can be seen in Figure 107 a) and b).

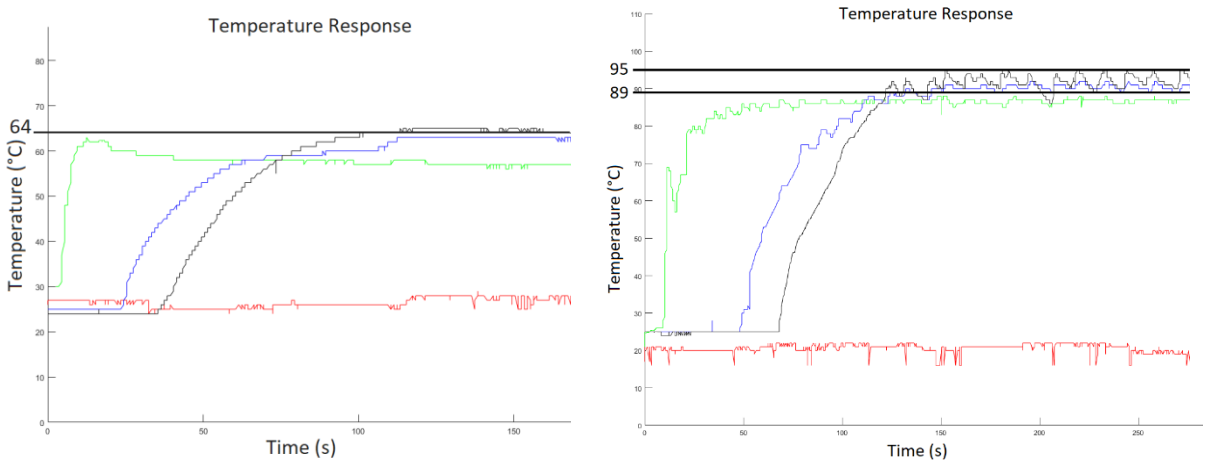

a) b)

Figure 107 - Implemented Live Control System a) Target Temperature 65 °C b) Target Temperature 90 °C

Figure 107 a) had a target temperature of 65 °C and the system achieved a steady state value of 64 °C with no overshoot. Figure 107 b) had a target temperature of 90 °C and the system achieved a steady state value between 89 °C and 95 °C. The reason for the "saw-tooth" shape on the graph is believed to be a product of the low flow rate causing media to boil slightly inside the applicator chamber. Pressure builds up inside the coil because liquid water turns into gaseous water at some points in the tube. This explanation comes from the observation that the peristaltic pump was observed to have a relatively constant rotational speed which did not match the aggressive "sputtering" of water coming out the outlet pipe. The sputtering was observed to occur roughly every 2 s. The results of this test concluded that the proportional-only control system designed in this chapter is able to control the output media temperature between 60 °C and 95 °C.

Chapter 9
Microbial Experiments

9.1 Chapter Summary

This chapter gives detailed insight into the methods used to prepare the media which was tested in the continuous flow system designed for this project. A step by step experimental procedure is presented which shows the apparatus used. The temperature response for the treatments are seen and comments are made with regards to the control system designed. The results are presented, and conclusions are drawn from the data.

9.2 Method for Media Preparation

The media prepared in this thesis was provided by the Microbiology Department of Stellenbosch University.

The microwave sterilisation treatment experiments were conducted with a strain of *Lactococcus lactis* (NZ9000) with an antibiotic marker (chloramphenicol at $10\ \mu g/ml$). The use of a single type of bacterium coupled with the antibiotic marker reduces the risk of unintended contamination.

The bacteria were inoculated from glycerol stocks into a $5\ ml$ M17 broth (supplemented with 0.5% glucose v/v and chloramphenicol at $10\ \mu g/ml$) and incubated overnight at $30\ °C$. The overnight culture was used to inoculate $200\ ml$ M17 broth (supplemented with 0.5% glucose v/v and chloramphenicol at $10\ \mu g/mL$) and incubated at $30\ °C$ until an OD_{600} value of 1.0 was reached. These cells were centrifuged at $8000\ rpm$ and washed in $200\ ml$ sterile saline (0.75% NaCl), cells were centrifuged again, and the wash step repeated. After the wash steps, cells were re-suspended in sterile saline to a final OD_{600} of 0.2-0.3 and placed in the media containers discussed in section 6.3.4 ready for transport and treatment.

Figure 108 - Received Media for Treatment

Figure 108 shows how the media was received prior to treatment. The tin foil seen in the picture was used to create a barrier between the breather holes in the lids and the external environment.

9.3 Method for Experiments

The steps followed for the bacterial treatment experiments included:

1. Clearing the laboratory bench of unnecessary tools.
2. Wiping down the immediate surfaces and the system parts with 70% ethanol solution and leaving to air-dry.

3. Pumping 70% ethanol solution into the system until the coiled pipe was completely filled and leaving to soak for 10 minutes.
4. Circulating the 70% ethanol solution for 5 minutes “just in case” an air bubble was present inside the system.
5. Thoroughly flushing the system with distilled water to remove any ethanol.
6. Pumping a small amount of saline containing bacteria (SCB) through the system into a waste beaker before starting a treatment.
7. Set the system to re-circulate SCB until desired output temperature is achieved.
8. Start treatment and fill the output container with $200\ \mathrm{ml}$ of treated SCB.
9. Drain the system of any SCB and circulate cold tap water to cool the system down. This was done so that every test can begin with the same starting characteristics.
10. Repeat steps 4 to 9 until all experiments are completed.

The four treated samples and the single control sample were collected and used for enumeration of viable cells. Cells were diluted in sterile saline and plated onto M17 agar (1.5% agar w/v; 0.5% glucose v/v) supplemented with chloramphenicol ($10\ \mu\mathrm{g/ml}$). Agar plates were incubated at $30\ ^{\circ}\mathrm{C}$ until visible colonies could be observed and counted for determination of colony forming units per millilitre ($\mathrm{CFU/ml}$).

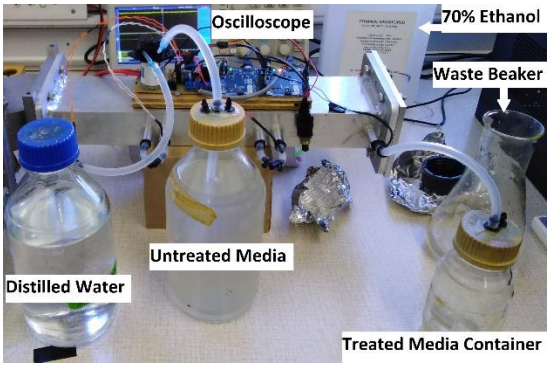

Figure 109 - Apparatus Used During Treatment

Figure 109 shows some of the apparatus used during the sterilisation experiments. The oscilloscope was connected to the output of the power detectors to ensure that microwave power is present during the test (the magnetron was unplugged between treatments to ensure user safety). This was necessary because the processing computer only generated power graphs after treatment cycles had been finished.

9.4 Temperature Response During Treatment

The decision to use 200 ml for the bacterial tests was done to ensure the system could be tested in both the “start-up” and “continuous” cases for the hybrid control system software.

The “control” sample (the sample not treated by microwave energy for comparison) of media was passed through the system at maximum flow rate while the magnetron was powered “off”. As expected, the temperature of the control sample did not change. The reason the control sample was sent through the system and not just set aside is because the peristaltic pump interacts with the media in a physical manner. This physical interaction could influence the samples in some way. Passing the control sample through the system ensures that the only difference between it and the treated samples is the addition of microwave energy.

The targeted control temperatures for the other four samples were designed to be 60 °C, 65 °C, 75 °C and 95 °C. The first test was designed to assess if the minimum attainable temperature achievable by the system could sterilise the targeted media. The second test was designed to compare the control system characteristics seen in chapter 8. The third test was designed after looking at bacterial death rate graphs. These graphs indicate the duration bacteria should be held at a specific temperature to ensure the death of the microorganism. For common non-thermal resistant bacteria, a temperature of 75 °C should completely denature the bacteria in a couple of seconds, if not less. The last test was implemented as the system's "best chance" of resulting in complete sterilisation.

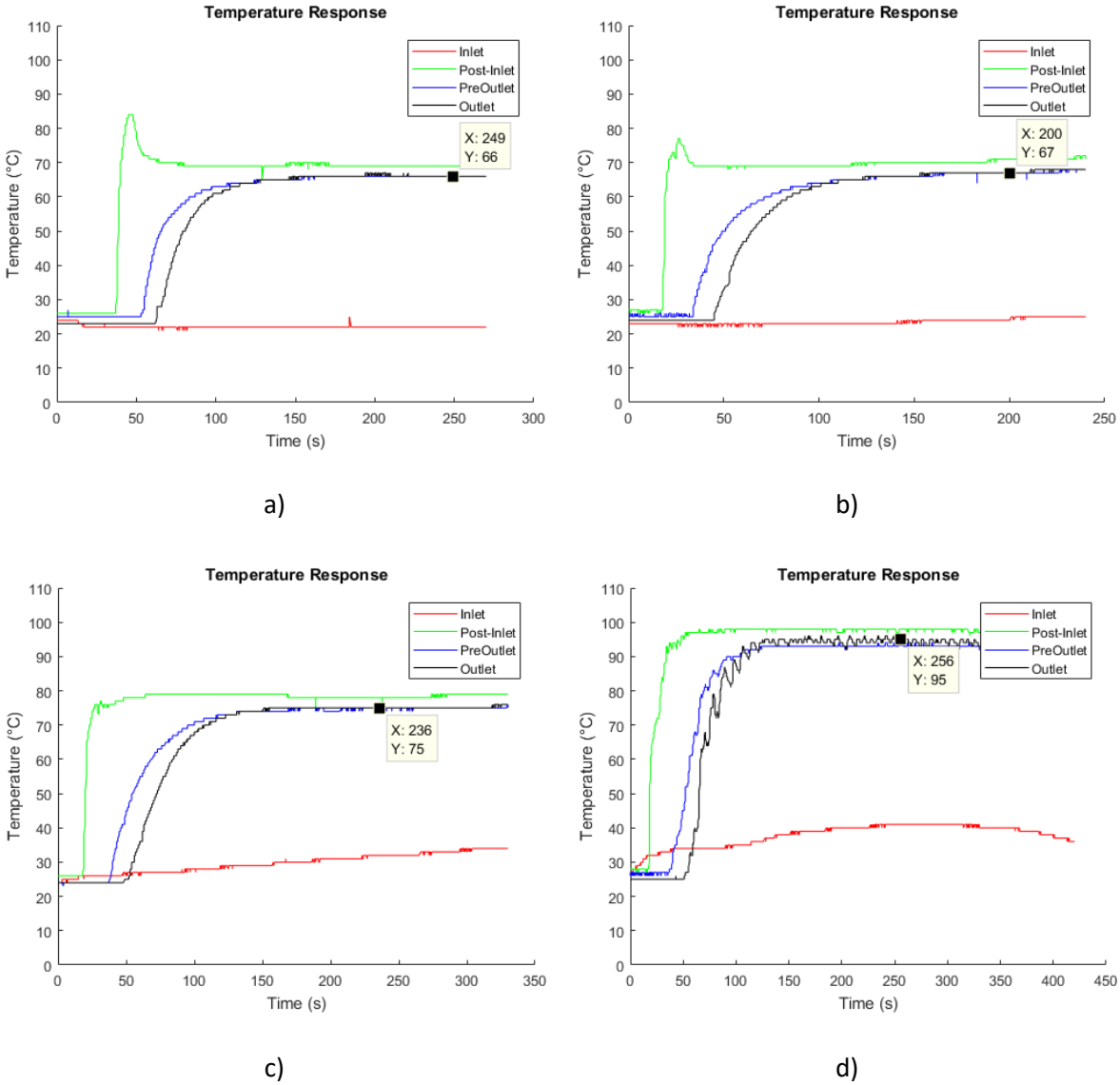

Figure 110 - Temperature Responses During Microbial Treatments a) Control Target = 60 °C b) Control Target = 65°C c) Control Target = 75°C d) Control Target = 95°C

The first test highlighted that the microwave response to the media was greater than anticipated. This can be seen in the large overshoot present in Figure 110 a). The steady state tracking error for this test was 6 °C. The control system was altered (by changing K_P) in an effort to improve performance on the three remaining tests.

The second test, illustrated in Figure 110 b), shows that the control software was not operating as well as it did during the design stages. This test, however, tracks the target temperature with a steady state error of $2\,°C$ which is within the design specifications but fails on the desired 5% overshoot allowed. The control system was altered further to improve performance for the other tests.

The third test seen in Figure 110 c) shows the control software performing perfectly. The target temperature is achieved with roughly $0\,°C$ ($\pm\,0.5\,℃$ decimal values rounded in software) steady state tracking error with no overshoot. At this temperature, recirculation of the media was required briefly, which in turn raised the input temperature of the media. This effect can be seen as an external disturbance signal to the system. The control system did not allow this change in input temperature to affect the targeted control temperature.

The fourth test seen in Figure 110 d) also shows the control system operating in the desired manner. The target temperature is achieved with no error($\pm\,0.5\,℃$) and no overshoot. The recirculated SCB posed a greater input disturbance to the system which did not alter the steady state. The control system in this test performed better than the designed system due to the fact that the media did not boil and sputter as it had previously causing steady state oscillations at similar temperatures.

9.5 Sterilisation Results

Figure 111 shows an example of the Petri dishes with the colonies of bacteria to be counted. A non-permanent marker was used during the counting process to ensure that the same colony of bacteria was not counted twice.

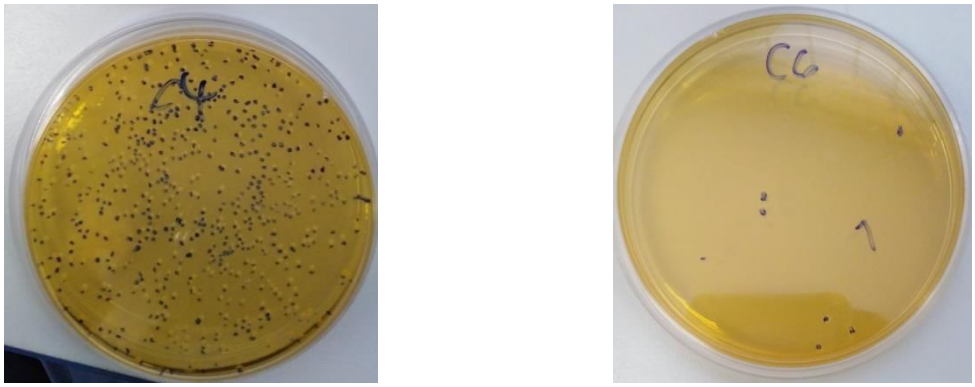

a) b)

Figure 111 - Incubated Control Samples a) 4 Dilutions b) 6 Dilutions

The purpose of the dilution process allowed results to be confirmed with each other as well as to make it easier to count the colonies. It is unrealisable to count millions of colonies. This means that a dilution series reduces the counting process and mathematical models can be used to determine the number of bacteria present in a sample. For example, if 10 colonies are counted in 1/100 dilution of the sample, then 100 colonies are expected in the sample with a 1/10 dilution. Similarly, 1000 colonies are expected in the sample with no dilutions.

Figure 112 shows that a fungal spore is present in the control sample. This means that cross-contamination occurred somewhere in the experimental chain. The source of the contamination is unknown and could have happened in either the Microbiology department or the Electrical Engineering department. The spore was only present in the fourth dilution of the control test and none of the other Petri dishes. This means that it is likely an isolated incident. The cross-

contamination does not make the experiments invalid because none of the treated samples had spores. This means spores were either never present, or the system destroyed them.

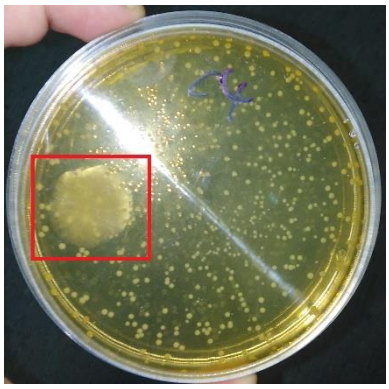

Figure 112 - Spore Contamination in Control

Table 15 shows the results after counting all the colonies in all the separate dilution series for the experiments.

Table 15 - Continuous Flow System Sterilisation Results

Continuous Flow Sterilisation Results						
	0 dilutions	2 dilutions	4 dilutions	6 dilutions	8 dilutions	
Control	n/a*	n/a*	574	7	0	5.74×10^7 CFU/mL
1 - 66 °C	1	0	0	2	0	TFTC#
2 - 67 °C	0	0	0	0	0	NOG$
3 - 75 °C	0	0	0	0	3	TFTC
4 - 95 °C	0	0	0	0	0	NOG
*Too many colonies to count, # Too few to count (< 10 CFU/mL), $ No observable growth						

The control test was calculated to have 5.74×10^7 CFU/ml on average based on the 1/1000 dilution as the next dilution is below 15. The treated samples in tests 1 and 3 had too few colonies to count deeming them successful. The few colonies counted are considered as errors as the dilution series cannot confirm the counts. Tests 2 and 4 had no colonies to count whatsoever which means complete sterilisation was achieved in these tests.

9.6 Chapter Conclusion

The control system dynamics were fully tested and although the system did not initially operate as designed, the simplicity of the proportional only control system allowed for the alteration of the design between tests. The control system was eventually tuned to the point where a steady state tracking error of $0\ ^\circ\mathrm{C} \pm 0.5\ ^\circ\mathrm{C}$ was achieved with no overshoot.

Complete sterilisation (i.t.o of *L. lactis*) was achieved in the microbiological experiments proving that the system designed in this thesis worked as intended.

Chapter 10
Recommendations & Conclusions

10.1 Chapter Summary

This chapter draws conclusions relating to the overall thesis system objectives highlighted in chapter 1 and briefly discusses and highlights potential improvements including future recommendations for the system designed in this project.

10.2 Recommendations

The recommendations discussed in this section include details about the pump, media recirculation techniques, the saturable reactor control selector, microprocessor, user interface, waveguide modules, control system, temperature sensors, methods of detecting when media is no longer inside the applicator and methods to reduce reflected power.

10.2.1 Pump

The control system in the design relies heavily on the variable flow rate of the pump in this system. A pump with a greater flow rate will allow a greater controllable temperature range at a higher output magnetron power level. This could enable the system to sterilise media at a faster rate. Furthermore, the ability to use a higher microwave power aligns with the decision of promoting a “non-thermal microwave effect” design discussed in section 3.2.

10.2.2 Media Recirculation

The recirculation hardware in this project makes use of manual irrigation taps. Electronic valves should be incorporated into the final design and controlled by the microprocessor. This feature would make the system fully autonomous.

10.2.3 Saturable Reactor Control

The three capacitors in the capacitor bank were physically plugged “in” and “out” of the system as required. This type of electronic manipulation would be impractical in a commercial environment. It is proposed that a manual “knob selector” be developed that “chooses” how many capacitors to incorporate.

The required power level supplied to the system is media dependant. This means that some applications require very high power for short periods of time whilst others require low power for longer periods of time.

10.2.4 Microprocessor

The Arduino Leonardo did not perform well enough in this project to have all system functionality on a single microprocessor.

The ESP32 microcontroller has two Xtensa 32-bit LX6 microprocessors enabling the device to perform coded tasks in parallel. Furthermore, this device has a $40\ \mathrm{MHz}$ crystal oscillator, provides 12-bit resolution for analogue readings and operates with $3.3\ \mathrm{V}$ logic [83]. Similarly, to the Arduino Leonardo, the ESP32 can be programmed through the Arduino IDE.

The ESP32 can connect to and create WiFi connections.

10.2.5 User Interface

The sterilisation unit developed in this project is “stand alone” as far as possible. The processing computer is not required for the system to operate and, as such, no graphical user interface (GUI) was developed. Plotted data was used during the design stages and may not be of use in a commercial product.

A user interface, however, may become necessary if the system could store different control system profiles for different media. Furthermore, the ESP32 comes with the capability of creating a wireless WiFi host which could interface with a mobile phone application.

10.2.6 Waveguide Modules

The waveguide components in this project were developed modularly. The final design only required the magnetron launcher to be attached the applicator with a reflective short termination.

The magnetron launcher is effectively “a hole” in the waveguide structure at a specific location. This means that the applicator can be made slightly bigger and the magnetron mounted directly onto the applicator.

10.2.7 Control System

The performance of the control system in this type of project is heavily dependent on the type of treatment media. Different control system profiles could be created and selected for various media types. These profiles could be downloadable from a website for a commercial product.

Alternatively, software configuration techniques for the system could be developed whereby the user could tell the system a new type of media is being passed through the system. The system would then record a step response for the new media and adjust the control software accordingly. The profiles can be saved and selected on start-up depending what the user would like to sterilise.

10.2.8 Temperature Sensors

The in-line thermistor temperature sensors used in this project worked very well, however, these sensors tended to lose their calibration and/or broke entirely and needed to be replaced and recalibrated.

The sensors were inserted into the side wall of the silicone tube by means of a small incision. Super glue was then used to seal the tube as well as hold the temperature sensors in place.

One can speculate as to why these sensors stopped working. The first reason may be because the system was continuously worked on and around. This factor could have caused the leads on the thermistor to move back and forth, eventually either thinning the leads or breaking them off inside the small component. The thinning of the leads could have caused a change in overall resistance and thus ruined the calibration.

The second possible reason could have been that the rapid heating followed by rapid cooling during the rigorous testing phases caused the insulation on the leads to crack creating potential short circuits.

Figure 113 shows the two different mounting styles used for the thermistors in this project:

Figure 113 - Thermistor Mounting Techniques a) Full Insertion b) Partial Insertion

All thermistor mountings made in the style of Figure 113 a) broke over time, whereas thermistors mounted in the style of Figure 113 b) did not break.

It is recommended that IR temperature sensors be used as this will provide a non-destructive method for capturing the temperature. The problem that the temperature will only measure the target container can be calibrate in software. This method should be thoroughly tested however, to ensure the change in response time for the temperature is adequate for the control system.

10.2.9 Detecting When No Media is Present in the Applicator

The axis and values presented in the graph seen in Figure 114 are not important for the explanation in this section. The image shows the produced temperature response during three stages. The first two stages have been discussed in detail during the course of this document. Stage 1 represents the transient response of the system recorded while the system fills up with media. Stage 2 represents the steady state response for continuous operation recorded while the system is completely full. Stage 3 represents the temperature response of the system recorded when the magnetron is kept "on" during drainage of the system.

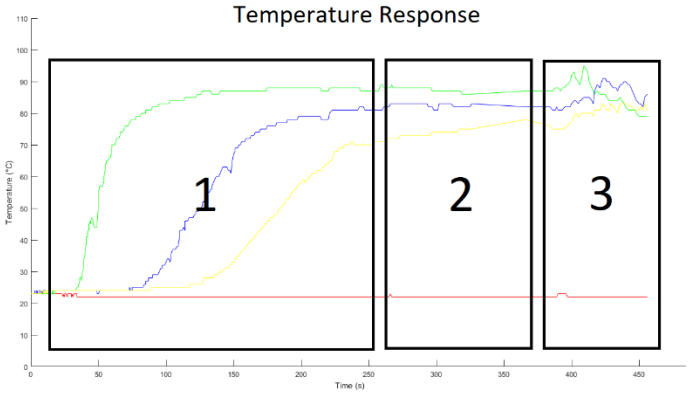

Figure 114 - Temperature Response During Magnetron Operation and Applicator Drainage

Stage 3 was always prevented because the treatment of media was either terminated through a software timer which turned the magnetron "off" and signalled the end of the treatment experiment. Alternatively, the microcontrollers were reset by pressing a "push" button. The start-up characteristics of the microcontrollers were such that the relay would keep the magnetron "off" until a treatment began. Stage 3, however, could prove to be a crucial element for the system when detecting the exact time when media leaves the treatment chamber.

Instead of waiting for the system to heat the magnetron through reflected power over time, the system could assess that a sudden large change has occurred in the steady state response. In turn

this could trigger a flag which states that errors exist in the system (and stop the treatment immediately).

This form of detection would occur more quickly than the magnetron overheating protection currently in the system.

10.2.10 Method to Reduce Reflected Power

The reason large reflections are present in the system is due to the fact that the full coil structure is not a matched load inside the waveguide applicator. This is because the full coil structure presents a large volume for the E-fields to immediately interact with.

If the shape of the coil was altered to present a more gradual increase in volume, reflections should decrease. This could be done by creating a tapered coil which starts with a small winding and gradually increases the winding radius. The "tip" of the tapered coil should be placed closest to the microwave source.

Alternatively, uniform coil rings could be placed increasingly further apart, the closer the coils get to the microwave source.

10.3 Conclusions

This section draws conclusions from all the material and topics presented in this thesis with particular focus on the objectives outlined, sterilisation effectiveness and the control system.

10.3.1 Microwave Sterilisation System Objectives

The objectives below are listed in chapter 1.

10.3.1.1 To develop a system capable of sterilising liquid to an industry standard

Complete sterilisation was achieved in the microbial sterilisation experiments performed on *Lactococcus lactis.* This achievement, however, does not necessarily mean that "an industry standard" has been met as outlined in section 2.5.3. There are many other types of microorganisms, all of which could behave differently under heat treatment. Some unicellular microorganisms can survive in harsh environments (e.g. temperatures above $100\ ^{\circ}\mathrm{C}$).

The system designed in this thesis currently has a controllable temperature range between $60\ ^{\circ}\mathrm{C}$ and $95\ ^{\circ}\mathrm{C}$. Higher temperatures than the range indicated inside the system causes the media to boil, which in turn ejects the media out of the outlet pipe aggressively. The aggressive ejection may result in the media not being held at the target temperature for long enough to achieve required sterilisation for a specific media. It is recommended that further testing of other, more resilient, microorganisms should be conducted before this objective can be confidently achieved.

Additionally, the results in this thesis have been achieved under "perfect" laboratory conditions with a single organism suspended in saline solution. Application specific media is likely to behave differently inside the system and may prove more difficult to sterilise.

10.3.1.2 To develop a predictable system where insight can be gained through simulation

Complete simulation, in terms of moving media, was not completed in this project. The project was instead broken up into various key parts and simulated to find the s-parameters for the system.

The applicator required the design of inlet and outlet microwave chokes intended to stop the structure from radiating. The simulated design was implemented on the applicator and no radiation was measured leaving the applicator. The applicators s-parameters were then determined. The simulated S_{11} yielded a value of $-6.655\ \mathrm{dB}$. The applicator was then measured on a VNA which

produced an S_{11} of -5.075 dB. These values predicted the reflected power in the system to be 75.6 W and 108.8 W respectively. The power detector used in conjunction with the bi-directional coupler suggested that the actual measured reflected power was closer to 90 W.

This objective was considered achieved because the design specifications outlined that the reflected power should be below 100 W. The simulation package allowed for a software design approach, resulting in only one applicator design reaching the fabrication stage at the same time as conforming to the design specification.

10.3.1.3 To have a continuous flow system as opposed to a batch system

The system designed in this thesis is continuous for as long as there is media present inside the system. The longest continuous test conducted with the system was 15 minutes. The magnetron and the high voltage transformer reached steady state temperatures below 40 °C. This level of temperature is not great enough to cause damage to the components. The response showed that these temperatures were maintained for the majority of the test, however, it is unknown what would happen to the system over a much longer period of time.

It is worth noting that the magnetron and high voltage transformer are air-cooled by a strong fan. When the fan is turned "off", the temperature began to rise. The limits of this test were never realised since this type of test could cause significant system damage. However, it could be concluded from this limit test that an air-cooling fan would be required for continuous operation.

10.3.1.4 To have a cost-effective design

The final system design, which did not incorporate a circulator, bi-directional coupler or power detectors, reduced the cost of the system dramatically. Furthermore, the power supply utilises conventional microwave oven parts which are mass produced and affordable. The other components in the system like the peristaltic pump, silicone tubing, polystyrene support structures and thermistor temperature sensors were all cheaper than their alternatives (diaphragm pump, PTFE tube and support, IR temperature sensors). The cost of these items, however, are irrelevant when compared to the cost of fabricating the WR340 waveguide structures used. Waveguide structures are expensive due to the accuracy required during the manufacturing process.

10.3.1.5 Create a system of comparable efficiency seen in other conventional sterilisation techniques

The validity of this objective was not fully realised because only one type of microorganism was tested.

Assuming, however, that complete sterilisation occurs for all media, this system may prove to be more efficient than that of a laboratory autoclave. This is because an autoclave could get "locked" into a treatment cycle for over an hour. Using the lowest flow rate in this project would yield 3.3 litres of treated media in that time. This means that the system designed in this thesis could potentially be more efficient than a laboratory autoclave for autoclave loads of less than 3.3 litres.

10.3.1.6 To detect when a treatment sample is no longer present in the treatment chamber

This objective was not focussed on during the development stages of this project due to its lack of necessity in the experimental system. This is because the circulator in the experimental design was intended to protect the magnetron. The power detectors functionality was relied on to determine the amount of reflected power in the system. It was evident that large amounts of reflected power were found even though there was no media present in the applicator.

The functionality of detecting when media was no longer present in the applicator was then lost once the power detector and circulator were removed in an effort to reduce the cost of the system.

The removal of the circulator, however, created a new source of data. Again, when media was not present in the applicator, large amounts of power were reflected. The reflected power now travelled back to the magnetron causing it to heat up. This change in heat can be sensed and the magnetron powered “off” due to no media presence inside the applicator.

A third method for detecting when no media is present in the applicator is recommended in section 10.2.9 which is beneficial in that it has the ability to protect the magnetron faster than the solution of waiting for the magnetron to reach potentially damaging temperature levels.

10.3.1.7 To ensure the temperature is controlled

The temperature was controlled through the hybrid proportional-only control system designed in chapter 8. The results showed evidence that the microwave heating effect relies heavily on the target media which was put through the system. The design modelled the effects of microwave heating on saline solution which proved to be a different from the model required for the bacterial tests conducted in chapter 9.

The first live test with the bacteria produced a steady state tracking error of $6\ ^{\circ}\mathrm{C}$. Although the error was greater than that designed for, the error was constant. This proves that the system was never unstable even though the model for the control system was incorrect. Alterations to the control system were easy enough to implement which produced results which were within the design specifications of the control system for the remaining bacterial tests. The control system also illustrated evidence which supports the rejection of input disturbance signals, deeming the control system robust.

10.3.2 Final Conclusion

The complete system designed in this thesis confidently achieved five out of the seven objectives outlined at the project’s inception. The objective to achieve comparable sterilisation efficiency for sterilisation techniques currently used in industry was not investigated. The objective to achieve sterilisation to an industry standard, outlined by the World Health Organisation and the Food and Agriculture Organisation, was not fully explored due to time constraints.

The tested system does however, provide a complete sterilisation solution for aqueous media through the use of microwave heating effects.

References

[1] A. E. Oberholzer and Prof J.B. de Swardt, “Development of a Continuous Flow Sterilisation System Using Microwaves,” Stellenbosch University, 2016.

[2] J. P. van der Merwe, “Magnetron Output Power Controller Used in the Application of Rooibos Tea Sterilisation,” Stellenbosch University, 2018.

[3] D. Ronica, “How Radiation Works,” *How Stuff Works*, 2008. [Online]. Available: https://science.howstuffworks.com/radiation.htm#. [Accessed: 17-Mar-2019].

[4] Health Physics Society, “What Is Radiation?,” *Health Physics Society*, 2016. [Online]. Available: http://hps.org/publicinformation/ate/faqs/whatisradiation.html. [Accessed: 17-Mar-2019].

[5] N. R. Center, “Nature of Radiation,” *NDT Resource Center*. [Online]. Available: https://www.nde-ed.org/EducationResources/CommunityCollege/RadiationSafety/theory/nature.htm. [Accessed: 17-Mar-2019].

[6] United States Nuclear Reglatory Commission, “Radiation Basics,” *United States Nuclear Reglatory Commission*, 2017. [Online]. Available: https://www.nrc.gov/about-nrc/radiation/health-effects/radiation-basics.html. [Accessed: 17-Mar-2019].

[7] Science10, “Atom,” *s.l.* [Online]. Available: https://atomsionsmolecules10.weebly.com/atoms.html. [Accessed: 17-Mar-2019].

[8] Commonwealth of Australia as represented by the Australian Radiation Protection and Nuclear Safety Agency, “What is ionising radiation?,” *s.l.* [Online]. Available: https://www.arpansa.gov.au/understanding-radiation/what-is-radiation/ionising-radiation. [Accessed: 17-Mar-2019].

[9] N. Patel, K. Vo, and M. Hernandez, “Electromagnetic Radiation,” *LibreTexts libraries*, 2015. [Online]. Available: https://chem.libretexts.org/Bookshelves/Physical_and_Theoretical_Chemistry_Textbook_Maps/Supplemental_Modules_(Physical_and_Theoretical_Chemistry)/Spectroscopy/Fundamentals_of_Spectroscopy/Electromagnetic_Radiation. [Accessed: 17-Mar-2019].

[10] J. Lucas, “What Is Electromagnetic Radiation?,” *Live Science*, 2015. [Online]. Available: https://www.livescience.com/38169-electromagnetism.html. [Accessed: 16-Mar-2019].

[11] W. D. Kimura, “What are electromagnetic waves?,” in *Electromagnetic Waves and Lasers*, Morgan & Claypool Publishers, 2017, pp. 1–33.

[12] Spazturtle, “File:EM-spectrum.svg,” *wikimedia*, 2015. [Online]. Available: https://commons.wikimedia.org/wiki/File:EM-spectrum.svg. [Accessed: 17-Mar-2019].

[13] I. The McGraw-Hill Companies, “microwave region,” *An Illustrated Dictionary of Aviation*, 2015. [Online]. Available: https://encyclopedia2.thefreedictionary.com/microwave+region. [Accessed: 16-Mar-2019].

[14] E. Ackerman, “A Brief History of the Microwave Oven,” *When Nuking Food Was Novel.*, 2016. [Online]. Available: https://spectrum.ieee.org/tech-history/space-age/a-brief-history-of-the-microwave-oven. [Accessed: 20-Jul-2019].

[15] New England Historical Society, “Percy Spencer Melts a Chocolate Bar, Invents the Microwave

Oven," *s.l.*, 2019. [Online]. Available: http://www.newenglandhistoricalsociety.com/percy-spencer-melts-chocolate-bar-invents-microwave-oven/. [Accessed: 20-Jul-2019].

[16] Encyclopedia Britannica inc, "The Magnetron," *Online*, 2004. [Online]. Available: http://mainland.cctt.org/istf2008/images/magnetron.jpg. [Accessed: 20-Jul-2019].

[17] M-Press Systems (M) Sdn. Bhd., "Magnetron Basics," *s.l.* [Online]. Available: https://www.m-press.com.my/en/technical_info/magnetron_basics.html. [Accessed: 21-Jul-2019].

[18] C. Wolff, "Radar Basics," *s.l.* [Online]. Available: http://www.radartutorial.eu/08.transmitters/Magnetron.en.html#this. [Accessed: 20-Jul-2019].

[19] T. Puiu and G. Retseck, "How the microwave oven was made from WWII radar tech," *ZME Science*, 2018. [Online]. Available: https://www.zmescience.com/science/physics/microwave-oven-from-ww2/. [Accessed: 20-Jul-2019].

[20] The Editors of Encyclopaedia Britannica, "Lorentz force," *Encyclopædia Britannica*, 2017. [Online]. Available: https://www.britannica.com/science/Lorentz-force. [Accessed: 21-Jul-2019].

[21] National MagLab, "How Microwaves Work," *s.l.*, 2017. [Online]. Available: https://www.youtube.com/watch?v=lVu11WWrNbQ. [Accessed: 20-Jul-2019].

[22] A. C. Metaxes and R. J. Meredith, "Industrial Microwave Heating," in *Power Engineering Series 4*, 1st ed., D. A. T. Johns, G. Ratcliff, and P. A. Write, Eds. London: Peter Peregrinus, 1983, pp. 238–276.

[23] J. P. van der Merwe and J. de Swardt, "Power Control of a Domestic Microwave Oven," *2017 IEEE AFRICON*, pp. 595–599, 2017.

[24] C. Perdomo, "Technical Guide, Microwave Ovens with Inverters," Secaucus, New Jersey.

[25] N. D. Tleis, *Power Systems Modelling and Fault Analysis*. Elsevier Ltd., 2008.

[26] Electronics Tutorials, "Series Resonance Circuit," *s.l.* [Online]. Available: https://www.electronics-tutorials.ws/accircuits/series-resonance.html. [Accessed: 08-Aug-2019].

[27] P. McNeil, "What are the ISM Bands, and What Are They Used For?," *Pasternack Blog*, 2018. [Online]. Available: https://blog.pasternack.com/uncategorized/what-are-the-ism-bands-and-what-are-they-used-for/. [Accessed: 09-Sep-2019].

[28] K. Umetsu and Y. Tomizawa, "Designing of Microwave Applicators by Electromagnetic Wave Analysis," 2004.

[29] M. Chaplin, "Water and Microwaves," *Water Structure and Science*, 2019. [Online]. Available: http://www1.lsbu.ac.uk/water/microwave_water.html. [Accessed: 09-Sep-2019].

[30] P. A. Mello and Et al., *Microwave-Assisted Sample Preparation for Trace Element Determination*. Elsevier B.V., 2014.

[31] J. Ahmed and S. Ramaswamy, *Microwave Pasteurization and Sterilization of Foods*, 2nd ed. CRC Press, 2007.

[32] Boundless, "1.2A Types of Microorganisms," *LibreTexts libraries*, 2019. [Online]. Available: https://bio.libretexts.org/Bookshelves/Microbiology/Book%3A_Microbiology_(Boundless)/1%3A_Introduction_to_Microbiology/1.2%3A_Microbes_and_the_World/1.2A_Types_of_Micr

oorganisms. [Accessed: 14-Sep-2019].

[33] Oxford, “peptidoglycan,” *Lexico.com*, 2019. [Online]. Available: https://www.lexico.com/en/definition/peptidoglycan. [Accessed: 14-Sep-2019].

[34] D. Moore, G. D. Robson, and A. P. J. Trinci, “16.2 Microsporidia,” *21st Century Guidebook to Fungi, SECOND EDITION*, 2019. [Online]. Available: http://www.davidmoore.org.uk/21st_Century_Guidebook_to_Fungi_PLATINUM/Ch16_02.htm. [Accessed: 14-Sep-2019].

[35] obpl, “Growth curve-orbit biotech,” *Orbit Biotech*, 2018. [Online]. Available: https://orbitbiotech.com/bacterial-growth-curve-generation-time-lag-phase-log-phase-exponential-phase-decline-phase/growth-curve-orbit-biotech/. [Accessed: 14-Sep-2019].

[36] M. W. Davidson and The Florida State University, “Bacteria Cell Structure,” *Molecular Expressions, Cell Biology and Microscopy*, 2015. [Online]. Available: https://micro.magnet.fsu.edu/cells/bacteriacell.html. [Accessed: 14-Sep-2019].

[37] Diffen LLC, “Gram-positive vs Gram-negative Bacteria,” *Diffen.com*. [Online]. Available: https://www.diffen.com/difference/Gram-negative_Bacteria_vs_Gram-positive_Bacteria. [Accessed: 14-Sep-2019].

[38] V. Greenwood and Quanta, “Why Does Heat Kill Cells?,” *theatlantic.com*, 2017. [Online]. Available: https://www.theatlantic.com/science/archive/2017/05/heat-kills-cells/526377/. [Accessed: 13-Sep-2019].

[39] T. K. Kovach, *Conformational stability: Protein folding and denaturation*. Khan Academy, 2013.

[40] T. K. Kovach, *Four levels of protein structure*. Khan Academy, 2013.

[41] Fitness Codes, “20 Facts About Protein You Probably Didn’t Know,” *FitnessCodes*, 2016. [Online]. Available: http://www.fitnesscodes.co.uk/20-facts-protein-probably-didnt-know/. [Accessed: 14-Sep-2019].

[42] P. J. Fellows, “Chapter 12 Heat sterilisation,” in *Food Processing Technology*, 4th ed., Woodhead Publishing, 2017, pp. 581–622.

[43] W. A. Rutala and D. J. Weber, “Chemical Disinfectants,” *Centers for Disease Control and Prevention*, 2016. [Online]. Available: https://www.cdc.gov/infectioncontrol/guidelines/disinfection/disinfection-methods/chemical.html. [Accessed: 10-Sep-2019].

[44] E. R. Sanders, “Aseptic laboratory techniques: volume transfers with serological pipettes and micropipettors,” *J. Vis. Exp.*, no. 63, p. 2754, May 2012.

[45] The Editors of Encyclopaedia Britannica, “Laminar flow,” 2018. [Online]. Available: https://www.britannica.com/science/laminar-flow. [Accessed: 10-Sep-2019].

[46] CLEATECH LLC, “Horizontal vs Vertical Laminar Flow Hoods,” *Lab Supply Network*. [Online]. Available: https://www.laboratory-supply.net/blog/horizontal-vs-vertical-laminar-flow-hoods/. [Accessed: 10-Sep-2019].

[47] Food and Agriculture Organization, “CODE OF HYGIENIC PRACTICE FOR ASEPTICALLY PROCESSED AND PACKAGED LOW-ACID FOODS,” *CAC/RCP 40-1993*. [Online]. Available: http://www.fao.org/input/download/standards/26/CXP_040e.pdf. [Accessed: 10-Sep-2019].

[48] Tetra Pak, “An introduction to commercial sterility,” *s.l.*, 2008. [Online]. Available:

https://endpoint895270.azureedge.net/static/documents/sterility_63601.pdf. [Accessed: 10-Sep-2019].

[49] C. Rougier, A. Prorot, P. Chazal, P. Leveque, and P. Leprat, “Thermal and Nonthermal Effects of Discontinuous Microwave Exposure (2.45 Gigahertz) on the Cell Membrane of Escherichia coli,” *Appl. Environ. Microbiol.*, vol. 80, no. 16, pp. 4832 LP – 4841, Aug. 2014.

[50] J. Berlan, P. Giboreau, S. Lefeuvre, and C. Marchand, “Synthese organique sous champ microondes : premier exemple d’activation specifique en phase homogene,” *Tetrahedron Lett.*, vol. 32, no. 21, pp. 2363–2366, 1991.

[51] A. de la Hoz, A. Diaz-Ortiz, and A. Moreno, “Review on non-thermal effects of microwave irradiation in organic synthesis,” *J. Microw. power Electromagn. energy a Publ. Int. Microw. Power Institute.*, vol. 41, no. 1, pp. 45–66, 2006.

[52] Sairem, “MANUAL 3-STUB TUNER,” 12 porte du Grand Lyon, 2017.

[53] C. Rhoda and J. Prof de Swardt, “Microwave heating for industrial food processing applications,” Stellenbosch University, 2018.

[54] D. K. Cheng, *Field and Wave Electromagnetics*, Second Edi. Pearson, 2014.

[55] C. A. Balanis, *Advanced Engineering Electromagnetics*, First Edit. Arizona: John Wiley and Sons Inc., 1989.

[56] E. Jensen, “Cavity Basics,” Geneva, 2012.

[57] P. J. Bevelacqua, “Slotted Waveguide Antennas.” [Online]. Available: http://www.antenna-theory.com/antennas/aperture/slottedWaveguide.php. [Accessed: 14-Feb-2019].

[58] U.S. Department of Health and Human Services, “Radiation-Emitting Products,” 2017. [Online]. Available: https://www.fda.gov/Radiation-EmittingProducts/ucm252762.htm. [Accessed: 14-Feb-2019].

[59] T. Abe and Y. Yamaguchi, “Propagation Constant Below Cutoff Frequency in a Circular Waveguide with Conducting Medium,” *IEEE Trans. Microw. Theory Tech.*, vol. MTT-29, no. 7, pp. 707–712, 1981.

[60] Electronicsnotes, “Waveguide Cutoff Frequency.” [Online]. Available: https://www.electronics-notes.com/articles/antennas-propagation/rf-feeders-transmission-lines/waveguide-cutoff-frequency.php. [Accessed: 14-Feb-2019].

[61] Pasternack, “Skin Depth Calculator,” *Infinite Electronics International, Inc.* [Online]. Available: https://www.pasternack.com/t-calculator-skin-depth.aspx. [Accessed: 14-Feb-2019].

[62] everythingRF, “Waveguide Sizes,” 2015. [Online]. Available: https://www.everythingrf.com/tech-resources/waveguides-sizes. [Accessed: 06-Nov-2019].

[63] S. K. Jain, D. K. Sharma, V. K. Senecha, P. Naik, and P. Hannurkar, “Study of microwave components for an electron cyclotron resonance source: Simulations and performance,” *Sa¯dhana¯*, vol. 39, no. 4, pp. 901–920, 2014.

[64] National Electronics, “YJ1530SP CW Magnetron,” La Fox, Illinois.

[65] henan xinhang, “manufacturers of rectangular waveguide for 1000w/1500w microwave magnetron,WR-340,” *Alibaba.com*. [Online]. Available: https://www.alibaba.com/product-detail/manufacturers-of-rectangular-waveguide-for-1000w_60390304891.html?spm=a2700.wholesale.maylikever.10.7474b396TdBIPR.

[Accessed: 06-Nov-2019].

[66] electronics-notes.com, “RF directional coupler basics tutorial.” [Online]. Available: https://www.electronics-notes.com/articles/radio/rf-combiner-splitter-coupler-hybrid/what-is-an-rf-directional-coupler.php. [Accessed: 07-Nov-2019].

[67] tutorialspoint.com, “Microwave Engineering - Directional Couplers,” 2019. [Online]. Available: https://www.tutorialspoint.com/microwave_engineering/microwave_engineering_directional_couplers.htm. [Accessed: 07-Nov-2019].

[68] www.Tpub.com, “Electronics Technician Volume 07-Antennas and Wave Propagation,” *Integrated Publishing*. [Online]. Available: http://electronicstechnician.tpub.com/14092/css/Waveguide-Plumbing-78.htm. [Accessed: 08-Nov-2019].

[69] Sairem, “Microwave Components – 915MHZ & 2,45 GHz,” 2019. [Online]. Available: https://www.sairem.com/microwave-radio-frequency-rf-products/microwave-generators-components/microwave-components/. [Accessed: 09-Nov-2019].

[70] Mepits, “DC Motor Driver Circuit,” 2015. [Online]. Available: https://www.mepits.com/tutorial/379/electrical/motor-driver. [Accessed: 11-Nov-2019].

[71] Global Pumps, “What Are the Differences Between Pump Types?,” 2016. [Online]. Available: https://www.globalpumps.com.au/blog/what-are-the-differences-between-pump-types. [Accessed: 11-Nov-2019].

[72] PumpScout Staff, “Pump Types Guide - Find the right pump for the job,” *LeadMethod, Inc.*, 2019. [Online]. Available: http://www.pumpscout.com/articles-scout-guide/pump-types-guide-aid100.html. [Accessed: 11-Nov-2019].

[73] R. Components, “RS PRO Diaphragm Electric Operated Positive Displacement Pump, 150mL/min, 1 bar, 1.5 → 4.5 V,” 2019. [Online]. Available: https://za.rs-online.com/web/p/products/7026894?cm_mmc=ZA-PLA-DS3A-_-google-_-PLA_ZA_EN_Plumbing_And_Pipeline-_-Central_Heating_And_Process_Pumps%7CPositive_Displacement_Pumps-_-PRODUCT_GROUP&matchtype=&aud-358527059426:pla-393276713923&gclid=CjwKCAiAqqTu. [Accessed: 11-Nov-2019].

[74] Micro Robotics, “Peristaltic Liquid Pump with Silicone Tubing,” 2019. [Online]. Available: https://www.robotics.org.za/AF1150?search=pump. [Accessed: 11-Nov-2019].

[75] ECCOSTOCK®, “DIELECTRIC MATERIALS CHART,” *Low Loss Dielectrics & Other Common Materials*. [Online]. Available: http://www.eccosorb.com/Collateral/Documents/English-US/dielectric-chart.pdf. [Accessed: 11-Nov-2019].

[76] Generation Communication, “THE ROLES OF VOLTAGE AND FREQUENCY IN THE TRANSMISSION OF ELECTRICITY,” *Fact Sheet*, 2017. [Online]. Available: http://www.eskom.co.za/AboutElectricity/FactsFigures/Documents/TD0004RolesVoltageFrequencyTxRev6.pdf. [Accessed: 12-Nov-2019].

[77] Vishay®, “NTC Thermistors, 2-Point Micro Chip Sensor Insulated Leads,” Malvern, Pennsylvania, 2011.

[78] P. Christensson, “Data Type Definition,” *TechTerms*, 2007. [Online]. Available: https://techterms.com/definition/datatype. [Accessed: 18-Nov-2019].

References

[79] Arduino, “string,” *Data Types*, 2019. [Online]. Available: https://www.arduino.cc/reference/en/language/variables/data-types/string/. [Accessed: 18-Nov-2019].

[80] Electrical4U, “Control System | Closed Loop Open Loop Control System,” 2019. [Online]. Available: https://www.electrical4u.com/control-system-closed-loop-open-loop-control-system/. [Accessed: 19-Nov-2019].

[81] tutorialspoint.com, “Control Systems - Controllers,” 2019. [Online]. Available: https://www.tutorialspoint.com/control_systems/control_systems_controllers.htm. [Accessed: 19-Nov-2019].

[82] K. ARI, F. T. ASAL, and M. COŞGUN, “PI, PD, PID CONTROLLERS.”

[83] Espressif Systems, “ESP32 Series Datasheet,” 2019.

Appendices

Appendix A – PCB Schematic

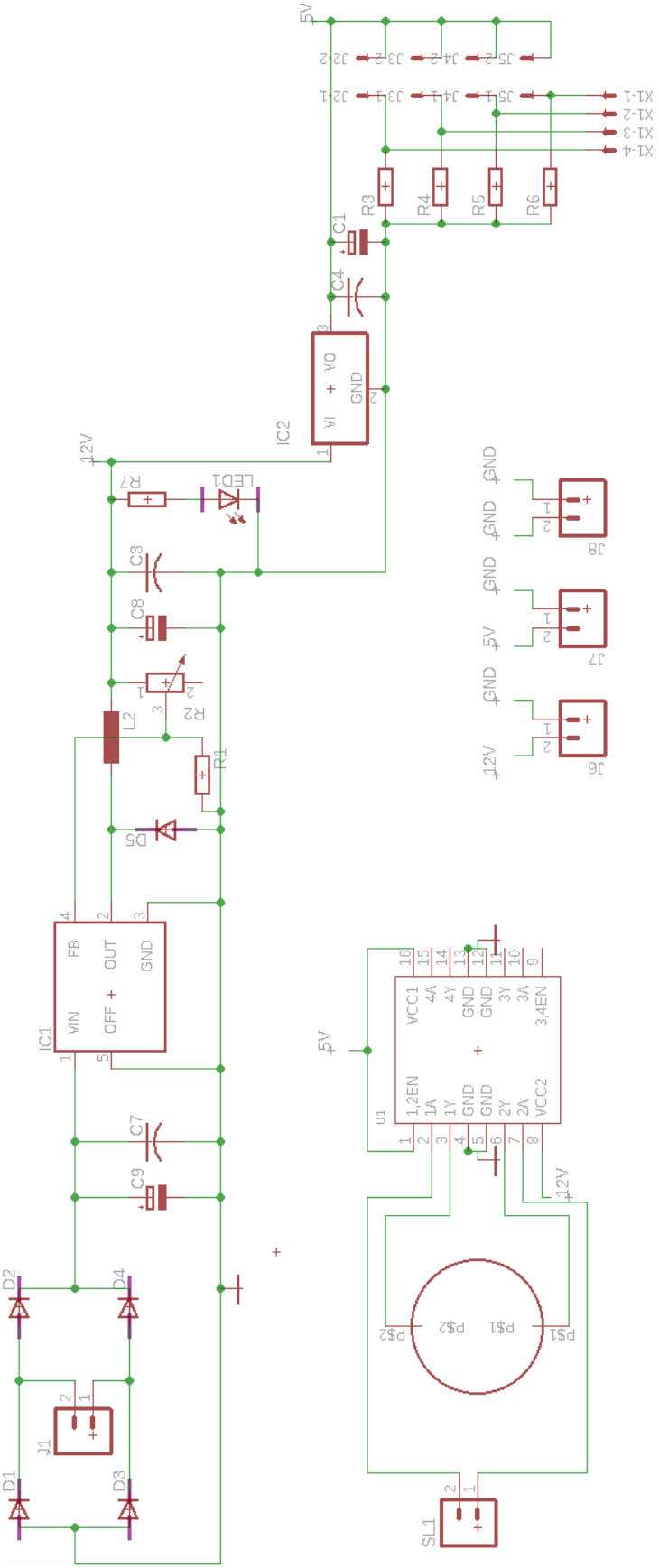

Appendix A – PCB Schematic

Table 16 - Parts List for Schematic and PCB

Part	Value
C1	100 n
C3	1000 µF
C4	100 µF
C7	1000 µF
C8	100 nF
C9	100 nF
D1	1N4007
D2	1N4007
D3	1N4007
D4	1N4007
D5	1N4007
IC1	LM2576
IC2	LM7805
J1	2 Terminal Screw Connector
J2	NTC Thermistor (Insulated Leads)
J3	NTC Thermistor (Insulated Leads)
J4	NTC Thermistor (Insulated Leads)
J5	NTC Thermistor (Insulated Leads)
J6	2 Terminal Screw Connector
J7	2 Terminal Screw Connector
J8	2 Terminal Screw Connector
L2	100 µH
LED1	Visible LED, Red, Single Chip, 5 mm Lamp
R1	1000 Ω
R2	Variable 8.86 kΩ
R3	680 Ω
R4	680 Ω
R5	680 Ω
R6	680 Ω
R7	1000 Ω
SL1	Female Header (2 Pins)
U$1	Peristaltic Pump Mounting
U1	L293D Driver IC - DIP
X1	Female Header (4 Pins)

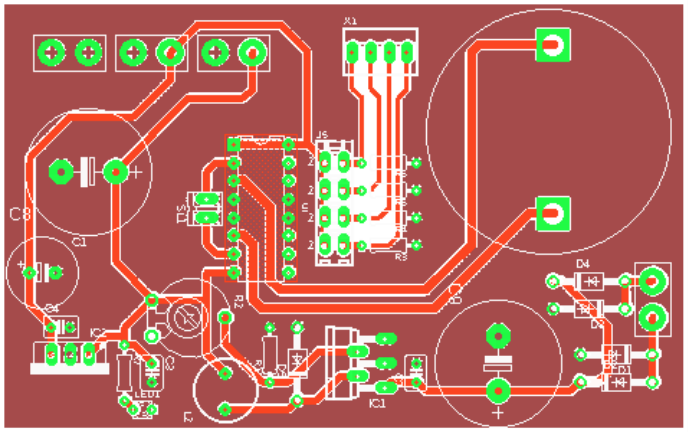

Figure 115 - PCB Layout

Appendix B – Risk Assessment

UNIVERSITEIT STELLENBOSCH UNIVERSITY

Department of Electrical & Electronic Engineering

Health and Safety Representative
Mr P Petzer 021-8084316

RISK ASSESSMENT / RISIKO ANALISE

REV. NR. 1

Building / Area / Project: Electrical & Electronic Engineering Room E322 M-Project: Directional Coupler and Microwave Oven Power Control	**US Number:** 17744687
	Assessment Undertaken: (Date) 15/09/2017
	People Involved: (Print Names) Student: BJ van der Merwe Supervisor: Prof. JB De Swardt
Job or Task: Design a directional coupler and use it in a microwave oven system. The output power of the microwave oven should be controlled. This may be used for sterilisation.	**Safety Supervisor Authorisation (Print Name)** Mr P. Petzer
	Assessment Review Date:

1 HAZARD AND HAZARD EFFECT	2 WHO / WHAT MIGHT BE HARMED?	3 IS THE RISK ADEQUATELY CONTROLLED?	4 WHAT FURTHER ACTION IS NECESSARY TO CONTROL THE RISK?	5 WHO IS RESPONSIBLE FOR THE ACTIONS?		
List Here:	**List groups of people who are especially at risk from significant hazards which you have identified**	**List existing controls here or note where the information may be found:**	**List the risks that are not adequately controlled and the action you will take where it is reasonably practicable to do more. You are entitled to take cost into account, unless the risk is high:**	**Person responsible and by when:**		
				Person	**Date for Completion**	**Date completed**
Future risk: RF Radiation: Leaking Microwaves can cause skin burns and eye damage.	Operator and people sharing the workspace can be harmed.	All connections between parts is insulated with aluminium tape to reduce the risk of leaking. A system that monitors continually is active in the lab and will warn when the power radiated is unsafe (5mW/cm^2 at 5cm from source). EM Stop has also been wired in.	The calibration of the system that continually monitors depends on the source of microwaves. Therefore, that system will be recalibrated every time microwave components are moved around.	BJ van der Merwe	To be determined	To be determined

Appendix B – Risk Assessment

1 HAZARD AND HAZARD EFFECT List Here:	2 WHO / WHAT MIGHT BE HARMED? List groups of people who are especially at risk from the significant hazards which you have identified	3 IS THE RISK ADEQUATELY CONTROLLED? List existing controls here or note where the information may be found:	4 WHAT FURTHER ACTION IS NECESSARY TO CONTROL THE RISK? List the risks that are not adequately controlled and the action you will take where it is reasonably practicable to do more. You are entitled to take cost into account, unless the risk is high:	5 WHO IS RESPONSIBLE FOR THE ACTIONS? Person responsible and by when:		
				Person	Date for Completion	Date completed
Electricity: 220VAC lines used in the power control circuit can cause severe, even lethal, electric shock.	Operator can be harmed	The high voltage part of the circuit is isolated from the rest. All high voltage wires are connected through connector blocks or with sufficient insolation tape to ensure no open live wires are present. Warning sign is placed on the circuit.	-	BJ van der Merwe	Ongoing	Ongoing
Lone working: Accidents or emergencies arising out of the work.	Lone worker/ operator can be harmed	Take reasonable care to look after own health and safety. Use tools and other equipment properly, in accordance with any relevant safety instructions.		BJ van der Merwe	Ongoing	Ongoing

Appendix B – Risk Assessment

1 HAZARD AND HAZARD EFFECT	2 WHO / WHAT MIGHT BE HARMED?	3 IS THE RISK ADEQUATELY CONTROLLED?	4 WHAT FURTHER ACTION IS NECESSARY TO CONTROL THE RISK?			5 WHO IS RESPONSIBLE FOR THE ACTIONS?		
List Here:	List groups of people who are especially at risk from significant hazards which you have identified	List existing controls here or note where the information may be found:	List the risks that are not adequately controlled and the action you will take where it is reasonably practicable to do more. You are entitled to take cost into account, unless the risk is high:			Person responsible and by when:		
				Person	Date for Completion	Date completed
Future potential hazard: High Temperature. Liquids being sterilised can reach temperatures between 70 – 120°C. Might also release steam. This can cause burn wounds.	Operator and people sharing workspace can be harmed.	The temperature of potentially hot containers is to be measured from a distance using a laser temperature 'gun'. This will determine whether they are too hot to touch.	The steam vent should be faced away from the operating area. Sterile liquid container should be placed in a safe area where accidental contact is minimised.	BJ van der Merwe	To be determined	To be determined
Future potential hazard: Environmental. The media that will be used during the project is a biochemical growth media that cannot be discarded in a normal drain.	Environment	The Biochemistry Department has waste containers and procedures of dealing with these substances.	All unused liquids should be labelled and set aside in a safe area during testing. These liquids should then be returned to the Biochemistry Department for proper disposal.	BJ van der Merwe	To be determined	To be determined

Appendix C - Determining Treatment Time

$10\ ml\ Water$

Time (s)	Starting Temperature (°C)	End Temperature (°C)	Thermal Image
10	13	22.6	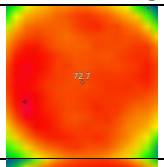
15	15	49.1	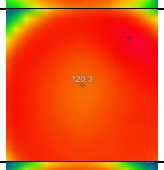
20	15	56.9	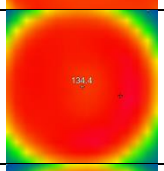
30	15	68.9	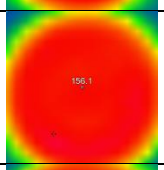
40	15	71.6	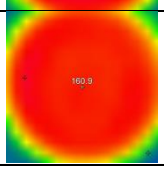

Rough Experimental Notes:

- Initial tests done with an uncovered Petri dish showed that it was difficult to raise the temperature above 60 °C.
- The temperature of the dish drops very quickly once placed on laboratory bench – need to consider death curves of bacteria.
- Initially even heating was seen or assumed – the higher temperatures caused the Petri dish to warp which in turn caused shallower regions in the middle of the dish. These shallower areas were seen to be colder and thus uneven heating was seen. Consider using glass Petri dish.
- Test done with a plastic Petri dish.

Appendix C - Determining Treatment Time

2 Teaspoons Dry Flour

Time (s)	Starting Temperature (°C)	End Temperature (°C)	Thermal Image
10	15	81.6	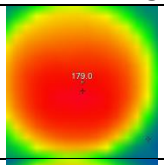
15	15	89.2	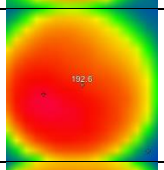
20	15	90.8	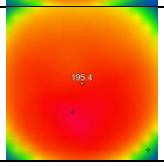

Rough Experimental Notes:

- The dry flower got very hot very quickly!
- Test done with a plastic Petri dish.

Appendix C - Determining Treatment Time

2 Teaspoons Flour, Teaspoons Water Mixed Into A Paste

Time (s)	Starting Temperature (°C)	End Temperature (°C)	Thermal Image
10	15	50.5	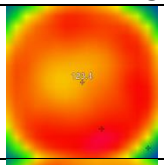
15	15	77.2	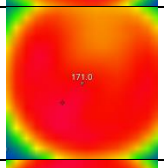
20	15	78.2	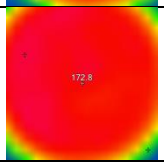

Rough Experimental Notes:

- Although the middle looks like a cold spot, the mixture was seen to rise in the centre. This could suggest that the middle was hotter. A potential reason for the thermal camera picking up a cold spot in the centre is that the mixture touched the lid of the Petri dish and dissipating the heat.
- Test done with a plastic Petri dish.

Appendix C - Determining Treatment Time

2 Teaspoons Grated Chocolate

Time (s)	Starting Temperature (°C)	End Temperature (°C)	Thermal Image
10	19	26.1	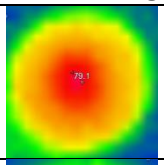
15	19	37.4	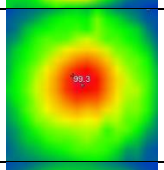
20	19	46.0	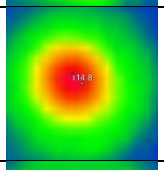
30	19	62.1	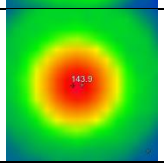

Rough Experimental Notes:

- Tests done with a glass Petri dish
- Heating seen to be very central